Modeling Transport in Polymer-Electrolyte Fuel Cells

Adam Z. Weber* and John Newman

Department of Chemical Engineering, University of California, Berkeley, California 94720-1462

Contents

1. Introduction

Fuel cells may become the energy-delivery devices of the 21st century. Although there are many types of fuel cells, polymer-electrolyte fuel cells are receiving the most attention for automotive and small stationary applications. In a polymer-electrolyte fuel cell, hydrogen and oxygen are combined electrochemically to produce water, electricity, and some waste heat.

During the operation of a polymer-electrolyte fuel cell, many interrelated and complex phenomena occur. These processes include mass and heat transfer, electrochemical reactions, and ionic and electronic transport. Only through fundamental modeling, based on physical models developed from experimental observations, can the processes and operation of a fuel cell be truly understood. This review examines and discusses the various regions in a fuel cell and how they have been modeled.

The focus of this review is to discuss the different fuel-cell models with the overall goal of presenting a picture of the various types of transport in fuel cells. Although the majority of the literature fuel-cell models have been examine, there are undoubtedly some that were left out. In terms of time frame, this review focuses mainly on models that have been published through the end of 2003.

In discussing the various models, this review starts with a historical background where the models are presented and their advantages and disadvantages are briefly discussed. However, direct comparisons of the different models to each other are hard to make because they vary in their approach and complexity, and one model may do a good job in one region (e.g., the membrane) but not in another (e.g., the electrode). Furthermore, almost all of them agree with some sort of experimental data. Therefore, the majority of this review delves into how the various regions and effects are modeled independently of each other. It is our feeling that the reader will get more by

* Corresponding author. E-mail: aweber@uclink.berkeley.edu. Telephone: 510-643-1972. Fax: 510-642-4778.

Figure 1. Fuel-cell schematic showing the different model dimensionalities. 0-D models are simple equations and are not shown, the 1-D models comprise the sandwich (z direction), the 2-D models comprise the 1-D sandwich and either of the two other coordinate directions (x or y), and the 3-D models comprise all three coordinate directions.

Adam Weber was born in 1976 in Fort Lauderdale, FL. He studied chemical engineering at Tufts University, where he earned B.S. and M.S. degrees in 1999. His thesis topic was on low-temperature carbon-monoxide oxidation using gold supported on ceria catalysts under the guidance of Maria Flytzani-Stephanopoulos. His work was supported by the EPA through a STAR graduate fellowship and through the Astronaut Scholarship Foundation. After spending a year on a Fulbright scholarship in Australia, he entered the Ph.D. program at University of California—Berkeley in chemical engineering under the guidance of John Newman. He once again earned an EPA STAR graduate fellowship for his dissertation work on the mathematical modeling of transport inside polymer-electrolyte fuel cells.

John Newman received his B.S. in chemical engineering from Northwestern in 1960 and his M.S. and Ph.D. from University of California—Berkeley in 1962 and 1963, respectively. Then he joined the faculty at U. C. Berkeley, where he has remained for the past 41 years. He also holds an appointment as a faculty senior scientist at Lawrence Berkley National Laboratory. Recently, he spent a semester in 2002 as the Onsager Professor at the Norwegian University of Science and Technology in Trondheim, Norway. His interests lie in understanding the fundamental processes in electrochemical engineering and other coupled phenomena. He is a member of the National Academy of Engineering and a Fellow of The Electrochemical Society as well as being a highly cited author of over 300 publications in the field of electrochemistry.

examining the modeling equations and approaches per region than through just an encyclopedic list and discussion of the various models. In this context, if the reader is just interested in a single region or effect, all of the relevant models, approaches, phenomena, and equations can easily be found. Finally, although the majority of the models discussed are for hydrogen polymer-electrolyte fuel cells, the underlying phenomena and many of the regions are applicable to other types of polymer-electrolyte fuel cells, such as direct-methanol fuel cells.

In this review, the discussion and models are classified by their geometric dimensionality. The zero-dimensional (0-D) models are mainly empirical

and model the fuel cell with a simple equation. The 1-D models treat the fuel-cell sandwich in varying degrees of complexity. These are the majority of the models, and they model the different regions of the fuel-cell sandwich with everything from simple equations to complex expressions derived from physical models. Furthermore, they can incorporate other (nongeometric) dimensional effects in terms of size, that is, microscopic and macroscopic effects (e.g., consumption of reactant in a pore of a particle which is within a porous electrode). The 1-D models are the major focus of this review. What we term the 2-D models deal with effects in the fuel cell that occur in the sandwich as well as in another direction, either across or along the gas channel. Finally, the 3-D models include the 1-D sandwich and consider effects in both directions in the flow field. Figure 1 shows a schematic of a fuel cell, showing the different (nonzero) modeling dimensions as defined in this article.

The outline of this review is as follows. First, the general overview of the models is presented in both a historical and research-group context. Next, the general modeling methodologies and overall phenomena are looked at, including the 0-D models. In the following section, the 1-D fuel-cell sandwich is discussed in detail by layer (catalyst layers, diffusion media, membrane, and multilayer). This section is the longest of the review because the sandwich has the most complex phenomena and is the heart of the fuel cell; it also is the most often modeled. Following this discussion, the multidimensional effects and models are considered. Next, nonisothermal and transient effects and models are examined. Finally, some related fuel-cell models are noted, and this is followed by a summary.

2. Overview of Models

The number of published fuel-cell-related models has increased dramatically in the past few years, as seen in Figure 2. Not only are there more models being published, but they are also increasing in complexity and scope. With the emergence of faster computers, the details of the models are no longer constrained to a lot of simplifying assumptions and analytic expressions. Full, 3-D fuel-cell models and the treatment of such complex phenomena as two-
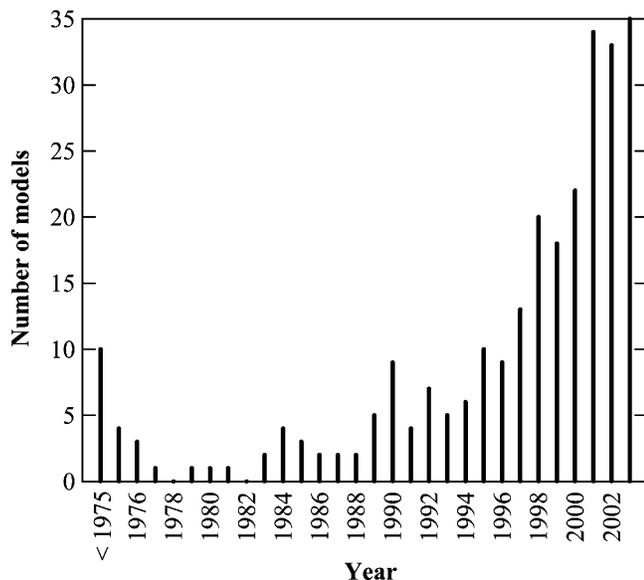
Figure 2. Bar graph showing the number of polymer-electrolyte related fuel-cell models published per year.

phase flow are becoming more common. In this section, an overview of the various fuel-cell models is presented with brief comments about their strengths and weaknesses. First, a short chronology of the major features and trends is outlined. This is followed by a description of the various models by research group. In both of these overviews, only select models are presented with a focus on macroscopic models that have a complete description of at least two layers of the 1-D fuel-cell sandwich. Other models, in addition to the ones below, are discussed in the appropriate sections of this review.

2.1. Historical

The beginning of modeling of polymer-electrolyte fuel cells can actually be traced back to phosphoric-acid fuel cells. These systems are very similar in terms of their porous-electrode nature, with only the electrolyte being different, namely, a liquid. Giner and Hunter[1] and Cutlip and co-workers[2-5] proposed the first such models. These models account for diffusion and reaction in the gas-diffusion electrodes. These processes were also examined later with porous-electrode theory.[6,7] While the phosphoric-acid fuel-cell models became more refined, polymer-electrolyte-membrane fuel cells began getting much more attention, especially experimentally.

Out of these experiments, simple 0-D models were used to analyze the data (for examples, see refs 8–12). These models normally fit the experimental data with a single equation, and although they demonstrate good fits and are quick and easy to implement, they are less reliable in predicting and explaining behavior. As the experiments and viability of polymer-electrolyte fuel cells became more widespread, models were designed to simulate their performance and gain understanding of the underlying fundamental transport processes. From these early models, the two main fundamental ones were those of Bernardi and Verbrugge[13] and Springer et al.[14] Both of them treat the fuel-cell sandwich,

composed of membrane, diffusion media, and catalyst layers, and are isothermal and 1-D. The Bernardi and Verbrugge model assumes a fully hydrated membrane and incorporates porous-electrode equations and Stefan−Maxwell diffusion in the diffusion media and catalyst layers. The model of Springer et al. does not use porous-electrode equations but does consider a changing water content in the membrane. This allows for variable properties in the membrane such as conductivity and the water diffusion coefficient. Most models today can trace their roots back to these models, and some are direct descendants, as discussed in the next section.

The next two major models were those by Fuller and Newman[15] and Nguyen and White,[16] who both examined flow effects along the channel. These models allowed for a more detailed description of water management and the effect of dry gas feeds and temperature gradients. Throughout the next few years, several more 0-D models and 1-D models were generated.[12,17−23] Also, some simulations examined more detailed 2-D effects, such as rib spacing.[24,25]

As interest grew in fuel cells in the late 1990s, more and more models were generated. Many of these models tried to understand and describe the cathode.[26−37] The interest was to optimize the catalyst layer and increase its efficiency, thereby reducing the precious-metal loading and increasing performance. Out of these models, those of Durand and co-workers[30−34] advocated strongly for the use of agglomerate models, where the microstructure of the cathode is considered explicitly. Another important model was that of Perry et al.,[36] which examined limiting behavior in the cathode and its possible diagnosis. Around this time as well, interest grew in membrane modeling,[38−43] as well as incorporating transient, nonisothermal, and multidimensional effects in complete fuel-cell models.[44−50]

In 2000 and 2001, fuel-cell models were produced by the dozens. These models were typically more complex and focused on such effects as two-phase flow[50−56] where liquid-water transport was incorporated. The work of Wang and co-workers[57−59] was at the forefront of those models treating two-phase flow comprehensively. The liquid-water flow was shown to be important in describing the overall transport in fuel cells. Other models in this time frame focused on multidimensional, transient, and more microscopic effects.[60−73] The microscopic effects again focused on using an agglomerate approach in the fuel cell as well as how to model the membrane appropriately.

In the last couple of years, the same trend toward more complex and complete models has continued, aided by the increases in computer processing speed. One way to address issues in more detail is through incorporating and examining complex effects such as flow-field design and two-phase flow.[74−88] The other way is to step back and examine a specific region of the fuel cell, such as the membrane or catalyst layer, and model that rigorously.[89−100] Whichever the case, the models today tend to be more complex, with detailed consideration of the important aspects of fuel cells, such as water management.

2.2. Detailed by Affiliation

Although the number of models is large, the number of modeling groups and approaches is significantly fewer. The obvious reason is that as a group becomes more familiar with a model, they continually upgrade it in terms of complexity to make it more physically realistic. For an approach, if it is general, then the community adopts and alters it. For this reason, it makes sense to give an overview of the models by these criteria. In this section, the models are discussed in terms of the research groups, where the progress of each group is highlighted and easily ascertained. These groups are loosely categorized by modeling approach. To save space, a research group is located only under the most appropriate heading, even if all of their models do not conform to that heading. Once again, the models discussed here are primarily those that model at least two layers of the 1-D sandwich of a single polymer-electrolyte fuel cell. Other models such as membrane, stack, impedance, electrode, empirical 0-D, and direct-methanol fuel-cell models and specific treatments of each layer can be found in later sections of this review and are not discussed below.

2.2.1. Springer et al. Model and Derivatives

As mentioned above, one of the first 1-D fuel-cell models was by Springer et al.[14] at Los Alamos National Laboratory (LANL). The model is isothermal and considers polarization and electrode effects only through a simple 0-D type of polarization equation. However, the membrane does have variable water content, although liquid water was not considered explicitly. The modeling results showed the importance of keeping the membrane well hydrated, and discussed the importance of water management. Springer et al.[101] took the original model and added a detailed cathode model to it. They examined utilization of the catalyst and the effects of performance on various parameters such as the diffusion-medium porosity and the inlet-gas composition. The cathode is treated as a uniformly distributed layer, and the model does not treat flooding. Springer et al.[102,103] also added impedance to their original model to explore other effects and compare to another set of data. They were one of the first to do this. Finally, recently, they have come up with a sophisticated anode model to go along with the overall model that includes the effects of carbon monoxide poisoning.[104]

Several groups were influenced by the work of the group at LANL. Models by these groups treat the membrane and fuel cell in a similar fashion, while adding various complexities. While not necessarily truly a derivative of Springer, the model of Wang and Savinell[17] has a very similar approach, except that they incorporate an agglomerate model of the catalyst layer. They examine the effects of feed concentration and humidity, although they do not consider changes down the gas channel. They also examine carbon monoxide poisoning and discuss the structure of the anode.

Similar to the above model, that of Ridge et al.[105] examines the microstructure of the cathode catalyst layer in more detail. Their analysis is thorough and shows the effect of such factors as Teflon loading and proton conductivity. Their implementation of an agglomerate model is perhaps the first application of this to polymer-electrolyte fuel-cell catalyst layers. Similar to this model, that of Rho and Srinivasan[19] looks at effects in the cathode in terms of operating conditions using a detailed agglomerate model. Their model was also relatively early and does a good job in describing observations in terms of interactions at the agglomerate scale. Finally, Weisbrod et al.[106] incorporated a porous-electrode model into the Springer et al. model to examine both kinetic and mass-transfer losses in more detail.

Perhaps the most renowned researcher to follow the Springer modeling concept is Trung Van Nguyen. His first model examined 2-D effects along the gas channel.[16] It is a pseudo-2-D model and has a very similar basis to that of the Springer et al. model. Although its membrane model assumes only a linear gradient in water concentration, it accounts for liquid-water flow and is nonisothermal. The model clearly showed that water and heat management are interrelated and very important for optimal fuel-cell operation. The model also examined the effects of having a nonuniform current-density distribution down the flow channel. Finally, although liquid water was considered in terms of energy, it had a negligible volume, and the electrodes were treated as interfaces.

Nguyen's group at the University of Kansas continued to upgrade this model. They also examined other effects in the fuel cell. Yi and Nguyen[107] took essentially the same model as that of Nguyen and White[16] above and added coolant-plate and heat-exchange equations. They also examined further the effects of differential pressures and humidification conditions of the anode. The research group reduced some of the limitations of the model and made it two-phase and a true two-dimensional model, where the flow-field structure of ribs and channels was examined.[48,52,108] The models that first did this were for interdigitated flow fields and, along with the model of Kazim et al.,[46] were some of the very first models to address this type of flow field.[48,52] Nguyen and co-workers were also some of the first researchers to examine two-phase flow, and they clearly showed how important saturation effects are at the cathode. The two-phase flow models use empirical expressions for the saturation functions taken from matching experimental data. However, these models assume a net water flux through the membrane and infinitely thin catalyst layers, which somewhat limits their applicability. The recent models of Natarajan and Nguyen[56,87] examined transient and 3-D effects, as well as limitations due to flooding in the catalyst-layer interfacial regions. Overall, the work of this group has pioneered examining two-phase flow effects.

Other Springer model derivatives include those of Ge and Yi,[109] van Bussel et al.,[44] Wohr and co-workers,[26,45] and Hertwig et al.[99] Here, the models described above are slightly modified. The model of Hertwig et al. includes both diffusive and convective transport in the membrane. It also uses a simplified two-phase flow model and shows 3-D distributions

of various properties in the fuel cell. The model of van Bussel et al. mainly focused on 2-D and dynamic water transport in the membrane by diffusion and electroosmotic flow. They showed agreement with polarization curves and explained the experimental results for counterflow and coflow operation and stability with dry gases based on the water-content distribution of the membrane. This is one of the first transient models. Another early transient model is that of Wohr et al.[45] Similar to the model of van Bussel et al., the membrane is accounted for by diffusion, but Wohr et al. also include liquid saturation and nonisothermal effects. The model does a good job in showing temperature spikes in single cells as well as in stacks. The catalyst-layer and diffusion-media models for this model were based on the earlier work by Bevers et al.[26] Here, the cathode side of a membrane was simulated including liquid-water and energy effects. The simulation results demonstrate good agreement with experimental data and allow for an increased understanding and calculation of meaningful physical parameters. Finally, the model of Ge and Yi is 2-D and uses the same kind of membrane model as van Bussel et al. They examine the effect of differential pressures, flow arrangement, and temperature.

2.2.2. Bernardi and Verbrugge Model and Derivatives

Around the same time as the model of Springer et al., Bernardi and Verbrugge[13] published their fuel-cell model. This model was based on their gas-diffusion electrode model[110] and that of Verbrugge and Hill.[111] Prior to their fuel-cell model, Bernardi[112] published a relatively simple study of the water balance in a fuel cell, highlighting the importance of water management and the sensitivity of the water balance to changes in operating conditions such as humidity, temperature, and pressure. The Bernardi article was a seminal paper and the first to stress water management. The fuel-cell model of Bernardi and Verbrugge includes transport of both gas and liquid in the diffusion media, detailed porous-electrode models for both electrodes, and a membrane model based on Schlogl's equation (see eq 34) with gas crossover. The model is 1-D and isothermal, and the main limitation of the model is that the membrane is assumed to be fully hydrated. This limits the applicability of the model to humidified feeds and/or thin membranes. Another limitation of the model is the neglect of true two-phase flow; the model only uses constant volume fractions for the various phases. Notwithstanding these limitations, the model allows for a detailed examination of liquid water pressure profiles and how many different operating and structural parameters affect overall fuel-cell performance.

Not surprisingly, the Bernardi and Verbrugge model forms the basis for many other models that came after it, most notably the computational-fluid-dynamics (CFD) models, as discussed in the next section. In terms of direct descendants of this model, the model of Chan et al.[113] takes the Bernardi and Verbrugge model and incorporates carbon monoxide effects at the anode as per the Springer et al.[104] description. The models of Li and co-workers[50,71,114−116]

start with the Bernardi and Verbrugge framework and include additional effects. The model of Marr and Li[114] uses an agglomerate catalyst-layer model in order to ascertain more easily the effects of changing various layer properties such as porosity and membrane loading. Baschuk and Li[50] took the Marr and Li model further by incorporating mass-transfer limitations in the cathode due to water flooding. They did this using an additional liquid-film resistance as an unknown parameter and were able to predict different levels of flooding as a function of cell polarization. The model of Rowe and Li[71] built on the other models and includes nonisothermal operation, which allows for a better study of water management in the 1-D fuel-cell sandwich. Finally, some of the models of Li and co-workers focus on carbon monoxide poisoning of the anode electrocatalysts.[115,116]

The last main group of models that directly follow the Bernardi and Verbrugge model are those from Italy by Murgia et al.[95,117] and Pisani et al.[78,91,118] In the first of these models, the original Bernardi and Verbrugge model is simplified to help its convergence.[95] This was done by integrating over the catalyst layers and using that result in the 1-D simulation. They argued that numerical accuracy was not compromised and computational cost and numerical instability were greatly reduced. The next of the models added two-phase flow effects and an agglomerate model for the catalyst layer, which addressed the need for a changing water content. A recent model from this group[91] examines analytic expressions for the catalyst layer. It does a good job in examining effects on the agglomerate scale and looks at how the shape and distribution of electro-catalyst agglomerates affect polarization behavior. They also use their models to understand direct-methanol fuel-cell electrodes.

2.2.3. Computational-Fluid-Dynamics Models

With the increased computational power of today's computers, more detailed simulations are possible. Thus, complex equations such as the Navier−Stokes equation can be solved in multiple dimensions, yielding accurate descriptions of such phenomena as heat and mass transfer and fluid and two-phase flow throughout the fuel cell. The type of models that do this analysis are based on a finite-element framework and are termed CFD models. CFD models are widely available through commercial packages, some of which include an electrochemistry module. As mentioned above, almost all of the CFD models are based on the Bernardi and Verbrugge model. That is to say that the incorporated electrochemical effects stem from their equations, such as their kinetic source terms in the catalyst layers and the use of Schlogl's equation for water transport in the membrane.

The first major CFD models were those by Liu and co-workers[25,119] at the University of Miami. They are nonisothermal and the first multidimensional models. They allowed for a more in-depth study of the effects along the channels than the models described above. While the original model by Gurau et al.[25] did not include liquid-water transport, it did have a variable water content in the membrane. To study

flooding effects, Gurau et al.[120] modeled the cathode region of the fuel cell by a simple approach where the cathode diffusion medium is broken down into regions of different gas-phase volume fractions. They developed analytic expressions and showed how flooding can limit fuel-cell performance. Later models by Liu and co-workers[79,121] incorporated the multiphase mixture model of Wang and co-workers[57-59] to study the effect of liquid water in their CFD simulations.

As mentioned, almost all of the CFD models use the Bernardi and Verbrugge approach of Schlogl's equation. The exceptions to these are the models from the University of South Carolina.[51,54,60,73,82] These models use an approach similar to that of Springer et al. in that water transport in the membrane is due to diffusion and the diffusion coefficient is a function of water content; they assume a linear concentration profile of water in the membrane. Out of these models, Shimpalee and Dutta[60] generated one of the first with CFD. It examined primarily the 3-D temperature profile. Later models by Dutta et al.[51,54] also examined mass-transfer and complete 3-D effects. While these examined the fuel cell in more depth, liquid water was not really treated in these models. It was assumed to be part of the gas phase in thin film or droplet form and for the most part ignored. A recent model by Lee et al.[82] demonstrated good agreement with experiment and allowed for an understanding of the nonuniform current-density and membrane-conductivity distributions.

The next step forward in CFD models came from the work of Wang and co-workers.[57,64,76,122-124] Their first model[64] was similar to Garua et al.[25] except that it was transient. Their next model incorporated liquid effects rigorously using the multiphase mixture model of Wang and Cheng.[58,59] Their approach is similar to the South Carolina one above, but by considering mixture parameters and the appropriate saturation equations, the liquid-phase flow was calculated. The modeling domain for this model was basically the cathode side of the fuel cell, where a net water flux through the membrane was assumed. Very recent models examine the effects of solid-phase properties such as electronic conductivity[124] and wettability,[123] as well as interdigitated flow fields.[76]

Around the same time as the other models were the models of Djilali and co-workers.[47,80,125] The first of these[47] was 2-D, and while it accounted for liquid-water flow, saturation effects were neglected, since they assumed two independent networks for liquid and gas. Their next model used the same approach but was 3-D.[125] Their most recent model accounted for saturation effects and coupled the liquid and vapor flows.[80] It was able to show temperature, concentration, and water distributions in the 3-D flow field.

Recently, other CFD models have been published. The model of Siegel et al.[90] used an agglomerate approach instead of the porous-electrode approach of the other CFD models. They showed that the agglomerate approach enables good comparisons to experimental data and showed the effects of agglomerate radius and membrane loading on perfor-

mance. However, they did not include liquid flow in their model. The two models by Mazumder and Cole[84,85] considered simulations with and without liquid-water flow. They showed better agreement when liquid-water flow and flooding were considered, and this was done with the multiphase mixture model. Furthermore, both models were 3-D and utilized complete porous-electrode descriptions of the catalyst layers with simple membrane models. The final CFD models are those of Costamagna[65] and Bradean et al.[126] Both of these models considered the same types of effects as the other CFD ones. The model of Costamagna is notable in that it considered both convective and diffusive flow in the membrane.

2.2.4. Other Macrohomogeneous Models

There are some modeling methodologies and research groups that do not fit exclusively into the above categories but should be mentioned. The foremost among these are the models by Newman and co-workers. Their models focus on fundamental phenomena and are usually simple in their dimensionality. In terms of fuel cells, Newman[127] used a simple pseudo-2-D model to look at optimization of hydrogen utilization in a phosphoric-acid fuel cell. Polymer-electrolyte fuel-cell modeling started with the models of Fuller[128] and Fuller and Newman.[15] In these models, concentrated solution theory was used to describe diffusive transport in the membrane, which was a slight improvement to the Springer et al. framework. The Fuller and Newman model was one of the first to examine water and thermal management simultaneously and along the gas channel, although it did not contain a description of liquid-water flow. West and Fuller[24] took a similar model and used it to model the 2-D effects of ribs and channels. Dannenberg et al.[129] basically used the same model as Fuller and Newman, but they incorporated agglomerate effects in the catalyst layer and a different water uptake isotherm in order to examine the effect of changing operating conditions. Finally, the models by Meyers and Newman[130-132] also improved upon the Springer et al. framework by using a thermodynamically rigorous treatment of transport in the membrane for the optimization of direct-methanol fuel cells.

The next set of Newman group models were aimed at demonstrating the applicability of models to diagnostic techniques. Perry et al.[36] examined the changes in the Tafel slope due to changes in the controlling phenomena in the cathode side of the fuel cell. This model was updated by Weber et al.,[133] who added explicit oxygen mass-transfer limitations in the diffusion media, and again later by Jaouen et al.,[98] who treated the catalyst layers as agglomerates.

Recently, Weber and Newman[89,93,94,134] introduced a framework for bridging the gap between the Bernardi and Verbrugge and the Springer et al. membrane approaches. The membrane model was used in a simple fuel-cell model, and it showed good agreement with experimentally measured water-balance data under a variety of conditions.[134] The fuel-cell model was similar to the model of Janssen,[55] who used chemical potential as a driving force in the

membrane, but Weber and Newman also accounted for such effects as Schroeder's paradox. Other membrane-modeling approaches in fuel-cell models besides those mentioned above include those by Datta and co-workers,[63,72,92] who use a dusty-gas approach, and Hsing and co-workers,[41,61,62] who use Flory−Huggins theory. Finally, Weber et al.[74] and Weber and Newman[88] have recently developed models to account for saturation effects and flooding phenomena. Along with the model of Nam and Kaviany,[86] they are some of the first to account for composite and hydrophobic diffusion media.

Within the last five years, many fuel-cell models have come out of the Research Center in Julich, Germany. These models have different degrees of complexity and seek to identify the limiting factors in fuel-cell operation. The model of Kulikovsky et al.[37] examined a 2-D structure of rib and channel on the cathode side of the fuel cell, and is similar to that of Springer et al. Other models by Kulikovsky included examination of depletion along long feed channels[67,83] and effects in the catalyst layers.[69,96,135] The most recent model by Kulikovsky[81] relaxed the assumption of constant water content in the membrane and examined quasi 3-D profiles of it. Also at the research center, Eikerling et al.[28,40,70,136−138] developed many different models. Most of these were concerned with modeling the membrane[40,70,136,138] and cathode side of the fuel cell.[28,137] These models were complex and focused on statistically relating macroscopic phenomena to structural properties. In both systems, they developed fundamental equations for the transport processes and examined different limiting cases, leading toward optimization analysis.

3. General Aspects and Equations

The performance of a fuel cell is most often reported in the form of a polarization curve. Such a curve is shown in Figure 3. Roughly speaking, the polarization curve can be broken down into three main regions. At low currents, the behavior of a fuel cell is dominated by kinetic losses. These losses
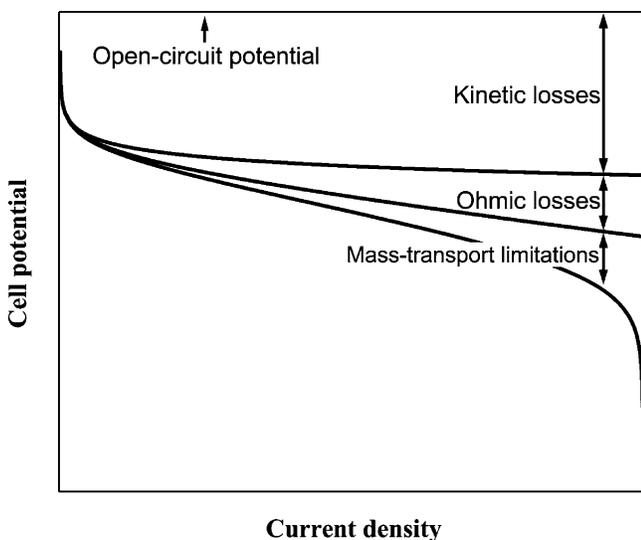
Figure 3. Example of a polarization curve showing the typical losses in a polymer-electrolyte fuel cell.

mainly stem from the high overpotential of the oxygen-reduction reaction (ORR), although the presence of carbon monoxide will produce a similar effect at the anode. As the current is increased, ohmic losses become a factor in lowering the overall cell potential. These ohmic losses are mainly from ionic losses in the electrodes and separator, although contact and electronic resistances can be important under certain operating conditions and cell configurations. At high currents, mass-transport limitations become increasingly important. These losses are due to reactants not being able to reach the electrocatalytic sites. Typically, oxygen is the problem due to flooding of the cathode by liquid water, but protons and electrons can also result in mass-transfer limitations. Before examining general polarization-curve models, some discussion should be made of the approach used for modeling and the equations used for the general regions of the polarization curve.

3.1. Modeling Methodologies

There are different global methodologies for modeling fuel cells and, in particular, the fuel-cell sandwich. The easiest division to make is between macroscopic and microscopic models. The microscopic models seek to model transport on an individual pore level, whereas the macroscopic ones are continuum and average over this level. Although the microscopic models may provide more realistic conditions and factors, they require a lot more knowledge of the microstructure and are much more expensive in terms of computation time. Macroscopic models are more common for fuel cells, although some microscopic details should be incorporated into them. An example of this is the agglomerate model for fuel-cell catalyst layers, as discussed below. This review focuses mainly on macroscopic models.

In a macrohomogeneous approach, the exact geometric details of the modeling domain are neglected. Instead, the domain is treated as a randomly arranged porous structure that can be described by a small number of variables such as porosity and surface area per unit volume. Furthermore, transport properties within the domain are averaged over the electrode volume. Thus, all variables are defined at all positions within the domain. Averaging is performed over a region that is small compared to the size of the electrode but large compared to the microstructure.

3.2. General Equations

3.2.1. Thermodynamics

As shown in Figure 3, the open-circuit potential represents the highest voltage obtainable for a single cell. This potential is derived from thermodynamics. The overall fuel-cell reaction can be broken down into the two global electrode reactions. If hydrogen is the primary fuel, it oxidizes at the anode according to the reaction

$$H_2 \rightleftarrows 2H^+ + 2e^- \qquad (1)$$
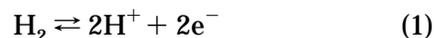
At the cathode, oxygen is reduced

$$4H^+ + 4e^- + O_2 \rightarrow 2H_2O \qquad (2)$$
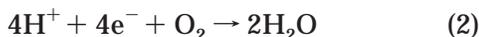
Although the above reactions are written in terms of the global species, no specific mention has been made about how the reaction proceeds. For example, each reaction can be broken down into single electron-transfer reactions, and the gas probably dissolves into the membrane that is covering the electrocatalyst sites (e.g., platinum on carbon). Some more comments about this can be found in section 4.4. Adding eqs 1 and 2 yields the overall reaction

$$2H_2 + O_2 \rightarrow 2H_2O \qquad (3)$$

A typical polymer–electrolyte fuel cell can be represented as

$$
\begin{array}{c|c|c|c|c}
\alpha & \beta & \gamma & \beta' & \alpha' \\
\text{Graphite} & \text{Pt}_{(s)} & \text{Membrane} & \text{Pt}_{(s)} & \text{Graphite} \\
 & H_{2(g)}, H_2O_{(g)} & H^+_{(m)}, H_2O_{(m)} & O_{2(g)}, H_2O_{(g)} &
\end{array} \qquad (4)
$$
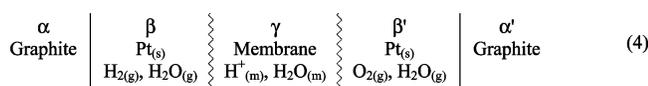
where each Greek letter identifies a distinct phase and the wavy lines imply that the membrane phase boundary is not sharp; rather, the membrane extends into adjacent regions and may include water activity gradients. The potential of this cell is[139]

$$FU = -F(\Phi^\alpha - \Phi^{\alpha'}) = \mu_{e^-}^\alpha - \mu_{e^-}^{\alpha'} \qquad (5)$$

where F is Faraday's constant, U is the thermodynamically defined reversible cell potential, Φ^α is the electrical potential of phase α, and $\mu_{e^-}^\alpha$ is the electrochemical potential of electrons in phase α. After introducing expressions for the activities of the various components,[139] this becomes

$$FU = FU^\theta + \frac{RT}{2}\ln a_{H_2}^\beta + \frac{RT}{4}\ln a_{O_2}^{\beta'} - \frac{RT}{2}\ln a_w^{\beta'} + (\mu_{H^+}^\beta - \mu_{H^+}^{\beta'}) \qquad (6)$$

where a_i^β is the activity of species i in phase β and the subscript w stands for water, R is the ideal-gas constant, T is the absolute temperature, and U^θ is the standard cell potential, a combination of appropriately chosen reference states that is a function of temperature and can be unit dependent. This equation reduces to a Nernst equation[139,140]

$$U = U^\theta + \frac{RT}{2F}\ln\left(\frac{p_{H_2}\sqrt{p_{O_2}}}{p_w}\right) \qquad (7)$$

when the gases are assumed to be ideal and gradients in the electrolyte are zero or neglected. Values and expressions for the parameters in the above equation, as well as further thermodynamic discussions, can be found in various books.[139–144]

3.2.2. Kinetics

The initial drop in the polarization curve is due to the sluggish kinetics of the ORR at the temperatures normally used for current polymer-electrolyte fuel-cell operation (<100 °C). A typical electrochemical

reaction can be expressed as

$$\sum_k \sum_i s_{i,k,h} M_i^{z_i} \rightarrow n_h e^- \qquad (8)$$
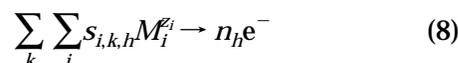
where $s_{i,k,h}$ is the stoichiometric coefficient of species i residing in phase k and participating in electron-transfer reaction h, n_h is the number of electrons transferred in reaction h, and $M_i^{z_i}$ represents the chemical formula of i having valence z_i.

The rate of an electrochemical reaction depends on the concentrations of the various species and the potential drop across the reaction interface between phases k and p, which are normally the electrode and electrolyte, respectively. In general, a Butler–Volmer expression can be used to describe the kinetics

$$i_{h,k-p} = i_{0_h}\left[\prod_i^a \frac{p_i}{p_i^{ref}}\exp\left(\frac{\alpha_a F}{RT}(\Phi_k - \Phi_p - U_h^{ref})\right) - \prod_i^c \frac{p_i}{p_i^{ref}}\exp\left(\frac{-\alpha_c F}{RT}(\Phi_k - \Phi_p - U_h^{ref})\right)\right] \qquad (9)$$

where $i_{h,k-p}$ is the transfer current between phases k and p due to electron-transfer reaction h, the products are over the anodic and cathodic reaction species, respectively, α_a and α_c are the anodic and cathodic transfer coefficients, respectively, p_i and p_i^{ref} are the partial pressure and reference partial pressure for species i, respectively, and i_{0_h} and U_h^{ref} are the exchange current density per unit catalyst area and the potential of reaction h evaluated at the reference conditions and the operating temperature, respectively. The reference potential can be determined using a Nernst equation (e.g., see eq 7); if the reference conditions are the same as the standard conditions (i.e., 100 kPa pressure for the different gas species), then U_h^{ref} has the same numerical value as U_h^θ.

The term in parentheses in eq 9 can be written in terms of an electrode overpotential

$$\eta_{h,k-p} = \Phi_k - \Phi_p - U_h^{ref} \qquad (10)$$

In this review, the reference electrode used is defined as a platinum metal electrode exposed to hydrogen at the same temperature and electrolyte (e.g., Nafion) as the solution of interest. With this reference electrode, the electrode overpotential defined in eq 10 is the same as having the reference electrode located next to the reaction site but exposed to the reference conditions (i.e., it carries its own extraneous phases with it). Typical values for the reference conditions are those in the gas channels. If the reference electrode is exposed to the conditions at the reaction site, then a surface overpotential can be defined

$$\eta_{s_{h,k-p}} = \Phi_k - \Phi_p - U_h \qquad (11)$$

where U_h is the reversible potential of reaction h (e.g., see eq 7). The surface overpotential is the overpotential that directly influences the reaction rate

across the interface. Comparing eqs 10 and 11, one can see that the electrode overpotential contains both a concentration and a surface overpotential for the reaction.

For the hydrogen-oxidation reaction (HOR) at the anode, eq 9 becomes, in the absence of poisons,

$$i_{\text{HOR},1-2} = i_{0_{\text{HOR}}}\left[\frac{p_{\text{H}_2}}{p_{\text{H}_2}^{\text{ref}}}\exp\left(\frac{\alpha_a F}{RT}(\eta_{\text{HOR},1-2})\right) - \exp\left(\frac{-\alpha_c F}{RT}(\eta_{\text{HOR},1-2})\right)\right] \quad (12)$$

where 1 and 2 denote the electron- and proton-conducting phases, respectively. Because the electrolyte is a polymer of defined acid concentration, the proton concentration does not enter directly into eq 12. Furthermore, due to the reference electrode used, the reference potential and reversible potential are both equal to zero. Equation 12 reduces to a Nernst relationship when the ratio i/i_0 becomes small, which is normally the case for the HOR.[13,17,145–149]

The oxygen-reduction reaction (ORR), on the other hand, is slow and represents the principal inefficiency in many fuel cells. Due to its sluggishness, the ORR is modeled reasonably well with Tafel kinetics with a first-order dependence on oxygen partial pressure[10,150,151]

$$i_{\text{ORR},1-2} = -i_{0_{\text{ORR}}}\left(\frac{p_{\text{O}_2}}{p_{\text{O}_2}^{\text{ref}}}\right)\exp\left(\frac{-\alpha_c F}{RT}(\eta_{\text{ORR},1-2})\right) \quad (13)$$

A linear fit on a Tafel plot of overpotential versus the log of the current density yields the commonly reported Tafel slope

$$b = 2.303\frac{RT}{\alpha_c F} \quad (14)$$

For the kinetic region, the values of the theoretical and experimental Tafel slopes have been shown to agree with α_c equal to 1.[9,10,150,152–157]

If eq 13 were to be written with respect to the surface overpotential, as defined by eq 11, instead of the electrode overpotential, then it would read

$$i_{\text{ORR},1-2} = -i_{0_{\text{ORR}}}\left(\frac{p_{\text{O}_2}}{p_{\text{O}_2}^{\text{ref}}}\right)^{3/4}\exp\left(\frac{-\alpha_c F}{RT}\eta_{s_{\text{ORR},1-2}}\right) \quad (15)$$

The power or the exponent with respect to oxygen is different because of the overpotential being used. As discussed by Newman,[139] the difference is due to how the exchange current density is defined and its dependence written, and both equations are consistent with a reaction order of 1. Mathematically, one can show that the exponent on oxygen changes from 1 to $^3/_4$ if α_c is equal to 1.[158] While eq 15 has perhaps a better defined overpotential and contains only a kinetic term and not also a thermodynamic term, eq 13 is often easier to use in simulations and in conceptualizing the dependence of the kinetics on gas concentration. Either equation is correct, and one must recognize which one is being used when analyz-

ing or comparing data and modeling results, as pointed out by Gasteiger et al.[158] Furthermore, the exchange current densities in the two equations are not necessarily equal because they are (perhaps different) functions of the reference pressures.

As noted, the equations above are a general starting point for describing the ORR, the HOR, and the kinetic regime. More detailed models, which examine such effects as the nature of the reaction interface, are discussed in later sections.

3.2.3. Ohmic Losses

The second part of the polarization curve is the ohmic regime. In this region, the potential varies linearly with the current density. This allows for Ohm's law to be used for modeling purposes

$$\Delta\Phi = iR' \quad (16)$$

where R' is the overall resistance in the fuel cell. For the ohmic region, this resistance is essentially constant; that is, it is not a strong function of the current density or potential. The resistance can either be measured experimentally by fitting polarization curves or be determined through modeling. It is a composite of the general electronic and ionic resistances through the fuel cell and is similar to a contact resistance. It does not include those resistances resulting from mass-transfer effects such as membrane dehydration, which are discussed below. In later sections, models that calculate R' are discussed in detail.

3.2.4. Mass-Transfer Limitations

The last part of the polarization curve is dominated by mass-transfer limitations (i.e., concentration overpotential). These limitations arise from conditions wherein the necessary reactants (products) cannot reach (leave) the electrocatalytic site. Thus, for fuel cells, these limitations arise either from diffusive resistances that do not allow hydrogen and oxygen to reach the sites or from conductive resistances that do not allow protons or electrons to reach or leave the sites. For general models, a limiting current density can be used to describe the mass-transport limitations. For this review, the limiting current density is defined as the current density at which a reactant concentration becomes zero at the diffusion medium/catalyst layer interface.

As mentioned, membrane dehydration can result in a problem where the membrane conductivity decreases to the point that it no longer conducts protons away from the reaction sites. Also, the distributed ohmic effects coupled with mass transfer in the porous electrode can result in a concentration overpotential that limits performance. In addition, if the diffusion media are composed mainly of insulating solids such as Teflon, electron conduction can become limiting. However, the most common cause for mass-transfer limitations is due to oxygen being inhibited from reaching the cathode reaction sites. This is normally due to flooding in either the catalyst layer or the diffusion medium because air and hydrogen are normally fed into a fuel cell, water is

produced at the cathode, and the diffusion coefficient of hydrogen is greater than that of oxygen.[142,149]

For typical fuel-cell designs, mass transport through the fuel-cell sandwich occurs mainly by diffusion. The simplest way to describe diffusion is by Fick's law[149]

$$\mathbf{N}_i = -\frac{D_i}{RT}\nabla p_i \qquad (17)$$

where $\mathbf{N}_i$ is the superficial flux density of species i and D_i is the diffusion coefficient of species i in the mixture. As discussed later, many models use more complex expressions and effective diffusion coefficients. These complexities allow the nature of the fuel-cell porous media to be accounted for, as well as counterdiffusion of water vapor and flooding of the porous media by liquid water.

An expression for the limiting current density due to oxygen transport can be derived by the following procedure. With Faraday's law for the oxygen flux in the ORR and rearrangement of Fick's law, the oxygen partial pressure at the catalyst layer, $p_{O_2}^{CL}$, can be related to the limiting current density, i_{lim}, and the oxygen partial pressure in the bulk, $p_{O_2}^{bulk}$,[127]

$$p_{O_2}^{CL} = p_{O_2}^{bulk}\left(1 - \frac{i}{i_{lim}}\right) \qquad (18)$$

Equation 18 can be used to write the ORR rate in eq 13 or 15 in terms of the limiting current density, an experimentally measurable quantity, rather than the oxygen partial pressure.

3.3. Zero-Dimensional Models

The simplest fuel-cell models describe the polarization behavior by a single equation; hence, they are 0-D. Even though these models are relatively simple and usually empirical, they are valuable for determining kinetic parameters as well as comparing the various losses in the system to one another. The 0-D modeling equations can be derived by combination of the above governing equations for each regime. The drawbacks of these models are that they do not yield true mechanistic behavior and fundamental understanding and that they are not good for predicting performance or optimization.

0-D models are very helpful in determining kinetic parameters and general ohmic resistance from data.[9,10,21,23,152,159−161] A typical expression for this type of analysis is

$$V = U + b\log(i_0) - b\log(i) - R'i \qquad (19)$$

where V is the cell potential and i is the superficial current density through the membrane. The first and second terms may be combined to form a potential intercept, U'; this quantity is a convenient way to group terms pertaining to (possibly unknown) thermodynamic and kinetic constants.

Upon comparison to data, the models demonstrate the aforementioned value of α_c being equal to 1. Not only are exchange current densities measured, but the effect of temperature can be studied in more detail, as well as the type and thickness of mem-

brane. For example, the model of Amphlett et al.[21] accounts for all of the temperature dependences through empirical fitting parameters. 0-D models also allow for deviations from the theoretical expression presented above to be investigated. For example, fitting eq 19 to some experimental data yields a double Tafel slope at higher current densities. This change in the Tafel slope is caused by transport limitations, something not explicitly taken into account in the above equation. In other words, the equation cannot fit the whole polarization curve with just one set of parameter values.

To make the model less empirical, gas-phase mass-transport limitations can be incorporated into the modeling equation explicitly[12]

$$V = U - b\log(i) - R'i - m\exp(ni) \qquad (20)$$

where m and n are fitting parameters. Although the above expression yields good fits with the data, it is more empirical than if the limiting current density is used[97,139,161]

$$V = U - b\log(i) - R'i + b\log\left(1 - \frac{i}{i_{lim}}\right) \qquad (21)$$

Other modifications to include mass-transport limitations deal with changing the last term to be a more complicated function of current with more fitting parameters.[118,162,163]

The final 0-D equation presented here stems from incorporating the gas-pressure dependences directly instead of through a limiting current density, which normally only considers oxygen effects. This equation was proposed by Newman[127] for phosphoric-acid fuel cells and predates the above polymer−electrolyte fuel-cell expressions. It has the form

$$V = U^\theta + \frac{RT}{F}\ln(a_{1,2}i_0L) - \frac{RT}{F}\ln\left(\frac{i}{p_{O_2}}\right) + \frac{RT}{2F}\ln(p_{H_2}) - R'i \qquad (22)$$

where $a_{1,2}$ is the interfacial area of the catalyst per unit volume of electrode and L is the thickness of the cathode catalyst layer. Thus, the quantity $a_{1,2}L$ is a roughness factor, a ratio of catalyst area to superficial electrode area. Out of all the approaches to include mass transport, eqs 21 and 22 are the most phenomenological, but with the fewest fitting parameters, they do not fit the data the best.

To examine how well the models agree with the data, Figure 4 shows model fits using eq 20. As can be seen, the model fits the data very well even with different operating conditions of oxygen mole fraction and gas pressure. Of course, the model parameters are adjusted for the conditions. As mentioned, such polarization-equation fits are useful for getting parameter values and perhaps some gross understanding, but they cannot really be used for optimization, prediction, or in-depth examination of the underlying phenomena. In essence, they are curve fits. It is difficult for them to treat interacting phenomena in
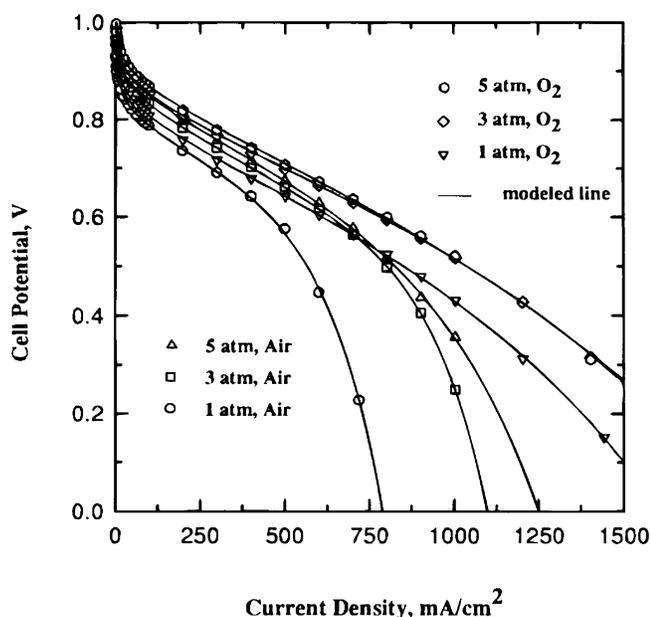
Figure 4. Model and experiment comparison of polarization curves for air or oxygen at different gas pressures and at 70 °C using eq 20. (Reproduced with permission from ref 12. Copyright 1995 The Electrochemical Society, Inc.)

Figure 5. 3-D schematic showing the various layers of the fuel-cell sandwich.

a clear way, such as drying of a membrane with current density or temperature or flooding with liquid water.

More complicated expressions than those above can be used in the 0-D models, but these usually stem from a more complicated analysis. For example, the equation used by Ticianelli and co-workers[29,156] comes from analysis of the catalyst layer as a flooded agglomerate. In the same fashion, eq 21 can be embedded and used to describe the polarization behavior within a much more complicated model. For example, the models of Springer et al.[14] and Weber and Newman[74] use a similar expression to eq 21, but they use a complicated 1-D model to determine the parameters such as i_{lim} and R'. Another example is the model of Newman,[127] who uses eq 22 and takes into account reactant-gas depletion down the gas channels by, in essence, having a limiting current density that depends on the hydrogen utilization. All of these types of models, which use a single equation to describe the polarization behavior within a more complicated model, are discussed in the context of the more complicated model.

4. Fuel-Cell Sandwich Modeling

The fuel-cell sandwich describes the 1-D cross section of the fuel cell (see Figure 1) and is shown in Figure 5. For the single dimension, flow is taken to be normal to the various layers. Flow in the other directions is discussed in section 5. The fuel-cell sandwich contains the gas channels or flow fields, diffusion media, catalyst layers, and membrane. Additional layers are sometimes incorporated into the sandwich, such as separating the diffusion media into microporous and gas-diffusion layers. Fuel cells operate in the following manner.

The fuel is fed into the anode flow field, moves through the diffusion medium, and reacts electro-

chemically at the anode catalyst layer to form hydrogen ions and electrons. The diffusion medium is typically a carbon cloth or carbon paper, possibly treated with Teflon. The catalyst layer usually contains platinum or a platinum alloy supported on carbon and an ionomeric membrane material such as Nafion. The oxidant, usually oxygen in air, is fed into the cathode flow field, moves through the diffusion medium, and is electrochemically reduced at the cathode by combination with the generated protons and electrons. The water, either liquid or vapor, produced by the reduction of oxygen at the cathode exits the fuel cell through either the cathode or anode flow field. The electrons generated at the anode pass through an external circuit and may be used to perform work before they are consumed at the cathode.
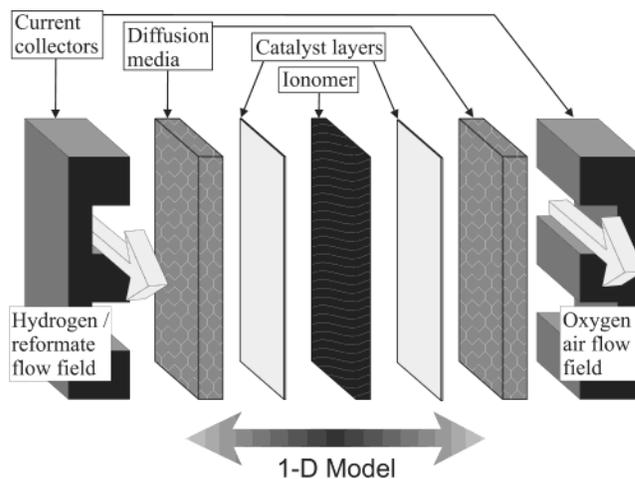
Mass and energy transport occur throughout all of the various sandwich layers. These processes, along with electrochemical kinetics, are key in describing how fuel cells function. In this section, thermal transport is not considered, and all of the models discussed are isothermal and at steady state. Some other assumptions include local equilibrium, well-mixed gas channels, and ideal-gas behavior. The section is outlined as follows. First, the general fundamental equations are presented. This is followed by an examination of the various models for the fuel-cell sandwich in terms of the layers shown in Figure 5. Finally, the interplay between the various layers and the results of sandwich models are discussed.

4.1. Conservation Equations

The number of equations and unknowns must balance. Thus, one can calculate the appropriate number of needed relationships from the degrees of freedom of a system, as shown for various systems by Newman.[164] In terms of the relations, the equations can be broken down into five main types. The first are the conservation equations, the second are the transport relations, the third are the reactions, the fourth are equilibrium relationships, and the fifth are the auxiliary or supporting relations, which include variable definitions and such relations as Faraday's law.

As noted in the Introduction, one of the defining characteristics of any fuel-cell model is how it treats transport. Thus, these equations vary depending on the model and are discussed in the appropriate subsections below. Similarly, the auxiliary equations and equilibrium relationships depend on the modeling approach and equations and are introduced and discussed where appropriate. The reactions for a fuel cell are well-known and were introduced in section 3.2.2. Of course, models modify the reaction expressions by including such effects as mass transfer and porous electrodes, as discussed later. Finally, unlike the other equations, the conservation equations are uniformly valid for all models. These equations are summarized below and not really discussed further.

It is necessary to write a material balance for each independent component in each phase. The differential form of the material balance for species i in phase k is[133]

$$\frac{\partial \epsilon_k c_{i,k}}{\partial t} = -\nabla \cdot \mathbf{N}_{i,k} - \sum_h a_{1,k} s_{i,k,h} \frac{i_{h,1-k}}{n_h F} + \sum_l s_{i,k,l} \sum_{p \neq k} a_{k,p} r_{l,k-p} + \sum_g s_{i,k,g} \epsilon_k R_{g,k} \quad (23)$$

The term on the left side of the equation is the accumulation term, which accounts for the change in the total amount of species i held in phase k within a differential control volume. This term is assumed to be zero for all of the sandwich models discussed in this section because they are at steady state. The first term on the right side of the equation keeps track of the material that enters or leaves the control volume by mass transport. The remaining three terms account for material that is gained or lost due to chemical reactions. The first summation includes all electron-transfer reactions that occur at the interface between phase k and the electronically conducting phase (denoted as phase 1). The second summation accounts for all other interfacial reactions that do not include electron transfer, and the final term accounts for homogeneous reactions in phase k.

In the above expression, $c_{i,k}$ is the concentration of species i in phase k, and $s_{i,k,l}$ is the stoichiometric coefficient of species i in phase k participating in heterogeneous reaction l (see eq 8). $a_{k,p}$ is the specific surface area (surface area per unit total volume) of the interface between phases k and p. $i_{h,k-1}$ is the normal interfacial current transferred per unit interfacial area across the interface between the electronically conducting phase and phase k due to electron-transfer reaction h, and it is positive in the anodic direction. In the above expression, Faraday's law

$$N_{i,k} = \sum_h s_{i,k,h} \frac{i_{h,1-k}}{n_h F} \quad (24)$$

was used to change the interfacial current density into an interfacial flux quantity. Furthermore, a current $i_{h,1-k}$, written with two subscripts, implies an interfacial, or transfer, current density. Conversely,

a current $\mathbf{i}_k$, written in boldface and with a single subscript, indicates the total current density carried within phase k

$$\mathbf{i}_k = F \sum_i z_i \mathbf{N}_{i,k} \quad (25)$$

where z_i is the valence or charge number of species i. Finally, $r_{l,k-p}$ is the rate of the heterogeneous reaction l per unit of interfacial area between phases k and p. $R_{g,k}$ is the rate of a strictly homogeneous reaction g in phase k per unit volume of phase k.

Because a large electrical force is required to separate charge over an appreciable distance, a volume element in the electrode will, to a good approximation, be electrically neutral. For fuel-cell models, electroneutrality is often assumed for each phase

$$\sum_i z_i c_{i,k} = 0 \quad (26)$$

The assumption of electroneutrality implies that the diffuse double layer, where there is significant charge separation, is small compared to the volume of the domain, which is normally the case. Because there is no accumulation of charge and electroneutrality has been assumed, the divergence of the total current density is zero

$$\sum_k \nabla \cdot \mathbf{i}_k = 0 \quad (27)$$

Equations 23 and 27 represent the mass and current conservation equations, respectively. These apply for all of the models discussed.

4.2. Membrane Modeling

One of the most important parts of the fuel cell is the electrolyte. For polymer-electrolyte fuel cells this electrolyte is a single-ion-conducting membrane. Specifically, it is a proton-conducting membrane. Although various membranes have been examined experimentally, most models focus on Nafion. Furthermore, it is usually necessary only to modify property values and not governing equations if one desires to model other membranes. The models presented and the discussion below focus on Nafion.

Nafion is a copolymer of poly(tetrafluoroethylene) and polysulfonyl fluoride vinyl ether. It has fixed anions, which are sulfonic acid sites, and consequently, by electroneutrality, the concentration of positive ions is fixed. Furthermore, the transference number of protons in this system is 1, which greatly simplifies the governing transport equations, as seen below. There can be different forms of Nafion in terms of the positive counterion (e.g., proton, sodium, etc.). Most models deal only with the proton or acid form of Nafion, which is the most common form used in polymer-electrolyte fuel cells due to its high proton conductivity.

Since the membrane is such a key element in the fuel cell, it has had a lot of attention in terms of modeling. There have been many microscopic and

physical models in addition to the macroscopic ones. The microscopic models focus solely on the membrane and examine single ions and pore-level effects. The macroscopic models are often more empirical and focus on describing the transport and relevant parameters of the membrane in a macrohomogeneous fashion. As per the overall approach of this review, discussion is mainly on the macroscopic models.

The macroscopic models can be sorted into two main categories, those that assume the membrane system is a single phase, and those that assume it is two phases. Each is discussed separately below. In either of these models, the membrane system is assumed to have three main components: membrane, protons, and water. For the three-species system, there should be $^1/_2 N(N - 1) = 3$ transport properties.[133] The above set of properties neglects any other kind of ions in the membrane, which is an assumption that almost all of the models make. Furthermore, the above property count does not consider hydrogen or oxygen crossover in the membrane. Such crossover results in only a small inefficiency and does not significantly influence proton or water transport. There are some models that take this into account, the most notable being by Bernardi and Verbrugge.[110] If desired, crossover can easily be added to any model.[94]

Before discussing the models and their approaches in more detail, some mention should be made on the microscopic models and the overall physical picture of Nafion. Since membrane-only models, especially the microscopic ones, are covered in another review,[165] the discussion below is shortened.

4.2.1. Microscopic and Physical Models

There have been many microscopic models based on statistical mechanics,[38,136,166−172] molecular dynamics,[173−180] and macroscopic phenomena applied to the microscopic structure of the membrane.[63,111,138,181−201] These models provide the fundamental understanding of processes such as diffusion and conduction in the membrane on a single-pore level. They allow for the evaluation of how small perturbations like heterogeneity of pores and electric fields affect transport, as well as the incorporation of small-scale effects. These models are also the only ones to look at different forms of Nafion as well as the effect of other ions in the membrane (e.g., those from a salt solution).[42,43,111,192−201] They also divide the membrane into more than just the three species of the macroscopic models; as examples, the membrane may be broken down into ionic and backbone moieties, and proton conduction may be by different proton−water complexes. Finally, almost all of the microscopic models treat the membrane as a two-phase system. While the microscopic models yield valuable information about what goes on inside the membrane, in general, they are too complex to use in an overall fuel-cell model.

Many of today's models are based on the early physical models of Hsu and Gierke[182] and Yeager and Steck.[184] These models, along with the relevant experimental data, were reviewed recently by Weber and Newman.[89,93] Out of their analysis came a
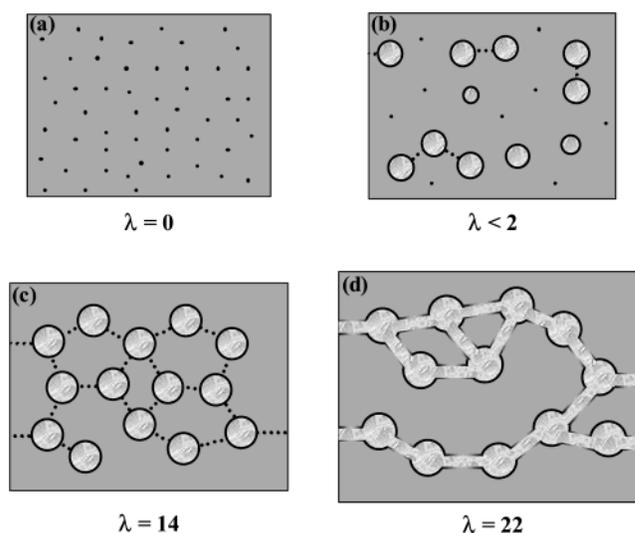
Figure 6. Evolution of the membrane structure as a function of water content, λ (moles of water per mole of sulfonic acid sites). The pictures are cross-sectional representations of the membrane where the gray area is the fluorocarbon matrix, the black is the polymer side chain, the light gray is the liquid water, and the dotted line is a collapsed channel. (Reproduced with permission from ref 89. Copyright 2003 The Electrochemical Society, Inc.)

physical model of transport in Nafion, which could be used as a foundation for a macrohomogeneous model. Figure 6 shows a schematic summary of the Weber and Newman model. The main focus of the model is how the membrane structure changes as a function of water content, where λ is the moles of water per mole of sulfonic acid sites and is measured by examining the weight gain of an equilibrated membrane.

In panel a, the dry membrane absorbs water in order to solvate the acid groups. This initial water is associated strongly with the sites. Additional water causes the water to become less bound, and inverted micelles form in the polymer matrix, panel b. With more water uptake, these clusters grow and form interconnections with each other. The connections, or collapsed channels, are transitory and have hydrophobicities comparable to that of the matrix. The cluster−channel network forms on the basis of a percolation-type phenomenon of the clusters; therefore, to form a transport pathway, the clusters must grow and be close enough together to be linked by the collapsed channels. From conductivity data, this percolation threshold is shown practically to occur around $\lambda = 2$.[94] Panel c corresponds to a membrane that is in contact with saturated water vapor, where a complete cluster−channel network has formed. When there is liquid water at the boundary of the membrane, structural reorganization occurs because the aqueous environment repels the fluorocarbon-rich skin of the ionomer. This inversion allows for the liquid water to infiltrate and expand the channels, causing them to stabilize and the various clusters to agglomerate along them; as a result, a porelike structure forms, panel d. In this structure, the channels are still hydrophobic on average. Because the channels are now filled with liquid, the uptake of the membrane has increased without a change in

the chemical potential of the water (i.e., Schroeder's paradox[202]).

In the physical model, there are two separate structures for the membrane depending on whether the water at the boundary is vapor or liquid; these are termed the vapor- or liquid-equilibrated membrane, respectively. The main difference between the two is that, in the vapor-equilibrated membrane, panel c, the channels are collapsed, while, in the liquid-equilibrated case, panel d, they are expanded and filled with water. These two structures form the basis for the two types of macroscopic models of the membrane.

4.2.2. Diffusive Models

The diffusive models treat the membrane system as a single phase. They correspond more-or-less to the vapor-equilibrated membrane (panel c of Figure 6). Because the collapsed channels fluctuate and there are no true pores, it is easiest to treat the system as a single, homogeneous phase in which water and protons dissolve and move by diffusion. Many membrane models, including some of the earliest ones, treat the system in such a manner.

Since the membrane is stationary, only the water and protons move in the membrane system. The simplest membrane models either neglect the water movement or treat it as a known constant. For the proton movement, the simplest treatment is to use Ohm's law (eq 16 in differential form)

$$\mathbf{i}_2 = -\kappa \nabla \Phi_2 \tag{28}$$

where κ is the ionic conductivity of the membrane. This can easily be integrated to yield a resistance for use in a polarization equation (see the 0-D models above). The above water and proton treatments are relatively trivial and are often used when the purpose of the model is to examine effects outside the membrane (e.g., cathode flooding)[26,48,52,56,57,69,80,85−87,101,105,120] or when only general trends are desired.[19,20,75,114,203,204] Below, more rigorous treatments are examined.

4.2.2.1. Dilute Solution Theory. Equation 28 is the result of using dilute solution theory.[139] Such an analysis yields the Nernst−Planck equation

$$\mathbf{N}_{i,2} = -z_i u_i F c_{i,2} \nabla \Phi_2 - D_i \nabla c_{i,2} + c_{i,2} \mathbf{v}_2 \tag{29}$$

The first term in the expression is a migration term, representing the motion of charged species that results from a potential gradient. The migration flux is related to the potential gradient ($-\nabla \Phi_2$) by a charge number, z_i, concentration, c_i, and mobility, u_i. The second term relates the diffusive flux to the concentration gradient. The final term is a convective term and represents the motion of the species as the bulk motion of the solvent carries it along. For the analysis of the one-phase systems, the solvent is the membrane, and thus, $\mathbf{v}_2 = 0$.

Dilute solution theory considers only the interactions between each dissolved species and the solvent. The motion of each charged species is described by its transport properties, namely, the mobility and the diffusion coefficient. These transport properties can

be related to one another at infinite dilution via the Nernst−Einstein equation[139,205,206]

$$D_i = RT u_i \tag{30}$$

So long as the solute species are sufficiently dilute that the interactions among them can be neglected, material balances can be written upon the basis of the above expression for the flux.

If water movement in the membrane is also to be considered, then one way to do this is to again use the Nernst−Planck equation. Because water has a zero valence, eq 29 reduces to Fick's law, eq 17. However, it is also well documented that, as the protons move across the membrane, they induce a flow of water in the same direction. Technically, this electroosmotic flow is a result of the proton−water interaction and is not a dilute solution effect, since the membrane is taken to be the solvent. As shown in the next section, the electroosmotic flux is proportional to the current density and can be added to the diffusive flux to get the overall flux of water

$$\mathbf{N}_{w,2} = \xi \frac{\mathbf{i}_2}{F} - D_w \nabla c_{w,2} \tag{31}$$

where ξ is the electroosmotic coefficient. The above equation, along with Ohm's law, has been used successfully for most of the models that treat the membrane as a single phase.[14,16,17,39,44,51,54,60,81,82,90,129,159,207] The deviations and complications in the models arise from what function to use for the transport properties, κ, ξ, and D_w, as well as the concentration of water in the membrane, $c_{w,2}$. To understand the differences in the models, a closer look at these functions is required, but first the models that use concentrated solution theory will be presented.

4.2.2.2. Concentrated Solution Theory. For an electrolyte with three species, it is as simple and more rigorous to use concentrated solution theory. Concentrated solution theory takes into account all binary interactions between all of the species. For membranes, this was initially done by Bennion[208] and Pintauro and Bennion.[209] They wrote out force balances for the three species, equating a thermodynamic driving force to a sum of frictional interactions for each species. As discussed by Fuller,[128] Pintauro and Bennion also showed how to relate the interaction parameters to the transport parameters mentioned above. The resulting equations for the three-species system are

$$\mathbf{i}_2 = -\frac{\kappa \xi}{F} \nabla \mu_{w,2} - \kappa \nabla \Phi_2 \quad \text{and} \tag{32}$$

$$\mathbf{N}_{w,2} = \xi \frac{\mathbf{i}_2}{F} - \alpha_w \nabla \mu_{w,2} \tag{33}$$

where μ_w represents the chemical potential of water and α_w is the transport coefficient of water. The equation for the membrane is ignored, since it is dependent on the other two equations by the Gibbs−Duhem equation. The above equations have also been arrived at using an irreversible thermodynamics approach.[210,211] Similar equations to those above were

used by Wohr et al.,[45] who put them in a Stefan–Maxwell framework.[149]

Upon comparison of eq 32 to 28, it is seen that the proton–water interaction is now taken into account. This interaction is usually not too significant, but it should be taken into account when there is a large gradient in the water (e.g., low humidity or high-current-density conditions). Upon comparison of eq 33 to 31, it is seen that the equations are basically identical where the concentration and diffusion coefficient of water have been substituted for the chemical potential and transport coefficient of water, respectively. Almost all of the models using the above equations make similar substitutions for these variables.[15,24,61,62,128]

The models by Janssen[55] and Weber and Newman[94] do not substitute for the chemical potential. Janssen took the transport coefficient as a fitting parameter. His model showed good agreement with water balance data under different conditions. Weber and Newman utilize the chemical-potential driving force directly and use a diffusion coefficient relative to that driving force for their vapor-equilibrated transport mode. Janssen states that using a chemical-potential driving force does not necessitate making the distinction between diffusive or convective flow in the membrane. However, as Meyers[212] points out, by assuming the membrane system is a single phase, it cannot support a pressure difference inside it. The only way that a single-phase membrane model can have a pressure difference across it is if the chemical potential or water concentration is being altered at the boundaries. This problem is why single-phase membrane models cannot adequately describe transport for fully hydrated membranes where the driving force is the liquid pressure. This point is discussed further in section 4.2.4.

4.2.2.3. Membrane Water Content. Whether the dilute solution or concentrated solution theory equations are used to model the membrane system, functional forms for the transport parameters and the concentration of water are needed. The properties are functions of temperature and the water content, λ.[94] In the models, empirical fits are used[14–17,24,44,51,54,60–62,82,128] or the properties are assumed constant.[39,81,90,159] A review of these properties and how each model implements them is beyond the scope of this paper. Weber and Newman[94] review many of the data and discuss the functional forms for the properties from a physical standpoint.

Different models determine λ in different ways. Nafion exhibits a water-uptake isotherm as shown in Figure 7. The dashed line in the figure shows the effects of Schroeder's paradox, where there is a discontinuous jump in the value of λ. Furthermore, the transport properties have different values and functional forms at that point. Most models used correlate λ with the water-vapor activity, a_w^G, since it is an easily calculated quantity. An exception to this is the model of Siegel et al.,[90] which assumes a simple mass-transfer relationship. There are also models that model the isotherm either by Flory–Huggins theory[41,61,62] or equilibrium between water and hydrated protons in the membrane and water vapor
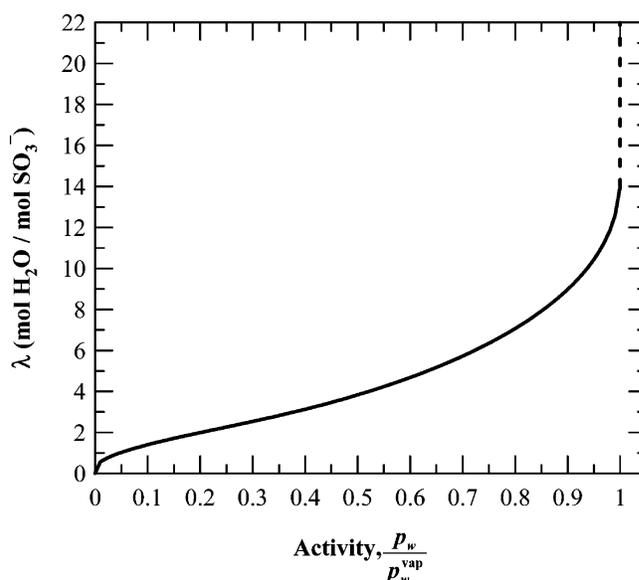
Figure 7. Equilibrium water-uptake or isotherm curve at 30 °C. The dashed line signifies the effect of Schroeder's paradox, a change in water uptake at the same chemical potential depending on the phase of water next to the membrane; liquid is at $\lambda = 22$.

next to it.[63,92,94,130] Finally, although it is known that the isotherm is a function of temperature, only a few models include this feature.[61–63,72,94,129] Most models just use an isotherm at a given temperature, usually 30 °C.

Schroeder's paradox is an observed phenomenon that needs to be considered in any model where the membrane is not either fully hydrated or dehydrated. There are various methods to account for Schroeder's paradox. The easiest way is to ignore it (i.e., either only vapor filled or fully hydrated), which a majority of the models do. Next, it can be treated as a discontinuity or by assuming a functional form of the water content such that λ and a_w^G continue to increase.[16,51,54,60,64,71,81,82,109,129] Hence, supersaturated conditions exist, which are only physically realistic if water is assumed to be a mist or suspended in the gas. More physical and rigorous models have also been generated.

Eikerling et al.[138] have a random network of pores that are filled with either bulklike water or bound water, and impregnation by liquid water is easier than condensation. They use effective medium theory to predict conductivity results from impedance data. Their model is more of a microscopic one in which λ is calculated by changing the number of pores that are filled and examining the types of liquid-film bonds between pores. Similarly, Weber and Newman[94] use capillary arguments where the liquid pressure expands the collapsed channels within the membrane. Thus, there is a continuous transition between the vapor- and liquid-equilibrated membranes that can occur within the membrane. The transition itself can be relatively sharp, which is not unexpected for a phase-change-type behavior. Finally, Choi and Datta[92] recently came up with an explanation of Schroeder's paradox that involves having evaporation at the liquid-filled pore mouth for a vapor-equilibrated membrane. The resulting me-

niscus causes a higher energy that the membrane must equilibrate with, thus lowering its water content. Out of the above three models, only that of Weber and Newman has been used in a fuel-cell sandwich model.

Those models that use an empirical expression for the isotherm often have different driving forces. One of the first models to use an isotherm was that by Springer et al.[14] In that model, λ was used as the driving force for water flow in the membrane, and an activity coefficient was used to account for the isotherm behavior. This same approach was used by van Bussel et al.[44] and Wang and Savinell.[17] The latter case examined the anode and assumed a flux of water through the membrane to help determine the membrane water concentration. Similar approaches to that of Springer et al. were used by Kulikovsky,[81] Fuller and Newman,[15] Dannenberg et al.,[129] and West and Fuller.[24] The models of Nguyen and White[16] and Shimpalee and co-workers[51,54,60,82] assume a linear change in water concentration in the membrane. Finally, Okada and co-workers[39,207] use analytic and perturbation expressions for how the concentration of water changes. They start with vapor-equilibrated membranes and treat them with either semi-infinite or finite boundary conditions.

4.2.3. Hydraulic Models

In opposition to the single-phase treatment of the membrane system mentioned above are the models that assume the membrane system is two phases. This type of model corresponds to the liquid-equilibrated membrane shown in panel d of Figure 6. In this structure, the membrane is treated as having pores that are filled with liquid water. Thus, the two phases are water and membrane.

The addition of a second phase means that there is also an additional degree of freedom. This results in the ability of the membrane system to sustain a pressure gradient in the water because of a possibly unknown stress relation between the membrane and fluid at every point in the membrane. However, diffusion of water becomes meaningless, since the water is assumed to be pure in the models discussed here. Furthermore, unlike the cases of the models discussed above, the water content of the membrane is assumed to remain constant ($\lambda = 22$) as long as the pores are filled and the membrane has been pretreated appropriately. For cases where the pores do not remain filled, see sections 4.2.4 and 4.2.5.

The first model to describe the membrane in the above fashion was that of Bernardi and Verbrugge,[13,110] which was based on earlier work by Verbrugge and Hill.[111,213,214] This model utilized a dilute solution approach that used the Nernst–Planck equation (eq 29) to describe the movement of protons, except that now **v** is not equal to zero. The reason is that, because there are two phases, the protons are in the water and the velocity of the water is give by Schlogl's equation[213,215]

$$\mathbf{v}_{w,2} = -\left(\frac{k}{\mu}\right)\nabla p_L - \left(\frac{k_\Phi}{\mu}\right)z_f c_f F \nabla \Phi_2 \qquad (34)$$

where k and k_Φ are the effective hydraulic and electrokinetic permeability, respectively, p_L is the hydraulic or liquid pressure, μ is the water viscosity, and z_f and c_f refer to the charge and concentration of fixed ionic sites, respectively.

In the above system, the movement of water can be attributed to a potential gradient and a pressure gradient. The movement of water by a pressure gradient is determined primarily by an effective permeability of water moving through the pore network. This approach is quite useful for describing fuel-cell systems where the membrane is well hydrated, but it requires that the water content be uniform across the membrane, with only a pressure gradient as a driving force for water movement. Such a treatment does not necessarily lend itself to describing the flux of water resulting when there is a water-activity gradient across the membrane (i.e., when the membrane is not fully hydrated).

The Bernardi and Verbrugge model also assumes that there is a gas volume fraction in the membrane that remains constant. This does not necessarily agree with the physical picture presented and experimental evidence. The reason for including the gas volume fraction was to allow for gas crossover through the membrane. Such a process though can be included using Fick's law for the gases in the membrane, since the diffusion coefficients of oxygen and hydrogen in Nafion are known. Many other models use the same approach and equations as Bernardi and Verbrugge, especially systems wherein the membrane is expected to be well hydrated (e.g., saturated gas feeds).[25,47,50,64,78,95,125]

Unlike the cases of the single-phase models above, the transport properties are constant because the water content does not vary, and thus, one can expect a linear gradient in pressure. However, due to Schroeder's paradox, different functional forms might be expected for the vapor- and liquid-equilibrated membranes.

Instead of the dilute solution approach above, concentrated solution theory can also be used to model liquid-equilibrated membranes. As done by Weber and Newman,[94] the equations for concentrated solution theory are the same for both the one-phase and two-phase cases (eqs 32 and 33) except that chemical potential is replaced by hydraulic pressure and the transport coefficient is related to the permeability through comparison to Darcy's law. Thus, eq 33 becomes

$$\mathbf{N}_{w,2} = \xi\frac{\mathbf{i}_2}{F} - \frac{k}{\mu \overline{V}_w}\nabla p_L \qquad (35)$$

where $\overline{V}_w$ is the molar volume of water.

4.2.4. Hydraulic–Diffusive Models

The two approaches above can be contrasted to one another. In the first approach, section 4.2.2, water moves by diffusion, and pressure-driven flow is excluded as a separate driving force. In the second approach, section 4.2.3, only pressure-driven flow is used, and there is no diffusive flow because the liquid

water in the pores is pure. To describe both effects, some other kind of model is needed.

As mentioned at the end of section 4.2.2.2, a one-phase open system cannot support a pressure gradient without experiencing bulk flow. One way around this restriction is to use the chemical potential as the overall driving force.[55,94] In essence, this driving force combines those of pressure and activity

$$\nabla \mu_{\mathrm{w},k} = RT \nabla \ln a_{\mathrm{w},k} + \overline{V}_{\mathrm{w}} \nabla p_k \qquad (36)$$

where p_k is the total pressure of phase k. For the single-phase system, there is not an additional degree of freedom to have both types of gradients. Thus, the above equation and approach requires that an additional relation is needed to specify both variables, and this is given by assuming local equilibrium (i.e., there is only one overall gradient, that of chemical potential).

Another way around the problem of pressure-driven flow in the single-phase membrane was presented by Meyers.[212] He worked around the problem by allowing for a discontinuity in pressure at the membrane/solution interface, even though the electrochemical potential of all soluble species is continuous. He argued that additional mechanical stresses compressing the membrane should be indistinguishable from the thermodynamic pressure, and thus, the thermodynamic pressure might be discontinuous at the interface.

There have been various models that try to incorporate both diffusive flow and convective flow in one type of membrane and using one governing transport equation.[63,65,71,72,79,99,107] They are based somewhat on concentrated solution theory where the concentration and total gas-phase pressure driving forces are used

$$\mathbf{N}_{\mathrm{w},2} = \xi \frac{\mathbf{i}_2}{F} - D_{\mathrm{w}} \nabla c_{\mathrm{w},2} - c_{\mathrm{w},2} \frac{k}{\mu} \nabla p_{\mathrm{G}} \qquad (37)$$

A dusty-fluid model[216] has also been used to combine the effects, which adds convection to the Stefan–Maxwell framework, as discussed in a later section.[63,72] This approach is akin to eq 37. As discussed above, the concentration of water may be replaced by a function of λ.

The problem with the above approach lies in the meaning of the two different gradients. As noted above, the pressure driving force does not make sense for a one-phase system. Thus, the model implicitly assumes a two-phase system. In a two-phase system, the interstitial concentration of water never varies, and the superficial concentration varies only if the volume fraction of water changes in the membrane. Furthermore, the use of a gas pressure means that a gas-phase is assumed to exist in the membrane, something that does not agree with experimental data. Overall, treatment in this manner is the same as that for the diffusive models except for an additional parameter to account for results that show a greater flux of water from cathode to anode when the fuel cell is operated with a pressure differential. This addition helps to fit some of the data, but it is not rigorous or consistent.

4.2.5. Combination Models

There is a need to be able to describe both types of behavior, diffusive and hydraulic, in a consistent manner, which also agrees with experimental data. For example, a membrane with a low water content is expected to be controlled by diffusion, and an uptake isotherm needs to be used (see Figure 7). The reasons for this are that there is not a continuous liquid pathway across the medium and that the membrane matrix interacts significantly with the water due to binding and solvating the sulfonic acid sites. A hydraulic pressure in this system may not be defined.

On the other hand, when the membrane is saturated, transport still occurs. This transport must be due to a hydraulic-pressure gradient because over-saturated activities are nonphysical. In addition, Buechi and Scherer[217] found that only a hydraulic model can explain the experimentally observed sharp drying front in the membrane. Overall, both types of macroscopic models describe part of the transport that is occurring, but the correct model is some kind of superposition between them.[94,218] The two types of models are seen as operating fully at the limits of water concentration and must somehow be averaged between those limits. As mentioned, the hydraulic–diffusive models try to do this, but from a non-physical and inconsistent standpoint that ignores Schroeder's paradox and its effects on the transport properties.

Weber and Newman[94] do the averaging by using a capillary framework. They assume that the two transport modes (diffusive for a vapor-equilibrated membrane and hydraulic for a liquid-equilibrated one) are assumed to occur in parallel and are switched between in a continuous fashion using the fraction of channels that are expanded by the liquid water. Their model is macroscopic but takes into account microscopic effects such as the channel-size distribution and the surface energy of the pores. Furthermore, they showed excellent agreement with experimental data from various sources and different operating conditions for values of the net water flux per proton flux through the membrane.[134]

Eikerling et al.[40,138] used a similar approach except that they focus mainly on convective transport. As mentioned above, they use a pore-size distribution for Nafion and percolation phenomena to describe water flow through two different pore types in the membrane. Their model is also more microscopic and statistically rigorous than that of Weber and Newman. Overall, only through combination models can a physically based description of transport in membranes be accomplished that takes into account all of the experimental findings.

4.3. Diffusion-Media Modeling

As shown in Figure 5, the diffusion media are the porous backings between the catalyst layers and the gas channels. They provide structural support, distribute the reactant gases, and provide a pathway for electrons, gases, and liquid water to move to or from the catalyst layers. The diffusion media are

often composed of either a single gas-diffusion layer or a composite structure of a gas-diffusion layer and a microporous layer. It should be noted that there are only a few models that treat composite diffusion media in a rigorous fashion.[86,88,122] Most models treat only gas-diffusion layers.

Besides gas and liquid transport in the diffusion media, there is also electronic conduction. Most models neglect this due to the high conductivity of the carbon in the diffusion media, although it can become a limiting factor due to geometry[124] or diffusion-media composition.[88] For those that take it into account, Ohm's law is used

$$\mathbf{i}_1 = -\sigma_0 \epsilon_1^{1.5} \nabla \Phi_1 \tag{38}$$

where ϵ_1 and σ_0 are the volume fraction and electrical conductivity of the electronically conducting phase, respectively. The above equation has been adjusted for porosity and tortuosity using a Bruggeman correction.[219−222] In the diffusion media, carbon is the conducting phase and the other solid component, Teflon, is insulating.

The mass balances of the species in the diffusion media can be deduced from eq 23. Furthermore, the fluxes of the various species are often already known at steady state. For example, any inert gases (e.g., nitrogen) have a zero flux, and the fluxes of reactant gases are related to the current density by Faraday's law (eq 24). Although water generation is given by Faraday's law, water can evaporate or condense in the diffusion media. These reactions are often modeled by an expression similar to

$$r_{evap} = k_m a_{G,L}(p_w - p_w^{vap}) \tag{39}$$

where r_{evap} is the molar rate of evaporation per unit volume, k_m is a mass-transfer coefficient per unit interfacial surface area, $a_{G,L}$ is the interfacial gas−liquid surface area per unit volume, p_w is the partial pressure of water in the gas phase, and p_w^{vap} is the vapor pressure of water, which can be corrected for pore effects by the Kelvin equation.[223] Although different models may write eq 39 in slightly different forms (e.g., with a switching function), the underlying equation and principles are the same. Finally, the two-phase models may also have an interfacial area that depends on the water content of the media (for example, see ref 86). Overall, the value of $k_m a_{G,L}$ is typically high enough that the gas is saturated if liquid water exists; that is, $p_w = p_w^{vap}$ (using this last expression means that a special treatment is needed to combine the vapor and liquid material balances for water so as to eliminate the net evaporation rate).

In terms of transport, both gas- and liquid-phase transport should be described. Below, approaches for both types of transport are examined, with the gas-phase transport being treated first.

4.3.1. Gas-Phase Transport

Almost every model treats gas-phase transport in the fuel-cell sandwich identically. The Stefan−Maxwell equations are used (one of which is dependent on the others, since the partial pressures sum to unity)

$$\nabla x_i = \sum_{j \neq i} \frac{x_i \mathbf{N}_j - x_j \mathbf{N}_i}{c_T D_{i,j}^{eff}} \tag{40}$$

where c_T is the total concentration or molar density of all of the gas species, x_i is the mole fraction of species i, and $D_{i,j}^{eff}$ is the effective binary interaction parameter between i and j, by the Onsager reciprocal relationships, $D_{i,j}^{eff} = D_{j,i}^{eff}$ for ideal gases. The effective diffusion coefficient is defined as

$$D_{i,j}^{eff} = \frac{\epsilon_G}{\tau_G} D_{i,j} \tag{41}$$

where ϵ_G and τ_G are the volume fraction and tortuosity of the gas phase, respectively. If liquid water is ignored, then ϵ_G is set to the value of the bulk porosity of the medium, ϵ_0. If liquid water is not ignored, then another treatment is required, as discussed in the next section. Typically, a Bruggeman expression is used for the tortuosity[219−222]

$$\tau_G = \epsilon_G^{-0.5} \tag{42}$$

However, the above expression can underpredict the tortuosity at low porosities.[86,102] Nam and Kaviany[86] have a very good discussion of the appropriate function to use for the tortuosity, in which changing values due to liquid saturation are also accounted for.

The gases in a fuel cell are typically hydrogen and water on the fuel side, and air and water on the oxidant side. Since there are not many components to the gases and one of the equations in eq 40 can be replaced by the summation of mole fractions equals 1, many models simplify the Stefan−Maxwell equations. In fact, eq 40 reduces to Fick's law for a two-component system. Such simplifications are trivial and are not discussed here.

As the pore size decreases, molecules collide more often with the pore walls than with each other. This movement, intermediated by these molecule−pore−wall interactions, is known as Knudsen diffusion.[224] Some models have begun to take this form of diffusion into account.[26,37,45,49,69,72,74,81] In this type of diffusion, the diffusion coefficient is a direct function of the pore radius.[149] In the models, Knudsen diffusion and Stefan−Maxwell diffusion are treated as mass-transport resistances in series[149,225] and are combined to yield

$$\nabla x_i = -\frac{\mathbf{N}_i}{c_T D_{K_i}^{eff}} + \sum_{j \neq i} \frac{x_i \mathbf{N}_j - x_j \mathbf{N}_i}{c_T D_{i,j}^{eff}} \tag{43}$$

where the $D_{K_i}^{eff}$ is the effective Knudsen diffusion coefficient. In effect, the pore wall, with zero velocity, constitutes another species with which the diffusing species interact, and it determines the reference velocity used for diffusion.[226] The above equation also can be derived from a dusty-gas analysis.[216]

From an order-of-magnitude analysis, when the mean-free path of a molecule is less than 0.01 times the pore radius, bulk diffusion dominates, and when it is greater than 10 times the pore radius, Knudsen diffusion dominates. This means that Knudsen diffusion is significant when the pore radius is less than about 0.5 μm. For reference, a typical carbon gas-diffusion layer has pores between 0.5 and 20 μm[227-229] in radius, and a microporous layer contains pores between 0.05 and 2 μm.[230,231] Thus, while Knudsen diffusion may not have to be considered for gas-diffusion layers, it should be accounted for in microporous and catalyst layers.

While most models treat gas-phase flow as purely due to diffusion (i.e., the total gas pressure or concentration remains uniform), some models take into account convection in the gas-phase.[25,45,48,51,52,54,60-64,72,80,82,90,122,125,126,216] This is usually done by the addition of Darcy's law for the gas phase

$$\mathbf{v}_G = -\frac{k_G}{\mu_G}\nabla p_G \qquad (44)$$

where k is the effective permeability. The above relation can be made into a flux by multiplying it by the total concentration of the gas species.

One way to include the effect of gas-phase pressure-driven flow is to use eq 44 as a separate momentum equation.[51,54,60-62,64,80,82,125] The models that do this are primarily CFD ones. Another way to include pressure-driven flow is to incorporate eq 44 into the Stefan–Maxwell equations, as per the dusty-gas model[45,63,90,126,216]

$$\nabla x_i = -\frac{x_i k_G}{D_{K_i}^{eff}\mu_G}\nabla p_G + \sum_{j\neq i}\frac{x_i\mathbf{N}_j - x_j\mathbf{N}_i}{c_T D_{i,j}^{eff}} - \frac{\mathbf{N}_i}{c_T D_{K_i}^{eff}} \qquad (45)$$

However, this is not necessarily a rigorously correct treatment, since the bulk-fluid velocity should not just be linearly combined with the transport equations. Instead, one of the Stefan–Maxwell equations should be replaced by eq 44, since it is in essence the summation of the mass velocities of the gas species.[226]

Although there are models that incorporate gas-phase pressure-driven flow in the diffusion media, the question can arise as to whether this is a significant effect. The results of almost all of the models show that the pressure difference through the sandwich is minimal, and the assumption of uniform gas pressure is probably fine for most conditions (for examples, see refs 13, 56, 57, and 134). This is as expected, since the gases flow parallel to the sandwich and, due to a no-slip condition, move through the diffusion media primarily by diffusion. There is a caveat to the above conclusion in that some models do show that even a small pressure difference hinders mass transfer if it is in the direction out of the sandwich; however, this effect depends greatly on the permeability of the diffusion media and is somewhat debatable. In addition, small pressure gradients when coupled with thermal gradients might affect water transport significantly, as discussed in later sections.

The main reason there are models that account for gas-phase pressure-driven flow is that these models are often multidimensional and are considering effects besides just through the 1-D fuel-cell sandwich. As discussed in a later section, the pressure difference down a gas channel is much more significant than that through the sandwich. The only type of fuel cell where gas-phase pressure-driven flow needs to be accounted for in the fuel-cell sandwich is one using an interdigitated flow field.[48,52,232] In these types of fuel cells, the gas channels are not continuous through the fuel cell, and thus, gas is forced by both convection and diffusion through the diffusion media to reach the next gas channel.

4.3.2. Treatment of Liquid Water

Liquid water has been modeled to various degrees in fuel cells, and the different approaches are discussed in terms of their complexity. The simplest way to account for liquid water, besides ignoring it, is to treat it essentially as a solid species that occupies a certain volume fraction. Its transport is not considered, and the only effect it has is to decrease the gas-phase volume. This decreases the effective diffusion coefficients of the gas species (see eq 41) and somewhat takes into account flooding. The models that do this approach usually use the volume fraction of water as a fitting parameter.[14,50,72,75,101,120] Out of these models, those of Chu et al.,[75] Gurau et al.,[120] and Baschuck and Li[50] use a liquid volume fraction that is a function of position to mimic flooding effects. Chu et al. showed the effect of different variations in the liquid volume fraction on various fuel-cell parameters including potential, oxygen mass fraction, and current density. Gurau et al. came up with an analytic solution for the cathode side of the fuel cell and showed how the limiting current density and polarization effects depended on the different liquid volume fractions. Baschuck and Li fit polarization curves by having different liquid volume fractions at each point. The resultant volume-fraction profile gives an idea about how flooding occurs and progresses.

The next more complicated treatment of liquid water is to have a way in which to model also its transport without going to a two-phase model. The models of this sort assume that the liquid water exists as droplets that are carried along in the gas stream.[16,25,65] Thus, while evaporation and condensation occur, a separate liquid phase does not have to be modeled. Instead, the liquid is assumed to be a component of the gas, and usually one that has a negligible effect on the gas-phase flow and velocity. There is a change in the gas-phase volume fraction due to the water, however. This type of model allows for the existence and location of liquid water to be noted, and to a limited extent the change in the water pressure or concentration.

The above two types of models are essentially one phase. To model liquid-water flow accurately, two-phase models are required. Liquid-phase transport is similar to the gas-phase pressure-driven flow described above. There is no diffusion component to water movement because the liquid water is assumed

to be pure. Thus, the flux form of Darcy's law models the flow of liquid water

$$\mathbf{N}_{w,L} = -\frac{k}{\overline{V}_w \mu} \nabla p_L \qquad (46)$$

where $\overline{V}_w$ is the molar volume of water and all of the properties are valid for pure water. Many models use the above equation with a set value of the liquid-phase volume fraction.[13,47,52,71,78,95,99,107,110,125] In essence, such a picture assumes that there are isolated gas and liquid pores in the medium. This makes some sense, since the medium contains hydrophilic and hydrophobic materials and pores, but in reality there should be some transfer between them as well as a changing volume fraction. Another way to look at it is that it is describing a thin film of liquid that coats a hydrophilic surface.

In the same fashion as that of the above models, those of Wohr et al.[45] and Bevers et al.[26,129] use a similar expression to eq 46 but instead use a surface diffusion coefficient instead of the effective permeability divided by the viscosity. Also, they use a water-loading gradient that one could relate to a water pressure. Bevers et al. also have a volume fraction that changes with respect to time. The model of Janssen[55] also has a similar equation to those of the other models but instead uses a driving force of chemical potential and a fitting parameter for the permeability. Weber and Newman[134] use a similar approach to that of Janssen but use a liquid-pressure-gradient driving force. They basically use the permeability as a fitting parameter that is set under only one set of operating conditions for each laboratory setup.

Finally, there are the models that use a phase mixture approach.[51,54,60,82] In this approach, the two phases are treated as a single-phase mixture. Thus, all parameters are mixture parameters for the two phases. However, unlike the cases of the single-phase models, eq 46 is used for the liquid, which effectively determines its mass flux. A problem with this approach is that the mixture moves with a single velocity (i.e., the gas and liquid move with the same velocity). Thus, the liquid pressure is a result of this velocity; it does not really have a separate driving force. Although these simplifications are made, usually to help in numerical stability and computation time, the models do a reasonable job in predicting the water balance of the fuel cell. This approach can be seen as a simplified version of the multiphase mixture model by Wang and Cheng,[58,59] as discussed below. While the above models describe liquid-water transport to some extent, the existence of partially saturated media requires the use of capillary equations and a rigorous two-phase description of two-phase flow.

4.3.2.1. Rigorous Two-Phase Flow Models. It is well-known that gas and liquid interact to a certain extent in a porous medium. Over the decades, many different modeling approaches have been developed for two-phase flow in porous media. These approaches range from a simple bundle-of-capillaries model to very complex 3-D network models incorpo-

rating a detailed description of a medium's microstructure. A complete description of the various modeling approaches is beyond the scope of this article, and the reader is referred to reviews and books on the subject.[223,233,234] In this section, only those models that are used for modeling the diffusion media in fuel cells are discussed.[56,57,74,78−80,85−87] These models are macroscopic and on the simpler end of the porous-media-model scale, which makes them easier to use although less accurate.

The interaction between liquid and gas is characterized by a capillary pressure, contact angle, surface tension, and pore radius[223,234−236]

$$p_C = p_L - p_G = -\frac{2\gamma \cos \theta}{r} \qquad (47)$$

where γ is the surface tension of water, r is the pore radius, and θ is the internal contact angle that a drop of water forms with a solid. Equation 47 is based on how liquid water wets the material; hence, for a hydrophilic pore, the contact angle is $0° \leq \theta < 90°$, and for a hydrophobic one, it is $90° < \theta \leq 180°$ (for examples, see refs 86 and 123).

One of the most important aspects of the two-phase models is their ability to predict the liquid saturation as a function of position. The saturation, S, is defined as the amount of pore volume that is filled with liquid; thus

$$\epsilon_G = \epsilon_0(1 - S) \qquad (48)$$

This equation shows that the saturation greatly affects the effective gas-phase diffusion coefficients. Hence, flooding effects are characterized by the saturation.

In the models, the saturation is normally calculated using an empirical function to relate the capillary pressure to the saturation. Nguyen and co-workers[56,87] use a function they developed from fitting data, and Pisani et al.[78] use a function with an unknown fitting parameter, while the other models use the empirically determined Leverett J-function.[57,79,80,85,86,123] A different approach than that using a functional form for the capillary pressure−saturation relationship is to calculate the saturation using a model. Weber and Newman[74] do this using a random cut-and-rejoin bundle-of-capillaries model[223] in order to integrate analytically the pore-size distribution of the diffusion media to get the saturation. In their analysis, they also explicitly account for the mixed wettability of the diffusion media (i.e., eq 47 is an integration limit, and there are separate hydrophobic and hydrophilic pore-size distributions). Along with Nam and Kaviany,[86] they have the only model to account for such effects. The use of a bundle-of-capillaries type of model is not necessarily rigorous because it idealizes the actual porous network.

Only a handful of models treat the diffusion media as at least partially hydrophobic;[74,78,86,123] the others treat the medium as entirely hydrophilic. Although in principle it does not change the approach, the physical picture and boundary conditions must change. An entirely hydrophilic medium means that the liquid pressure must always be below the gas pres-

sure or the medium is flooded. This is taken into account in the models by assuming that the saturation equals zero at the interface of a diffusion medium with a gas channel. In principle, this seems fine, yet it also means that the liquid pressure is much lower than the gas pressure (and can even approach a value of zero) at this interface. The hydrophobic models assume that at this interface the capillary pressure is equal to zero, or in other words the liquid pressure equals the gas pressure. This assumption is not necessarily true due to menisci formation in the diffusion media, but it seems to be a more valid assumption, especially since the diffusion media have added Teflon to keep them from flooding (i.e., there is a need to have hydrophobic pores). The true boundary condition is probably a thermodynamic balance that also considers multidimensional flow effects.

To determine the saturation for any of the models, the capillary pressure must be known at every position within a diffusion medium. Hence, the two-phase models must determine the gas and liquid pressure profiles. In typical two-phase flow in porous media, the movement of both liquid and gas is determined by Darcy's law for each phase and eq 47 relates the two pressures to each other. Many models utilize the capillary pressure functionality as the driving force for the liquid-water flow

$$\mathbf{N}_{w,L} = -\frac{k}{\bar{V}_w \mu}\nabla p_L = -\frac{k}{\bar{V}_w \mu}(\nabla p_C + \nabla p_G) =$$
$$-\frac{k}{\bar{V}_w \mu}\nabla p_C \quad (49)$$

where the last equality is justified by the assumption of a uniform gas pressure in the fuel-cell sandwich. A useful relation in calculating the effective permeability, k, is to define a relative permeability, k_r,

$$k = k_r k_{sat} \quad (50)$$

where k_{sat} is the saturated permeability, or the permeability at complete saturation, of the medium. k_{sat} depends only on the structure of the medium and has either been assumed,[57,80,85] used as a fitting parameter,[56,74,87] or estimated using a Carman–Kozeny equation.[86]

If the dependence of k_r on saturation is known, then it can be used in eq 49 (via eq 50) directly. Nguyen and co-workers[56,87] and Berning and Djilali[80] assume a linear dependence of k_r on saturation, and most of the other models use a cubic dependence;[57,78,79,85,86] the model of Weber and Newman[74] yields close to a cubic dependence. This last model differs from the others because it obtains an analytic expression for k_r as a function of the capillary pressure (the independent variable). Furthermore, they also calculated and used residual or irreducible saturations, which are known to exist[59,223,234,235] but have only been incorporated into a few other models.[78,86] In accordance with typical data, a cubic dependence is the most often observed, although the other dependences help in the mathematical convergence of the models
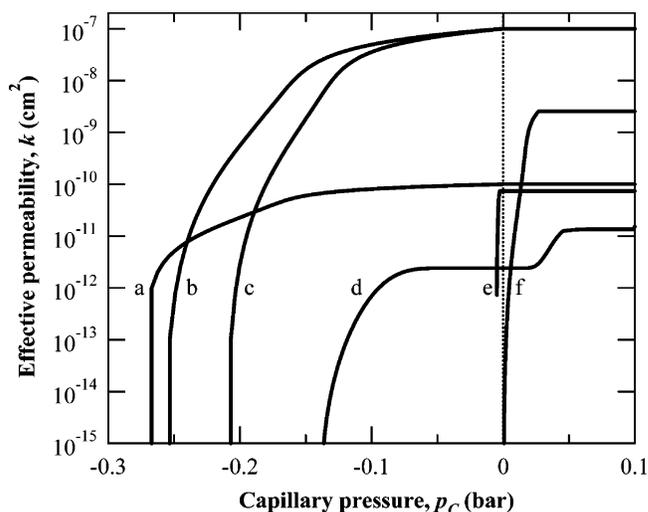
Figure 8. Effective permeability as a function of capillary pressure for the different two-phase models for the gas-diffusion layer. The lines correspond to the models of (a) Berning and Djilali,[80] (b) You and Liu[79] and Mazumder and Cole,[85] (c) Wang et al.,[57] (d) Weber and Newman,[74] (e) Natarajan and Nguyen,[56] and (f) Nam and Kaviany.[86]

without increasing the overall error of the simulations too much.

The different capillary pressure, saturation, and permeability relationships of the different models can be compared. To do this, the effective permeabilities from some of the different models are plotted as a function of the capillary pressure in Figure 8. In the figure, the capillary pressure at which the effective permeability no longer changes is where the medium is fully saturated. Also, the values of the effective permeability are dependent on the diffusion media being tested. Furthermore, the value of the effective permeability at the right end of the curves corresponds to the saturated permeability, except for the model of Weber and Newman, who use a gas-phase residual saturation.

The values of the effective permeabilities vary over orders of magnitude, and this corresponds to the different results of the models. Furthermore, as discussed in various papers,[56,80,85] the effective permeability of Natarajan and Nguyen (curve e) varies significantly over a very small pressure range, although they state that their capillary-pressure equation mimics data well. With respect to the various equations, the models that use the Leverett J-function[57,79,80,85,86] all have a similar shape except for that of Berning and Djilali (curve a), who used a linear variation in the permeability with respect to the saturation. The differences in the other curves are due mainly to different values of porosity and saturated permeability. As mentioned above, only the models of Weber and Newman (curve d) and Nam and Kaviany (curve f) have hydrophobic pores, which is why they increase for positive capillary pressures. For the case of Weber and Newman, the curve has a stepped shape due to the integration of both a hydrophilic and a hydrophobic pore-size distribution.

The addition of the gas and water mass balances (eq 39 with eq 23) along with the above transport equation (eq 46) and constitutive relationships com-

pletely specifies the system of equations. In making these equations, some of the models include the effect of gravity and an additional advection or convection term. These other terms are secondary effects and, in a fashion similar to that of the full Navier–Stokes equations, are not as important as the Darcy effects due to the small pore sizes and low permeability. Even though there is a closed set of equations, it is often hard to get the simulations to converge, especially if they are multidimensional. Thus, the computational-fluid-dynamics models[57,79,80,85] use the multiphase mixture model.[58,59]

As mentioned above, this approach treats each phase as a constituent to a mixture. Thus, all parameters are mixture parameters and must be averaged, usually by the saturation. Unlike the models mentioned at the end of the previous section, the models here use capillary phenomena. Furthermore, although the mixture moves at a mass-average velocity, interfacial drag between the phases and other conditions allow each separate phase velocity to be determined. The liquid-phase velocity is found by[57,59]

$$\mathbf{v}_L = \lambda_L \frac{\rho_m}{\rho_L} \mathbf{v}_m + \frac{k \lambda_L (1 - \lambda_L)}{\epsilon_0 \rho_L \nu_m} [\nabla p_C + (\rho_L - \rho_G) \mathbf{g}] \quad (51)$$

where the subscript m stands for the mixture, ρ_k and ν_k are the density and kinematic viscosity of phase k, respectively, and λ_L is the relative mobility of the liquid phase

$$\lambda_L = \frac{k_{r,L}/\nu_L}{k_{r,L}/\nu_L + k_{r,G}/\nu_G} \quad (52)$$

In eq 51, the first term represents a convection term, and the second comes from a mass flux of water that can be broken down as flow due to capillary phenomena and flow due to interfacial drag between the phases. The velocity of the mixture is basically determined from Darcy's law using the properties of the mixture. The appearance of the mixture velocity is a big difference between this approach and the others, and it could be a reason the permeability is higher for simulations based on the multiphase mixture model.

The overall gain of the multiphase mixture model approach above is that the two-phase flow is still considered, but the simulations have only to solve pseudo-one-phase equations. Problems can arise if the equations are not averaged correctly. Also, the pseudo-one-phase treatment may not allow for pore-size distribution and mixed wettability effects to be considered. Furthermore, the multiphase mixture model predicts much lower saturations than those of Natarajan and Nguyen[56,87] and Weber and Newman[74] even though the limiting current densities are comparable. However, without good experimental data on relative permeabilities and the like, one cannot say which approach is more valid.

Finally, some of the models use an equation of the type[52,80,85]

$$\mathbf{N}_{w,L} = -D_S \nabla S \quad (53)$$

where D_S is a so-called capillary diffusivity

$$D_S = \frac{k}{\mu \overline{V}_w} \frac{dp_C}{dS} \quad (54)$$

Although the above equation is valid, it gives the false impression that the saturation is the driving force for fluid flow and that a saturation condition should be used as a boundary condition. Furthermore, care must be taken in the interpretation of the capillary diffusivity.

4.4. Catalyst-Layer Modeling

Electrochemical reactions take place at the catalyst layers of the fuel cell. At the anode and cathode, hydrogen is oxidized (eq 1) and oxygen is reduced (eq 2), respectively. These layers are often the thinnest in the fuel-cell sandwich but are perhaps the most complex because this is where electrochemical reactions take place and where all of the different types of phases exist. Thus, the membrane and diffusion media models must be used in the catalyst layer along with additional expressions related to the electrochemical kinetics on the supported electrocatalyst particles.

A schematic of a typical fuel-cell catalyst layer is shown in Figure 9, where the electrochemical reactions occur at the two-phase interface between the electrocatalyst (in the electronically conducting phase) and the electrolyte (i.e., membrane). Although a three-phase interface between gas, electrolyte, and electrocatalyst has been proposed as the reaction site, it is now not believed to be as plausible as the two-phase interface, with the gas species dissolved in the electrolyte. This idea is backed up by various experimental evidence, such as microscopy, and a detailed description is beyond the scope of this review. Experimental evidence also supports the picture in Figure 9 of an agglomerate-type structure where the electrocatalyst is supported on a carbon clump and is covered by a thin layer of membrane.[162,237–240] Sometimes a layer of liquid water is assumed to exist on top of the membrane layer, and this is discussed in section 4.4.6. Figure 9 is an idealized picture, and
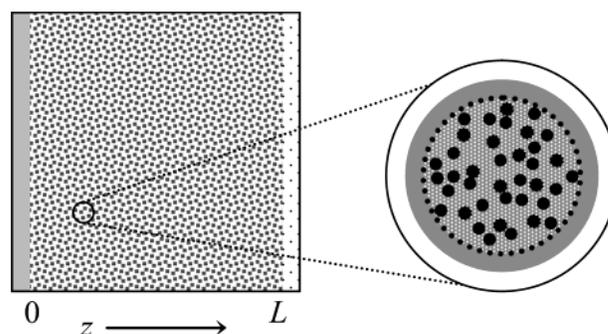
Figure 9. Idealized schematic of the cathode catalyst layer (going from $z = 0$ to $z = L$) between the membrane and cathode diffusion medium showing the two main length scales: the agglomerate and the entire porous electrode. Gray, white, and black indicate membrane, gas, and electrocatalyst, respectively, and the gray region outside of the dotted line in the agglomerate represents an external film of membrane or water on top of the agglomerate.

the actual structure is probably more of a "spaghetti and meatball" structure, where the carbon agglomerates are connected to each other and covered by thin tendrils of membrane.

Various modeling approaches have been used for the catalyst layers, with different degrees of success. The approach taken usually depends on how the other parts of the fuel cell are being modeled and what the overall goal of the model is. Just as with membrane modeling, there are two main classes of models. There are the microscopic models, which include pore-level models as well as more detailed quantum models. The quantum models deal with detailed reaction mechanisms and elementary transfer reactions and transition states. They are beyond the scope of this review and are discussed elsewhere, along with the issues of the nature of the electrocatalysts.[151,241−243]

The other type of model is the macrohomogeneous model. These models are macroscopic in nature and, as described above, have every phase defined in each volume element. Almost all of the models used for fuel-cell electrodes are macrohomogeneous. In the literature, the classification of macrohomogeneous models is confusing and sometimes contradictory. To sort this out, we propose that the macrohomogeneous models be subdivided on the basis of the length scale of the model. This is analogous to dimensionality for the overall fuel-cell models.

In this scheme, the first type of model is the 0-D-type models or interface models, where a single equation is used without regard to the structure of the catalyst layers. Next are the 1-D-type models, which either account for changes across the layer or account for only local effects in the agglomerate. Typically, those that account for changes across the layer are called porous-electrode, macrohomogeneous, or thin-film models, and those that account for changes in the agglomerate are called agglomerate models. However, the agglomerate models are still macrohomogeneous models, and they may include effects across the layer as well. In the same fashion, some porous-electrode models include agglomerate-scale interactions. The models that include effects on only one length scale are termed simple. They are further subdivided on the basis of the length scale modeled, such that porous-electrode and agglomerate correspond to the length scales of the layer and agglomerate, respectively. Those models that include effects on both length scales (i.e., 2-D-type models) are known as embedded macrohomogeneous models. Finally, there are no 3-D-type models because there are only two primary length scales (the catalyst layer and the agglomerate) in these regions.

An examination of the catalyst-layer models reveals the fact that there are many more cathode models than anode ones. In fact, basically every electrode-only model is for the cathode. This arises because the cathode has the slower reaction; it is where water is produced, and hence, mass-transfer effects are much more significant; and it represents the principal inefficiency of the fuel cell. In other words, while the cathode model can be separate from the anode model, the converse is not true due to the

above reasons. Finally, the anode can almost always be modeled as a simplified cathode model, with the exception of poisoning of the electrocatalyst. For these reasons, the discussion below focuses mainly on the cathode models; the anode models require only a switch in the kinetic expression and various property values.

In this section, the reactions and general equations for the catalyst layers are presented first. Next, the models are examined starting with the interface models, then the microscopic ones, and finally the simple and embedded macrohomogeneous ones. Finally, at the end of this section, a discussion about the treatment of flooding is presented.

4.4.1. General Governing Equations

Although the various models contain their own equations, they are derived from basically the same set of governing expressions, regardless of the effects being modeled. As mentioned, the reactions at the anode and cathode are termed the HOR and ORR, respectively. For the HOR, the reaction is fast and can be described by a Butler−Volmer kinetic expression, eq 12. However, if the feed stream is reformate or contains poisons such as carbon monoxide, the reaction rate is quite different. In this situation, the carbon monoxide adsorbs to the electrocatalyst sites and effectively decreases the reaction rate. There have been various models that account for this by doing a carbon monoxide site balance and examining the reaction steps involved.[17,104,113,115,244−248] Of these models, the one by Springer et al.[104] is probably the most comprehensive and does the best job in terms of agreement with experimental data. The treatment of the effect of poisons on kinetics is beyond the scope of this review and is not discussed further. For the ORR, a Tafel expression, eq 13, is normally used due to the slow kinetics of the four-electron-transfer reaction. As discussed in section 3.2.2, either eq 13 or eq 15 can be used, with the difference being in the overpotential used (i.e., whether the surface and concentration or just the surface overpotential is used, respectively). As discussed, this difference basically corresponds to the placement of the, perhaps imaginary, reference electrode.

In general, catalyst layers contain many phases: liquid, gas, different solids, and membrane. Because the layers have multiple phases, effective values must be used for the transport properties such as membrane conductivity; this is typically done using a Bruggeman expression (see eqs 41 and 42). Because of the complexity of the layers, it is worthwhile to do a variable and equation count. In the most general case, the membrane, diffusion medium, and kinetic equations are used. This gives the set of variables and equations as listed in Table 1. It should be noted that since there are multiple phases in the catalyst layer, appropriate volume fractions and Bruggeman expressions are required for such equations as Ohm's law in the membrane phase. Another point is that the complete set of equations is seldom used in modeling. Often, simplifying assumptions are used. For example, the ohmic drop in the matrix or solid is often ignored due to its high conductivity. Also,

Table 1. List of Important Variables and Their Governing Equations or Conditions for the Catalyst Layer

variable		equation
overall liquid water flux	$\mathbf{N}_L$	23
overall membrane water flux	$\mathbf{N}_w$	23
gas-phase component flux	$\mathbf{N}_{G,i}$	23
gas-phase component partial pressure	$p_{G,i}$	43
liquid pressure	p_L	49
membrane water chemical potential[a]	μ_w	33 or 34
electronic-phase current density	$\mathbf{i}_1$	38
membrane current density	$\mathbf{i}_2$	32 or 28
electronic-phase potential	Φ_1	27
membrane potential	Φ_2	55 or 64
temperature	T	set or 76 or 78
total gas pressure	p_G	set or 44
liquid saturation	S	see section 4.3.2.1

[a] This can be directly related to the liquid pressure depending on what equation or approach is used.

treatment of the membrane phase is usually done using Ohm's law and ignoring the water flux through the membrane. While Table 1 lists all of the governing variables and equations, it does not necessarily say how to relate the variables to each other, since more than one variable may occur in a given equation.

The membrane and diffusion-media modeling equations apply to the same variables in the same phase in the catalyst layer. The rate of evaporation or condensation, eq 39, relates the water concentration in the gas and liquid phases. For the water content and chemical potential in the membrane, various approaches can be used, as discussed in section 4.2. If liquid water exists, a supersaturated isotherm can be used, or the liquid pressure can be assumed to be either continuous or related through a mass-transfer coefficient. If there is only water vapor, an isotherm is used. To relate the reactant and product concentrations, potentials, and currents in the phases within the catalyst layer, kinetic expressions (eqs 12 and 13) are used along with zero values for the divergence of the total current (eq 27).

The kinetic expressions result in transfer currents that relate the potentials and currents in the electrode (platinum on carbon) and electrolyte (membrane) phases as well as govern the consumption and production of reactants and products. To simplify the equations and approaches for the case of one ionically and one electronically conducting phase, it is useful to use the relation

$$\nabla\cdot\mathbf{i}_2 = -\nabla\cdot\mathbf{i}_1 = a_{1,2}i_{h,1-2} \qquad (55)$$

where $-\nabla\cdot\mathbf{i}_1$ represents the total anodic rate of electrochemical reactions per unit volume of electrode and $i_{h,1-2}$ is the transfer current for reaction h between the membrane and the electronically conducting solid (i.e., eqs 12 and 13 for the HOR and ORR, respectively). The above charge balance assumes that faradaic reactions are the only electrode processes; double-layer charging is neglected (as is appropriate under steady-state conditions). This equation can be used in the conservation-of-mass equation

(eq 23) to simplify it. For example, if the ORR is the only reaction that occurs at the cathode, the following mass balance results

$$\nabla\cdot\mathbf{N}_{O_2,G} =$$
$$-\frac{1}{4F}a_{1,2}i_{0,ORR}\left(\frac{p_{O_2}}{p_{O_2}^{ref}}\right)\exp\left(-\frac{\alpha_c F}{RT}(\eta_{ORR,1-2})\right) = \frac{1}{4F}\nabla\cdot\mathbf{i}_1 \qquad (56)$$

This equation is often used in the various cathode models.

Before discussing the models, a note should be made concerning catalyst loading. Many models use platinum loading in their equations, especially for optimizing designs and in normalizing the current produced (equivalent to a turnover frequency in catalysis). In this respect, the catalyst loading, m_{Pt}, is the amount of catalyst in grams per geometric area of the fuel-cell face (x,y in Figure 1). If a turnover frequency is desired, the reactive surface area of platinum, A_{Pt}, can be used (usually given in m^2/g). This area can be related to the radius of a platinum particle, assuming perhaps a certain roughness factor, but more often it is experimentally inferred using cyclic voltammetry measuring the hydrogen adsorption. These variables can usually be determined and then used to calculate the specific interfacial area between the electrocatalyst and electrolyte,

$$a_{1,2} = \frac{m_{Pt}A_{Pt}}{L} \qquad (57)$$

where L is the thickness of the catalyst layer. This assumes a homogeneous distribution of electrocatalyst in the catalyst layer.

A factor closely related to the catalyst loading is the efficiency or utilization of the electrode. This tells how much of the electrode is actually being used for electrochemical reaction and can also be seen as a kind of penetration depth. To examine ohmic and mass-transfer effects, sometimes an effectiveness factor, E, is used. This is defined as the actual rate of reaction divided by the rate of reaction without any transport (ionic or reactant) losses. With this introduction of the parameters and equations, the various modeling approaches can be discussed.

4.4.2. Interface Models

The simplest way to treat the catalyst layers is to assume that they exist only at the interface of the diffusion media with the membrane. Thus, they are infinitely thin, and their structure can be ignored. This approach is used in complete fuel-cell models where the emphasis of the model is not on the catalyst-layer effects but on perhaps the membrane, the water balance, or multidimensional effects. There are different ways to treat the catalyst layer as an interface.

If a detailed potential is not required in the model, then the catalyst layer can be treated as simply the location where oxygen and hydrogen are consumed and water is produced. Hence, Faraday's law (eq 24) is used as a generation/consumption term in the

boundary condition for the mass balance between the membrane and the diffusion medium. The models that focus mainly on water management, a quantity tied to the current density, use this type of treatment of the catalyst layers.[55,81,112,126,134] A slightly more sophisticated treatment is to model the catalyst layers as described above but then use an overall polarization equation (e.g., eq 21) with the simulation results to yield a potential for the cell at the specific current density.[14,65,74,86,127,203]

A more sophisticated and more common treatment of the catalyst layers still models them as interfaces but incorporates kinetic expressions at the interfaces. Hence, it differs from the above approach in not using an overall polarization equation with the results, but using kinetic expressions directly in the simulations at the membrane/diffusion medium interfaces. This allows for the models to account for multidimensional effects, where the current density or potential changes,[16,24,46−48,51,52,54,56,60−62,66,80,82,87,107,125] although some of the earlier and water-management models are 1-D and treat the catalyst layer in this manner.[20,57,75,109] This treatment means that both Faraday's law and the kinetic expressions are used as boundary conditions at the diffusion media and membrane interfaces. This type of treatment also allows for nonuniform current density distributions to exist, because the potential is constant in a cell due to the equipotential surfaces of the bipolar plates. Another way to look at these models is that the surface overpotential and reactant gas concentrations are assumed uniform throughout the catalyst layers, and this is used in the kinetic expressions to calculate the current density. In fact, it is common for these models to use the overpotential as a fitting parameter.

Overall, the interface models are basically 0-D. They assume that all of the relevant variables in the catalyst layers are uniform in their values across the layer. This has some justification in that the catalyst layers are very thin, and it is adequate if other effects that are modeled are more significant; however, the catalyst layers should be modeled in more detail to ensure that all the relevant interactions are accounted for and to permit optimization of such parameters as catalyst loading.

4.4.3. Microscopic and Single-Pore Models

The earliest models of fuel-cell catalyst layers are microscopic, single-pore models, because these models are amenable to analytic solutions. The original models were done for phosphoric-acid fuel cells. In these systems, the catalyst layer contains Teflon-coated pores for gas diffusion, with the rest of the electrode being flooded with the liquid electrolyte. The single-pore models, like all microscopic models, require a somewhat detailed microstructure of the layers. Hence, effective values for such parameters as diffusivity and conductivity are not used, since they involve averaging over the microstructure.

There are two main types of single-pore models. In the first, the approach of Giner and Hunter[1] is taken in which there are straight, cylindrical gas pores of a defined radius. These pores extend the length of the catalyst layer, and reaction takes place at their surface. These models are termed the gas-pore models.[249−252] The second type of model follows the scheme of Grens[253] and Cutlip.[2] In this approach, there are still gas pores, but there are also pores filled with electrolyte and catalyst. It is in these other pores that reaction, diffusion, and migration occur. These models are termed the flooded-agglomerate models.[3−5,254−257] Although there are the two approaches, the distinction between them is often blurred.

The equations used in these models are primarily those described above. Mainly, the diffusion equation with reaction is used (e.g., eq 56). For the flooded-agglomerate models, diffusion across the electrolyte film is included, along with the use of equilibrium for the dissolved gas concentration in the electrolyte. These models were able to match the experimental findings such as the doubling of the Tafel slope due to mass-transport limitations. The equations are amenable to analytic solution mainly because of the assumption of first-order reaction with Tafel kinetics, which means that eq 13 and not eq 15 must be used for the kinetic expression. The different equations and limiting cases are described in the literature models as well as elsewhere.[258,259]

Of these models, the flooded-agglomerate one shows better agreement with experimental data. This is not unexpected, since it probably models the actual microstructure better and also has more parameters. A problem with the single-pore models is that in reality there are multiple pores that are tortuous. Furthermore, the driver of having analytic expressions becomes less important, as computer power has progressed. Overall, the single-pore models represent a good first start in simulating fuel-cell electrodes and form the core of many more complicated models as discussed below. However, macrohomogeneous and more sophisticated models provide for more physically realistic simulations. Finally, while these models do a good job for phosphoric-acid fuel cells, it is unknown how well they work for polymer-electrolyte fuel cells where, since the electrolyte is a solid, it does not necessarily penetrate the pore space.

The only other truly microscopic models for the catalyst layers are those by Durand and co-workers.[30−33,260] In these models, spherical agglomerate structures are assumed to exist in regular 3-D hexagonal arrays. Between the agglomerates, either there are gas pores or the region is flooded with electrolyte. The reason these models are microscopic and not macrohomogeneous is that they examine interactions in such a way that there is a dependence on the exact way in which the agglomerates are placed. Furthermore, not all of the phases are defined in every volume element. The equations solved are mainly Ohm's law and Fick's law with kinetic expressions. The results of the models show the concentration contours around a particle and agree with experimental current densities and trends. Such a model also allows for the detailed placement of the electrocatalyst particles to be studied, even though it may not be possible to make such an arrangement experimentally. To expand on the last comment, the

benefit of these microscopic models is that they clearly show how the HOR occurs next to the membrane and how the packing and structure of the agglomerate particles help to enhance or reduce the overall efficiency of the anode, something that the classical models above could not demonstrate.

4.4.4. Simple Macrohomogeneous Models

There are many models that use essentially only one length scale but average over the microscopic details of a region. These models are termed simple macrohomogeneous models. As described in section 3.1, the macrohomogeneous approach assumes that all phases exist at all points in the volume and that properties and phases can be categorized by a handful of parameters including the volume fraction and surface area per volume. Although these models do not include microstructural details, they do use many of the same equations and physical ideas of the single-pore models. The two main length scales studied are over the whole catalyst layer or over the agglomerate (see Figure 9), and each are discussed below.

4.4.4.1. Porous-Electrode Models. The porous-electrode models are based on the single-pore models above, except that, instead of a single pore, the exact geometric details are not considered. Euler and Nonnenmacher[261] and Newman and Tobias[7] were some of the first to describe porous-electrode theory. Newman and Tiedemann[6] review porous-electrode theory for battery applications, wherein they had only solid and solution phases. The equations for when a gas phase also exists have been reviewed by Bockris and Srinivasan[262] and DeVidts and White,[263] and porous-electrode theory is also discussed by Newman[139] in more detail.

Porous-electrode theory is concerned about the overall reaction distribution in the catalyst layer. Thus, it is assumed that the main effects do not occur within the agglomerates. In other words, the agglomerates all have a uniform concentration and potential. Conceptually, porous-electrode theory can be visualized as a resistor network, as shown Figure 10. Physically, the figure is showing that electron, proton, and kinetic resistances govern the reaction distribution. Thus, the overpotential and transfer current in the electrode are functions of position because the current travels along the path of least resistance. The effect of concentration is accounted for in the calculation of the charge-transfer resistance, which is derived directly from the kinetic expressions and likely to be nonlinear. Finally, to be
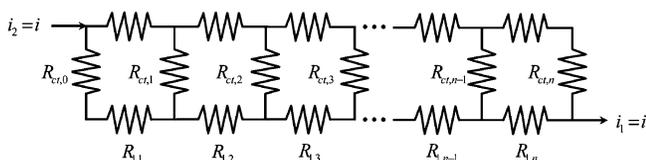
Figure 10. Resistor-network representation of porous-electrode theory. The total current density, i, flows through the electrolyte phase (2) and the solid phase (1) at each respective end. Between, the current is apportioned on the basis of the resistances in each phase and the charge-transfer resistances. The charge-transfer resistances can be nonlinear because they are based on kinetic expressions.

rigorous, the charge-transfer resistances in Figure 10 should be in parallel with a capacitor representing double-layer charging. However, this can be neglected for the steady-state operation of fuel cells and introduced if transients or impedance is studied.

The governing equations for the simple porous-electrode models are as referenced in Table 1. The characteristic length scale is the thickness of the catalyst layers. There are also some variations in the treatment of the simple porous-electrode models. In the first set of models, the catalyst layers are integrated over, and the expression is included as a boundary condition in calculating the cell potential or current density.[37,95,99] This treatment is very similar to that of the interface models, except that potential drops for the matrix and solution phases are accounted for. The reason for doing the integration is that, if the reaction distribution is mainly uniform, then there is no loss in numerical accuracy and there is a gain in numerical stability and easier convergence.

The next set of models treats the catalyst layers using the complete simple porous-electrode modeling approach described above. Thus, the catalyst layers have a finite thickness, and all of the variables are determined as per Table 1 with a length scale of the catalyst layer. While some of these models assume that the gas-phase reactant concentration is uniform in the catalyst layers,[15,67,69] most allow for diffusion to occur in the gas phase.[13,25,26,28,45,71,72,110,121,133,204] These models are essentially macrohomogeneous versions of the single-gas-pore models.

The final simple macrohomogeneous porous-electrode models are the ones that are more akin to thin-film models. In these models, the same approach is taken, but instead of gas diffusion in the catalyst layer, the reactant gas dissolves in the electrolyte and moves by diffusion and reaction.[17,36,50,64,101,114,264] The governing equations are more-or-less the same as above, except that now a concentration instead of a partial pressure appears in the kinetic expressions and the governing equations for mass transport of the reactant and product gas species become ones of diffusion in the membrane or water (if a water layer is assumed to exist). The reason these models are still simple models is that only the length scale of the catalyst layer is considered, and the concentrations of the species are assumed to be in equilibrium with their respective gas-phase partial pressures (i.e., Henry's law applies).

As mentioned, the reaction distribution is the main effect on the catalyst-layer scale. Because of the facile kinetics (i.e., low charge-transfer resistance) compared to the ionic resistance of proton movement for the HOR, the reaction distribution in the anode is a relatively sharp front next to the membrane. This can be seen in analyzing Figure 10, and it means that the catalyst layer should be relatively thin in order to utilize the most catalyst and increase the efficiency of the electrode. It also means that treating the anode catalyst layer as an interface is valid. On the other hand, the charge-transfer resistance for the ORR is relatively high, and thus, the reaction distribution is basically uniform across the cathode. This means
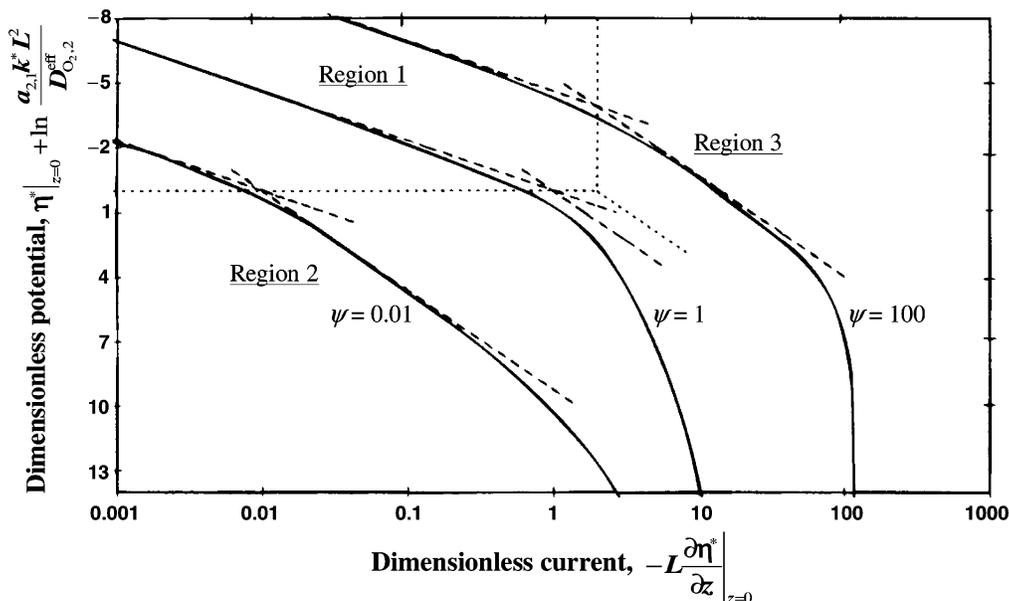
Figure 11. Tafel plot of flooded porous-electrode simulation results for the cathode at three different values of $\psi = 2.3nFD_{O_2,2}^{\text{eff}}c_{O_2,2}|_{z=L}/bk^{\text{eff}}$. The z coordinate ranges from 0 (catalyst layer/membrane interface) to L (catalyst layer/diffusion medium interface), the dimensionless overpotential is defined as $\eta^* = -\alpha_c F/RT(\eta_{\text{ORR},1-2})$, and the ORR rate constant is defined as $k^* = i_{0_{\text{ORR}}}/nFc_{O_2,2}^{\text{ref}}$. (Reproduced with permission from ref 36. Copyright 1998 The Electrochemical Society, Inc.)

that simplifying assumptions such as a uniform surface overpotential ($\eta_{s_{\text{ORR},1-2}}$) can be justified, and basically all of the catalyst is being utilized in the layer as long as the mass-transfer of oxygen does not become limiting. In this case, the charge-transfer resistance next to the membrane becomes much higher than the other ones, and the catalyst is less utilized in that region, since there is less oxygen. One should note that with Tafel kinetics, which prevail for the ORR, the nonuniformity of the reaction distribution is governed by the current density and electrode thickness and not by the exchange current density.

The above effects can also be seen in the different regimes of the polarization curve. To study these effects, Perry et al.[36] made Tafel plots of their simulation results, which used a flooded porous-electrode model of the cathode catalyst layer. These plots are shown in Figure 11, where they are a function of a dimensionless parameter that is essentially a ratio of oxygen mass transfer to ionic conduction. The Tafel plots show a doubling of the Tafel slope when either the mass-transfer or ionic limitations are controlling, regions 2 and 3, respectively. In region 1, kinetics is controlling. Figure 11 allows one to understand and visualize how the interplay between the different phenomena and variables, such as current, gas diffusion both inside and outside the catalyst layer, and proton conduction inside the catalyst layer, affects polarization behavior. Although the model is for the cathode, it is equally valid for the anode, where the parameter values normally result in kinetic control (region 1).

The results of Perry et al. allow for the development of a diagnostic method that determines the limiting behavior from simple experimental data. In a similar analysis, Weber et al.[133] added mass transport in the diffusion media explicitly and analyzed

their results in terms of ohmic, kinetic, or mass-transfer control situations. Like Perry et al., they discuss how simple experiments such as oxygen gain, the gain in performance with oxygen instead of air, can help determine a given fuel cell's controlling phenomena. Eikerling and Kornyshev[28] also show the same behavior, and they analyze the resistances with analytic expressions for the various limiting cases. Finally, Jaouen et al.[98] examine similar cases to those above but include agglomerate effects, as discussed in detail in section 4.4.5.

4.4.4.2. Agglomerate Models. The simple macro-homogeneous agglomerate models consider only effects that occur on the agglomerate length scale. In essence, they assume a uniform reaction-rate distribution, that is, a uniform gas concentration and surface overpotential through the thickness of the catalyst layer. As mentioned above, the simple agglomerate models more accurately represent the structure of the catalyst layers than the simple porous-electrode models. These models are very similar to the microscopic models of Durand and co-workers discussed above, except that the geometric arrangement is averaged over and each phase exists in each volume element.

For the agglomerate model, the characteristic length scale is the radius of the agglomerate, R_{agg}, and all of the agglomerates are assumed to be the same shape and size. In the model, the reactant or product diffuses through the electrolyte film surrounding the particle and into the agglomerate, where it diffuses and reacts. Hence, there is a concentration and possibly a potential distribution within the agglomerate. The equations for modeling the agglomerate are similar to those listed in Table 1, except that either spherical or cylindrical coordinates are used for the gradients. The reason they are not identical is that the agglomerate scale is es-

sentially a subscale or microscopic scale in the catalyst layer. This is the same as examining a bed of sand, where the normal resolution looks at changes across the box and the agglomerate scale looks at changes within individual grains (see Figure 9). In a macrohomogeneous model, it is necessary to average over the agglomerate scale, and hence, effectiveness factors, both internal and overall,[265] are often used.

The analysis below is given for the ORR, since the agglomerate and embedded models mainly examine the cathode; reaction at the anode can be derived in a similar manner. The analysis is basically the same as that of reaction and diffusion in a catalyst pellet. For the analysis, an effectiveness factor is used, which allows for the actual rate of reaction to be written as (see eq 55)

$$\nabla \cdot \mathbf{i}_2 = a_{1,2} i_{h,1-2} E \tag{58}$$

Since the ORR is a first-order reaction following Tafel kinetics, the solution of the mass conservation equation (eq 23) in a spherical agglomerate yields an analytic expression for the effectiveness factor of[149,265]

$$E = \frac{1}{3\phi^2}(3\phi \coth(3\phi) - 1) \tag{59}$$

where ϕ is the Thiele modulus for the system[266]

$$\phi = \zeta \sqrt{\frac{k'}{D_{O_2,\text{agg}}^{\text{eff}}}} \tag{60}$$

where ζ is the characteristic length of the agglomerate (volume per surface area), $R_{\text{agg}}/3$ for spheres, $R_{\text{agg}}/2$ for cylinders, and δ_{agg} for slabs, and k' is a rate constant given by

$$k' = \frac{a_{1,2} i_{0_{\text{ORR}}}}{4F c_{O_2}^{\text{ref}}} \exp\left(-\frac{\alpha_c F}{RT}(\eta_{\text{ORR},1-2})\right) \tag{61}$$

where the reference concentration is that concentration in the agglomerate that is in equilibrium with the reference pressure

$$c_{O_2}^{\text{ref}} = p_{O_2}^{\text{ref}} H_{O_2,\text{agg}} \tag{62}$$

where $H_{O_2,\text{agg}}$ is Henry's constant for oxygen in the agglomerate. Similar expressions to eq 59 have also been derived for other types of reactions and geometries,[149,265] and while eq 59 is derived for spheres, with the appropriate Thiele modulus, it results in deviations less than 10% in the value of the effectiveness factor for other geometries. The above rate constant can be related to the transfer current density, $i_{\text{ORR},1-2}$ (see eq 13). Also, one notices that the Thiele modulus is independent of the surface concentration for a first-order reaction.

If external mass-transfer limitations can be neglected, then the surface concentration in eq 58 (via eq 13) can be set equal to the bulk concentration, which is assumed uniform throughout the catalyst layer in the simple agglomerate models. Otherwise, the surface concentration is unknown and must be

calculated. To do this, an expression for the diffusion of oxygen to the surface of the agglomerate is written

$$W_{O_2}^{\text{diff}} = A_{\text{agg}} D_{O_2,\text{film}} \frac{c_{O_2}^{\text{bulk}} - c_{O_2}^{\text{surf}}}{\delta_{\text{film}}} \tag{63}$$

where $W_{O_2}^{\text{diff}}$ is the molar flow rate of oxygen to the agglomerate, A_{agg} is the specific external surface area of the agglomerate, and the film can be either membrane or water (if two or more films are desired, similar expressions can be written for each film). The above expression uses Fick's law and a linear gradient, which should be valid due to the low solubility of oxygen, steady-state conditions, and thinness of the film. At steady state, the above flux is equal to the flux due to reaction and diffusion in the agglomerate (as well as the flux through any other films), and thus, the unknown surface concentration(s) can be replaced. Doing this and using the resultant expression in the conservation equation (eq 56) yields

$$\nabla \cdot \mathbf{i}_1 = 4F c_{O_2}^{\text{bulk}} \left(\frac{1}{\dfrac{\delta_{\text{film}}}{A_{\text{agg}} D_{O_2,\text{film}}} + \dfrac{1}{k'E}} \right) \tag{64}$$

This equation is the governing equation for the agglomerate models for the cathode, and without external mass-transfer limitations, it results in eq 58. For the anode, a similar analysis can be done.

There is only a handful of models that simulate the catalyst layers using the simple agglomerate model,[44,90,105,120,160,267,268] because most agglomerate models are developed for comparison purposes (discussed in the following section) or are macrohomogeneous embedded models (i.e., take into account the catalyst-layer length scale as well) and are discussed in section 4.4.5. The results of the simple agglomerate models are helpful in trying to understand and optimize catalyst-layer parameters such as loading and agglomerate size. For example, it has been shown that fuel-cell performance increases with a decrease in agglomerate radius until a maximum plateau is reached.[90,105] This limit results because the effectiveness factor plateaus at a value of 1 at a finite radius. However, this result does not necessarily hold if the agglomerate is not at a uniform temperature throughout.

4.4.4.3. Model Comparison. The distinction between the two simple macrohomogeneous models deals with the length scales of the effects being studied. While both show similar effects such as doubling of the Tafel slope due to mass-transport limitations, the question arises as to where the limitations are occurring. To get a better grasp on the two different approaches, several researchers have compared them to each other and experimental data.[27,34,35,49,53] Of particular note is the analysis of Boyer et al.,[49] who examined the characteristic length scales for the various processes such as diffusion in the gas phase, diffusion in the agglomerate, proton migration in the catalyst layer, and so forth. These length scales are simple expressions and can let one
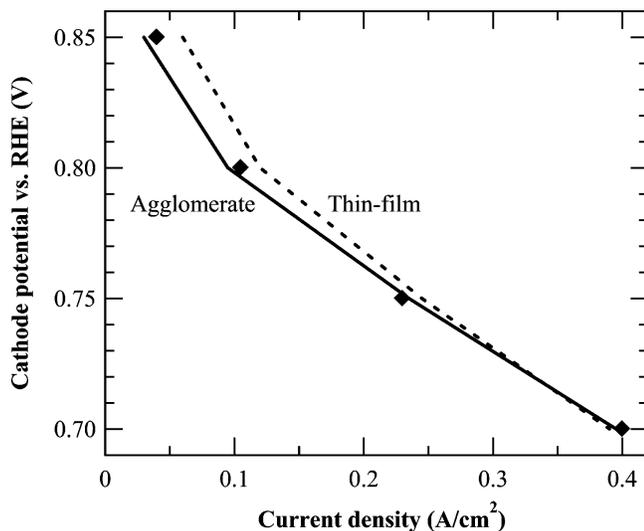
Figure 12. Comparison of simple macrohomogeneous agglomerate (solid line) and thin-film (dashed line) cathode models to experimental data (diamonds). Data are adapted from ref 34.

easily identify which scale is more important for the conditions being studied. Hence, one will know which model is the best to use. In general, they arrived at the conclusions that the simple agglomerate model is accurate for the cathode but that a porous-electrode approach is better in the anode due to the highly nonuniform reaction distribution. They also showed how to optimize various parameters such as Nafion loading.

The rest of the comparisons were done for the cathode. The results all showed that the agglomerate model fits the data better than the porous-electrode model. However, it should be noted that the porous-electrode model used was usually a thin-film model and so was not very robust. Furthermore, the agglomerate model has more parameters that can be used to fit experimental data. Finally, some of the agglomerate models compared were actually embedded models that account for both length scales, and therefore, they normally agree better with the experimental data.

The main problem with the porous-electrode models according to Gloaguen et al.[34,35] is that they overestimate oxygen transport limitations, but that is because they used thin-film models that did not contain gas pores. Chan and Tun[53] compared much more similar agglomerate and porous-electrode models and noted the effects of changing different parameters on performance. They showed that the agglomerate model is more sensitive to changes in mass-transport resistances caused by flooding than the porous-electrode models. A final comparison was done by Broka and Ekdunge.[27] They compared the models to experimental data and microscopy and arrived at the conclusion that the agglomerate model is a more accurate representation, although they also showed that with the addition of a mass-transfer coefficient in the porous-electrode model it can agree with the data as well as the agglomerate model.

A comparison of the two models with experimental data is given in Figure 12. In the figure, simulations were run with a simple agglomerate model and a simple thin-film model. As can be seen, the agglomerate model fits the data much better than the thin-film model, although the lack of a gas phase in the thin-film model makes it less rigorous than the simple porous-electrode model described above. The difference between the models declines at higher current densities where the reaction distribution is becoming nonuniform. In fact, for anode simulations the porous-electrode model should be better due to the much more nonuniform reaction distribution. At low current densities, the reaction distribution is uniform, and the most important effects happen at the agglomerate scale; that is why the agglomerate model fits the data better in that regime. While these simple models are acceptable, a more complex embedded model where both are used should be the best in terms of accuracy.

4.4.5. Embedded Macrohomogeneous Models

The above simple models account for only one length scale. To account for both the local agglomerate level and effects across the porous electrode, embedded macrohomogeneous models are used. Even though the simple agglomerate models account for many effects, they cannot truly consider reaction distributions and proton migration across the catalyst layer. As noted above, these effects are important in certain circumstances (e.g., within the anode catalyst layer, within a flooded catalyst layer, and within a catalyst layer with a dehydrated membrane). The application of embedded models is very straightforward. Finally, the original model of Iczkowski and Cutlip[5] was really a precursor of the embedded models, and agglomerate models rather than porous-electrode ones are more likely to become embedded models.

There are two ways in which the embedded model can be used. In the first, the porous-electrode modeling equations are used as discussed above and in Table 1. Next, a mass-transfer term is added to account for the flux to the agglomerate. In this situation, there is basically a film between the reaction site and the gas pore, although this exact structure is averaged over in the macrohomogeneous approach. Thus, in a single volume element, the diffusive and reaction fluxes are related at the boundary of the agglomerate film. This approach is basically the same as accounting for external mass-transfer limitations within each volume element. Because this approach adds only an additional resistance to charge transfer due to diffusion, it is not more computationally costly than the porous-electrode model and yields an extra fitting parameter if desired (the thickness of the film or the mass-transfer coefficient) and more realistic behavior, especially for incorporating flooding effects. There are a few models that use this approach.[19,84,85]

The other approach is more complicated and requires a deeper knowledge of the agglomerate structure or yields more fitting parameters. In this approach, the porous-electrode equations are used, but now the effectiveness factor and the agglomerate model equations are incorporated. Hence, eq 64 is used to get the transfer current in each volume element. The gas composition and the overpotential
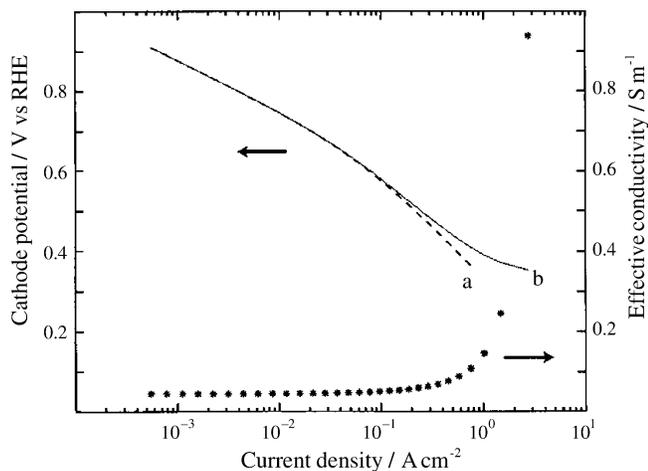
Figure 13. Plot of cathode potential as a function of current density for a macrohomogeneous embedded model where the proton conductivity is assumed to be uniform (0.044 S/m), curve a, or varies with water production (changing humidity) across the catalyst layer, curve b. (Reproduced with permission from ref 98. Copyright 2002 The Electrochemical Society, Inc.)

change across the catalyst layer due to ohmic, mass-transfer, and reaction effects. While this approach is slightly more complicated and requires knowing values for more parameters, the payoffs are greater in that it does the best job in representing the physical reality of the catalyst layer and includes all of the relevant effects. This is in agreement with the analysis of Pisani et al.,[91] who compared different agglomerate structures with each other and the porous-electrode model. Other models also use this approach.[36,78,98,129,269] Finally, it should be noted that an overall effectiveness factor that considers both external and internal mass transfer to and through the agglomerate can be used as a fitting parameter, thereby avoiding the necessity of detailed calculations and perhaps multiple fitting parameters on the agglomerate scale.

In terms of the cathode models, that of Maja et al.[269] in essence examined the effect of having two different agglomerate radii. They showed that this is important for being able to predict the correct limiting current density. Pisani et al.[78] used analytic expressions for cylindrical agglomerates that are basically flooded pores. They then integrated over the catalyst layer to get an overpotential and current density for use as a boundary condition in the overall 1-D fuel-cell model. As mentioned above, Jaouen et al.[98] examined the cathode polarization curve in a manner similar to those of Perry et al.[36] and Weber et al.[133] However, the addition of the agglomerate length scale allowed them to examine more complex behavior. This can be seen in Figure 13, where the embedded model shows a more complex cathode-potential curve due to tradeoffs between the two length scales. In the figure, consideration of a changing ionic conductivity due to water production hydrating the membrane causes the potential curve to move from a double Tafel slope back toward a single Tafel slope.

While it is evident that the embedded model is the best one to use, it requires additional complexity and

more parameters, not all of which may be known. If the controlling phenomena are known, which seldom are a priori, then the appropriate simple model can be used. Diagnostic techniques aimed at determining the controlling phenomena and perhaps parameter values are discussed by Perry et al.,[36] Weber et al.,[133] and Jaouen et al.[98] They advocate conducting simple experiments, such as oxygen gain and varying layer thickness, and analyzing the results. The analysis and results of their models can be summarized as follows for the different operating regimes. Control by oxygen diffusion in the agglomerate results in a double Tafel slope, and the total current density is proportional to the active layer thickness, is first-order in oxygen, and has a low sensitivity to gas humidity. Control by proton transport in the catalyst layer results in a double Tafel slope, and the current density is independent of the layer thickness, is half-order in oxygen, and increases with relative humidity. Control by both of the above results in a quadruple Tafel slope. Control by oxygen diffusion in both the agglomerate and covering film results in the progressive disappearance of quadruple and double Tafel slopes with increasing film thickness. Control by oxygen diffusion in the layer and either proton diffusion in the layer or oxygen diffusion in the agglomerate yields a double Tafel slope that also progressively disappears.

4.4.6. Catalyst-Layer Flooding

Flooding of the catalyst layer is treated in a separate section because various models with different approaches have addressed it and it is important, especially in the cathode. There are two main ways in which flooding is considered, and they depend on how the catalyst layer is modeled. If an agglomerate model is used and if liquid water exists in the fuel cell, a liquid film covering the membrane film of the agglomerates can be assumed. Thus, the flooding of the catalyst layer is easily incorporated into the external mass-transfer limitation (eqs 63 and 64) where the reactant gases have to diffuse through a water film as well as the membrane layer.[50,114] Due to the low diffusivity and solubility of oxygen in water, only a very thin liquid film is needed to inhibit reaction. All of the agglomerate models can easily incorporate flooding in this manner, with perhaps the thickness of the film used as a fitting parameter.

The other way to incorporate flooding in the catalyst layers is to use the two-phase modeling approach described in section 4.3.2.1. This involves calculating the liquid saturation in the catalyst layer and then adjusting the interfacial area accordingly. This is done by a linear expression

$$a_{1,2} = a_{1,2}^{\circ}(1 - S) \tag{65}$$

where $a_{1,2}^{\circ}$ is the maximum or dry specific interfacial area. There are a few models that use this approach.[52,56,57,87,109] Equation 64 assumes a homogeneous distribution of electrocatalyst through the catalyst layers, which is a fine first approximation, although accounting for the electrocatalyst location (e.g., hydrophilic versus hydrophobic pores) would be more rigorous.

In comparing the two approaches, it seems that the saturation approach allows for greater reaction rates (higher current densities). The reason is that the catalyst layers have small pores and are hydrophobic, and thus, it takes a high liquid pressure to flood them, whereas even a thin film can effectively shut down the reaction. Of course, the film is spread over a much larger surface area and depends on the agglomerate radius. It is tough to say which approach is better, but because the saturation equations for the diffusion media are well developed compared to having an unknown water film thickness that may vary with position, it is our belief that eq 65 should be incorporated into an embedded catalyst-layer model.

It is known that flooding is important at high current densities, especially at the cathode. However, one may wonder if the performance loss is due to blockage of the catalyst sites by water or by flooding of the diffusion media. In the literature models, flooding of the diffusion media has garnered more attention. Flooding of the diffusion media seems also to agree with the fact that the diffusion media are much thicker and more hydrophilic with larger hydrophobic pores than the catalyst layers, but they also have a higher porosity. Furthermore, due to the normally high surface area of active material in the catalyst layers, some flooding can occur without a significant detriment to performance.[123] Experimental data with microporous layers between the catalyst layer and diffusion media (for examples, see refs 270−272) are inconclusive. Some indicate that, due to their often hydrophobic nature, they keep water out of the diffusion media. However, other microporous layers are thought to wick water out of the catalyst layers due to their small pores. In reality, the physical situation is that flooding should be considered in both regions. Overall, the catalyst layers are complex and have been treated by various means, with macrohomogeneous embedded models agreeing the best with the physical picture, while also not being too complicated to use in fuel-cell simulations.

4.5. Multilayer Simulations

The purpose of this section is to describe the general results of models that contain more than one of the layers described above. It is beyond the scope of this article to analyze every model and its results in detail, especially since they have already been discussed to a certain extent in section 2. Many of the models make tradeoffs between complexity, dimensionality, and what effects are emphasized and modeled in detail. It is worth noting that those models that employ a CFD approach seem to be the best suited for considering multidimensional effects. In this section, the ways in which the multilayer models are solved and connected are discussed first. Next, some general trends and results are presented.

4.5.1. Numerical Solution and Boundary Conditions

Due to the complexity and interconnectivity of the governing equations and constitutive relationships, most fuel-cell models are solved numerically. Although analytic solutions are obtainable in certain instances, these usually involve assumptions that make the solution of limited significance. Furthermore, the power of digital computers is continually progressing such that the computational cost of running simulations becomes manageable.

For most numerically solved models, a control-volume approach is used. This approach is based on dividing the modeling domain into a mesh. Between mesh points, there are finite elements or boxes. Using Taylor series expansions, the governing equations are cast in finite-difference form. Next, the equations for the two half-boxes on either side of a mesh point are set equal to each other; hence, mass is rigorously conserved. This approach requires that all vectors be defined at half-mesh points, all scalars at full-mesh points, and all reaction rates at quarter-mesh points. The exact details of the numerical methods can be found elsewhere (for example, see ref 273) and are not the purview of this review article. The above approach is essentially the same as that used in CFD packages (e.g., Fluent) or discussed in Appendix C of ref 139 and is related to other numerical methods applied to fuel-cell modeling.[274,275]

The various layers of the fuel-cell sandwich described above are linked to each other through boundary conditions, which apply at the mesh point between two regions. There are two main types of boundary conditions, those that are internal and those that are external. The internal boundary conditions occur between layers inside the modeling domain, and the external ones are the conditions at the boundary of the entire modeling domain.

Typically, coupled conditions are used for internal boundaries wherein the superficial flux and interstitial concentration of a species are made continuous. However, as mentioned above, boundary conditions between the membrane and electrode can involve the fact that there is only ionic current in the membrane and that the uptake isotherms mean that water content changes from λ in the membrane to partial pressure in the electrode. On the other side of the electrode, the boundary condition should state that all of the current is electronic. Another common boundary condition is to have a change in concentration because a species dissolves. This is similar to the internal boundary condition in the membrane and is used sometimes for electrodes where phases are not continuous across the boundary. Finally, internal boundary conditions can represent modeling regions that are not modeled in depth. For example, a water flux and kinetic equation can be used at the boundary between the cathode diffusion medium and the membrane if the catalyst layer is not modeled rigorously. Another example is setting the flux of water through the membrane and its ohmic resistance at a single boundary point.

Depending on the modeling domain, the last boundary condition is sometimes also used as an external boundary condition (e.g., half-cell models). The external boundary conditions specify the concentrations and values for all of the species and variables at the boundary. Examples include specifying the inlet conditions, such as gas feed rates, composition,

temperature, and humidity, or specifying the current density or potential. The external boundary conditions are often the same as the operating conditions and, therefore, are very similar for most simulations, although there can be differences such as what condition is used for two-phase flow (i.e., zero saturation or zero capillary pressure).

4.5.2. General Multilayer Simulation Results

In terms of sandwich models, there are four main varieties. The first are those that treat only one layer in the sandwich, and they were discussed above. The second are those that treat multiple layers of the sandwich but not all of them.[26,37,50,56,57,75,86,105,110,120,153,252] These are typically cathode models that include the diffusion medium and perhaps a membrane water flux. Next are the models that treat all of the layers of the sandwich and are only 1-D.[13,14,17,20,45,71,72,74,78,95,98,99,101,112,203] Finally, there are those that are multidimensional and treat all of the layers; these are discussed in detail in section 5.

The models should duplicate the effects seen by experiment. Thus, as the temperature is raised, better performance is obtained up to a point. An optimum is reached because, even though property values are usually increasing, so does the water vapor pressure. Consequently, if the feeds are saturated, the reactant gas partial pressure is lower, which affects the kinetics, and if the feeds are dry, it is harder to hydrate the membrane and there are higher ohmic losses. These issues can become important during operation of high-temperature fuel cells. As discussed in section 5.1.1, water concentration effects down the gas channels need to be considered for dry feeds, and therefore, a 1-D model does not suffice. Gains in performance are also seen in fuel cells operating with pure oxygen or under elevated pressure. In these cases, fuel cells perform better not only because of higher reactant gas pressures but also because flooding is not as critical (i.e., the limiting current density increases due to lower mass-transport limitations).
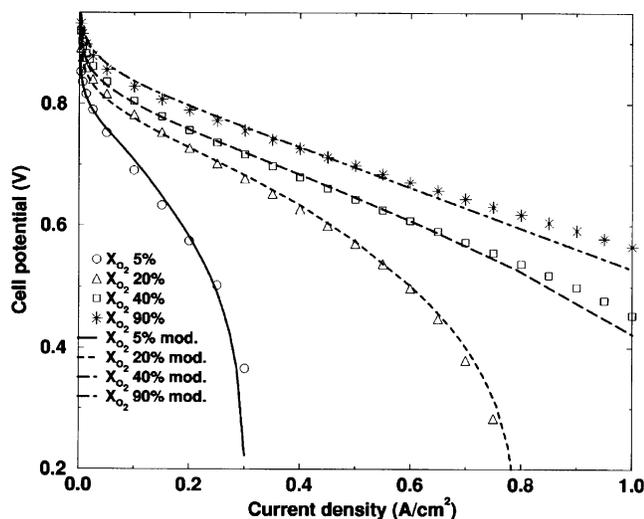
Figure 14. Comparison between experiment and simulation for different humidified oxygen feeds. (Reproduced with permission from ref 78. Copyright 2002 The Electrochemical Society, Inc.)
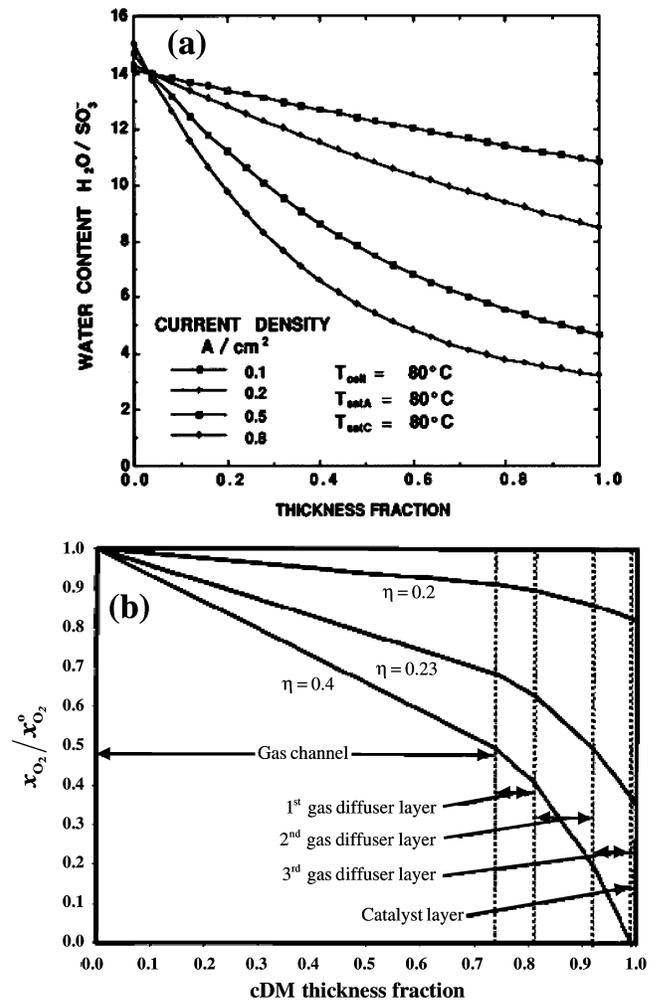
Figure 15. Simulation results showing membrane dehydration (a) and cathode flooding (b). (a) λ as a function of membrane position (cathode on the left) for different current densities. (Reproduced with permission from ref 14. Copyright 1991 The Electrochemical Society, Inc.) (b) Dimensionless oxygen mole fraction as a function of cathode-diffusion-medium position and cathode overpotential. (Reproduced with permission from ref 120. Copyright 2000 The Electrochemical Society, Inc.)

This last point is shown very well in Figure 14, where model and experimental data are compared for different oxygen concentrations. In some sense, this is an analogue to Figure 4, where a 1-D and not a 0-D model is used. Figure 14 demonstrates good fits between experiments and 1-D model simulations. In this model, flooding was accounted for in the diffusion media and the simple agglomerate model was used for the catalyst layers. The membrane model considered only the liquid-equilibrated transport mode, which is why the ohmic region in some of the curves deviates from the experimental data. Overall though, the 1-D sandwich model does a good job in fitting the data for humidified feeds and in predicting the full polarization curve, especially at low oxygen concentrations.

Most of the models show that fuel-cell performance is a balance among the various losses shown in Figure 3, in particular, ohmic losses and mass-transport limitations, which both increase with current. The reason for this is that the kinetic losses are hard to mitigate without significantly changing op-

erating conditions or using better catalysts, as discussed above. Models show that ohmic losses mainly result from the membrane drying out at the anode side of the membrane-electrode assembly. This is shown in Figure 15a. This is not to say that ohmic losses do not occur in other parts of the fuel cell, just that they are not as dominant. The mass-transport limitations are due mainly to flooding of the cathode side of the fuel cell, as shown in Figure 15b. The answers that models predict to the above tradeoffs focus mainly on increasing the flux of water in the membrane from cathode to anode and increasing the oxygen partial pressure in the cathode. To these extents, models agree with experiment in showing that thinner membranes, higher-oxygen-content feeds and pressures, and the use of a microporous layer between the catalyst layer and a gas-diffusion layer all yield better performing fuel cells.

Finally, fuel-cell models allow for optimization studies. For example, understanding the current distribution in the electrode allows one to understand the effect of changing its thickness and how to decrease catalyst loading by proper platinum placement. Such modeling results can be credited for the manufacturing of fuel cells that have thinner anodes than cathodes due to more of a nonuniform reaction distribution in the anode. Other optimization studies include looking at different structural and physical properties such as thicknesses, porosities, and so forth. However, optimization studies should be confined to those models that are more physical and complex. Overall, the best fuel-cell sandwich models have a physical basis; take into account all of the sandwich layers; have a minimum of fitting parameters; agree with experimental data trends; and adequately model the dominant transport phenomena.

5. Multidimensional Effects

Although the fuel-cell sandwich is the heart of a fuel cell, there are important effects that are not found when only a 1-D model is used. These effects basically arise from the fact that a fuel cell is in reality a 3-D structure, as shown in Figures 1 and 5. Many models explore these effects and are discussed in this section. These models always include the fuel-cell sandwich as one of the dimensions. First, the 2-D models are examined and then the 3-D ones. Because there is another review in this issue that focuses on these models in more depth, the discussion below is shortened.[276]

5.1. Two-Dimensional Models

As shown in Figures 1 and 5, there are two possible ways that 2-D effects can be incorporated, either along the channel (y,z) or under the rib (x,z). The modeling domains of these two effects are shown parts a and b, respectively, of Figure 16. The rib effects take into account the fact that there is a solid rib between two channels, which affects transport in the sandwich. This latter effect is germane to interdigitated flow fields. Both of the 2-D effects are discussed below, starting with the along-the-channel models.
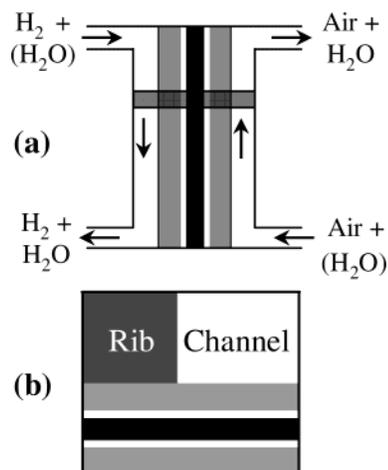
Figure 16. Schematic showing the modeling domain for the 2-D models. (a) Along-the-channel domain where the 1-D sandwich is highlighted for the pseudo-2-D case. (b) Rib domain showing only the cathode side rib and channel.

5.1.1. Along-the-Channel Models

There are two main ways that transport along the channel can be treated. The first is to assume that changes within the fuel-cell sandwich occur only in the direction perpendicular to it (z axis).[15,16,44,55,107,109,127,129,134] This assumption effectively means that the models have only to account for a change in the boundary conditions or values along the channel. This kind of treatment is termed pseudo-2-D. A limiting case of the pseudo-2-D model may be seen as those models that are 1-D but use an average concentration for each species in the gas channels.[14,74,88,101] The other kind of treatment is to use a full 2-D simulation in which equations and parameters change in both directions in the sandwich and gas channels.[25,47,61,62,64,66,79,90] With proper discretization, the pseudo-2-D models can accurately reflect the results of the full 2-D models.

For a full 2-D model, the only change in the equations is that the vector components now occur in two directions. The various regions are normally assumed to be isotropic so that the property-value expressions are the same for each direction. If data are known, then the expressions can be altered accordingly. The gas channels are the only new modeling domains introduced.

The gas channels contain various gas species including reactants (i.e., oxygen and hydrogen), products (i.e., water), and possibly inerts (e.g., nitrogen and carbon dioxide). Almost every model assumes that, if liquid water exists in the gas channels, then it is either as droplets suspended in the gas flow or as a water film. In either case, the liquid water has no affect on the transport of the gases. The only way it may affect the gas species is through evaporation or condensation. The mass balance of each species is obtained from a mass conservation equation, eq 23, where evaporation/condensation are the only reactions considered.

For movement of the gases, various treatments can be used. The simplest is to use mass balances down the flow channel. This is the same as saying that there is plug flow and the pressure remains uniform,

something that is not valid under certain operating conditions or with long or interdigitated flow fields. A robust treatment would be to use the Navier–Stokes equation

$$\mathbf{v}_G \cdot \nabla(\rho_G \mathbf{v}_G) = -\nabla p_G + \mu_G \nabla^2 \mathbf{v}_G \qquad (66)$$

where $\mathbf{v}_G$ is the mass-average velocity of the gas phase. For the gas channels, Darcy's law is not valid because they are not porous. If desired, diffusion terms (e.g., Stefan–Maxwell equations) can be used in conjunction with the above equation to result in convective-diffusion equations. However, axial dispersion is normally negligible compared to pressure-driven flow. Finally, simpler flow equations are also often used such as assuming plug flow or Poiseuille flow. If only a pressure drop down the channel is required, correlations from fluid dynamics can be used to determine it (e.g., Ergun equation).[149,277]

In terms of boundary conditions, the following apply. The gas-channel plates represent equipotential surfaces, which serve to set the overall cell potential. In terms of flows, the gases are usually assumed to be either in a coflow or counterflow arrangement, although the physical system may be in cross-flow. The inlet flow rates and concentrations must be specified; setting the stoichiometry of the inlet gases and the humidity serves to do this. The stoichiometries are normally based on the total current of the cell, and when they are time independent, the results are independent of the active area or the channel length. The reason for this is that all the fluxes become proportional to the active area, which can be canceled out. Setting the outlet pressure and the inlet temperature also serves as boundary conditions. A no-slip condition at the gas channel wall is also valid. The conditions needed at the interfaces of the gas channels and the diffusion media are now coupled, internal boundary conditions, which were discussed previously.

Now that the methodology and equations have been introduced, one may wonder what the effects along the channel are. The most significant effects deal with the changing gas composition. As the feed gases react, their concentration goes down unless the feed stoichiometries are very high. This means that the reaction rate decreases and a nonuniform current distribution is generated. In fact, with very long channels, the decrease in concentration of the feed gases might result in a type of limiting current density.[66] Such a distribution can have a variety of effects including nonuniform temperature distributions, places where the membrane dries out, and poorly utilized catalyst areas.

To expand on the last remark, the simulation results from Fuller and Newman[15] are shown in Figure 17. The curves clearly show a nonuniform current distribution that is mainly due to the change in the gas concentrations and the membrane hydration. In the simulation, the initial decrease in the current density is due to the change in the oxygen concentration. However, once enough water is generated to hydrate the membrane, the increased conductivity yields higher local current densities. What
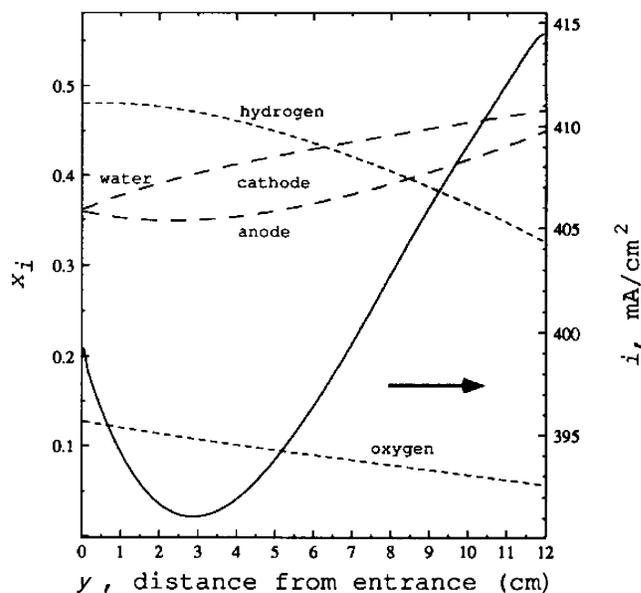
Figure 17. Mole fraction of water vapor, hydrogen, and oxygen in the gas channels at a cell potential of 0.72 V, at a temperature of 80 °C, and in a coflow arrangement. The local current density is shown by the solid line. (Reproduced with permission from ref 15. Copyright 1993 The Electrochemical Society, Inc.)

the figure shows is that these effects are significant, and if one were to use a 1-D model, these effects would be lost. Fuller and Newman also show that the membrane can dehydrate along the channel due to nonisothermal effects.

Because of gas composition changes along the channel, a 2-D model is necessary to describe dry feeds. This is true since not only does the oxygen concentration vary, but, perhaps more importantly, the water does as well. This is seen in Figure 17, where the increase in current density is due to the increase in water in the system. To study this further, Janssen[55] and Weber and Newman[134] ran simulations where the inlet gases were dry and the flow was countercurrent. They studied the water balance of the fuel cell, and some of their results are given in Figure 18. Figure 18a clearly shows that, with countercurrent operation, the water is recycled in that the water produced near the air inlet helps to keep the membrane hydrated near the dry hydrogen inlet. It is noted that Figure 18a is basically a composite of the cases where one gas is fed dry and the other humidified. The 2-D membrane hydration is shown in Figure 18b. This figure clearly shows Schroeder's paradox in the sharp drop off in the water content, where the drop signifies the point where liquid water and the liquid-equilibrated transport mode cease to exist in the membrane. It also shows that the highest water content is near the cathode inlet and that, although the water is recycled, dehydration problems can arise near the hydrogen inlet. However, these simulations assumed uniform current distributions, which is not valid but affects the potential of the cell more than the water balance. Figure 18 also shows that, due to the slower diffusion of water vapor in air than in hydrogen, it is more important for the anode to be humidified. Other models have also reached this conclusion.[16,25,44,47,129]
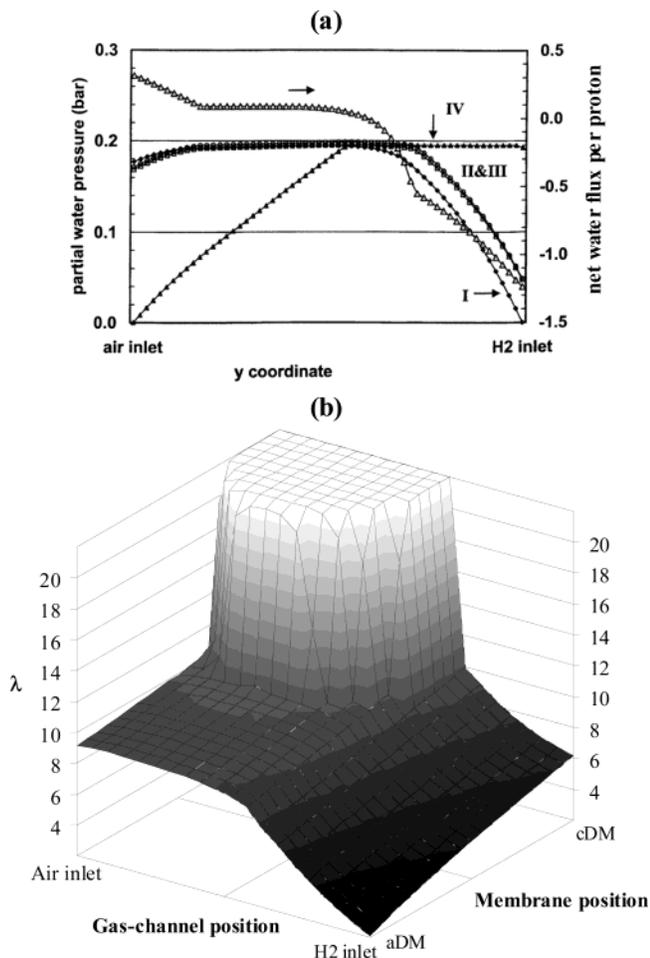
Figure 18. Pseudo-2-D simulation results at 0.4 A/cm² where the feed gases are dry and countercurrent. (a) Water partial pressure profiles at four positions in the fuel-cell sandwich as a function of distance along the channel; the positions are at the anode and cathode gas channels (I and IV) and catalyst layers (II and III), respectively. Also plotted is the value of β, the net flux of water per proton flux, as a function of position. The data are from Janssen.[55] (Reproduced with permission from ref 55. Copyright 2001 The Electrochemical Society, Inc.) (b) Membrane water content as a function of position both along the gas channel and through the thickness of the membrane for the same simulation conditions as above. The data are from Weber and Newman.[134] (Reproduced with permission from ref 55 and 134. Copyright 2004 The Electrochemical Society, Inc.)

The 2-D models also allow for different effects to be studied in depth. For example, the simulations show that, as mentioned above, countercurrent flow yields better performance than coflow due to water recycling.[16,25,44,47,109] This is something that a 1-D model cannot address. The 2-D models also have studied pressure differentials and design strategies to help boost performance.[64,107,109] Finally, the 2-D models allow for optimization studies to be conducted, such as minimizing cost and examining the effects of fuel utilization,[127] and seeing how structural variables change the performance.[16,25,44,47,79] This last is perhaps better addressed with a complex 1-D model rather than a simpler 2-D one.

Overall, effects along the channel are significant and need to be considered. This is especially true in cases where the composition in the gas channel is expected to vary significantly. Some examples of these conditions include low stoichiometry feeds, low humidity feeds, and temperature effects at high current densities. Furthermore, for the cases outlined above, such flow is the most important multidimensional effect. Although full 2-D models do not necessarily have to be done, flow along the channels needs to be accounted for in some fashion.

5.1.2. Under-the-Rib Models

As shown in Figure 16b, the 2-D rib models deal with how the existence of a solid rib affects fuel-cell performance.[24,37,46,56,57,126,278] They do not examine the along-the-channel effects discussed above. Instead, the relevant dimensions deal with the physical reality that the gas channel/diffusion media interfaces are not continuous. Instead, the ribs of the flow-channel plates break them. These 2-D models focus on the cathode side of the fuel-cell sandwich because oxygen and water transport there have a much more significant impact on performance. This is in contrast to the along-the-channel models that show that the underhumidification of and water transport to the anode are more important than those for the cathode.

As mentioned, the 2-D rib effects are crucial in understanding transport in interdigitated flow fields.[108,232] In these flow fields, the gas channels are not continuous, and thus, the gases must pass through the diffusion media. The benefit of such a configuration is that water removal and reactant gas distribution are better because of the convective flow of gases through the diffusion media. However, such flow also means that there is a much higher pressure drop. Some models, of note those of Nguyen and co-workers,[48,52] Um and Wang,[76] Zhukovsky,[77] and Kazim et al.,[46] have specifically looked at interdigitated flow fields. Their results show the importance of having more gas channels with smaller widths, among other things. Interdigitated flow fields are not discussed further in this review.

The equations for modeling the 2-D rib effects require a domain where the boundary conditions in terms of gas flow and composition are specified only at the channel. At the solid rib, there is no flux of gas and liquid, but all of the electronic current must pass through it. Furthermore, the modeling domain is usually as shown in Figure 16b; thus, only a half channel and rib is modeled, and symmetry conditions can be used to model the other half. Besides those noted above, the boundary conditions and equations are more-or-less the same as those discussed in section 4.

As can be seen in the different boundary conditions, the main effects of having ribs are electronic conductivity and transport of oxygen and water, especially in the liquid phase. In terms of electronic conductivity, the diffusion media are mainly carbon, a material that is fairly conductive. However, for very hydrophobic or porous gas-diffusion layers that have a small volume fraction of carbon, electronic conductivity can become important. Because the electrons leave the fuel cell through the ribs, hot spots can develop with large gradients in electron flux density next to the channel.[37,124] Furthermore, if the conductivity of the gas-diffusion layer becomes too small, a

nonuniform reaction distribution can be generated with the highest rate occurring across from the ribs.[37,124]

Although usually the transport of electrons is not limiting, the transport of oxygen can be. For example, at high overpotentials or low oxygen concentrations, the oxygen has a much higher concentration across from the channels and not the ribs.[37,56,278] What this means is that once again a nonuniform reaction distribution is generated, which results in a nonuniform current distribution and all of the associated effects with it (e.g., hot spots, flooding, membrane dehydration, etc.). Under these circumstances, mass transport is an important consideration. Oxygen diffusion is expected to cause the above problems, which are exacerbated by the presence of liquid water.

Figure 18 shows that, even when the cathode is relatively dry, liquid water exists in the cathode. What the 2-D rib models show is that this liquid water cannot be effectively removed if it is next to the rib because it has no way to get out of the cell.[24,56,126] In fact, this effect is perhaps more important in generating nonuniform reaction-rate distributions. Simulation results from Natarajan and Nguyen,[56] shown in Figure 19, clearly demonstrate the entrainment of liquid water in the gas-diffusion layer next to the rib. In fact, Figure 19a shows that the diffusion medium next to the rib is fully flooded. They correlated a more uniform reaction-rate distribution with a decrease in the extent of flooding. Furthermore, they showed that these effects become less important at higher cell potentials because the fuel cell operates in the kinetic regime in which mass-transport limitations are only minor (see Figure 3).

It is clear that the ribs can have a detrimental effect on fuel-cell performance by creating a nonuniform current distribution due to poor mass transfer of oxygen. This is shown in detail in Figure 19b, where the current distribution is shown for different rib and channels sizes. Clearly, the smaller channels and ribs provide more uniform current distributions. This is because there are smaller regions of flooding, since the water has more pathways to leave the gas-diffusion layer and enter the channel. This effect has also been modeled by others.[24,126] It is also interesting that, although the gas-diffusion layer is flooding, the ribs also are making sure the membrane is better hydrated due to the increased liquid pressure throughout the gas-diffusion layer. Consequently, there is a tradeoff between decreased ohmic losses in the membrane and mass-transfer limitations in the cathode diffusion medium. For dry systems, ribs might actually help performance, while, for saturated systems, they only hinder it.

Overall, the rib effects are important when examining the water and local current distributions in a fuel cell. They also clearly show that diffusion media are necessary from a transport perspective. The effect of flooding of the gas-diffusion layer and water transport is more dominant than the oxygen and electron transport. These effects all result in non-uniform reaction-rate distributions with higher current densities across from the channels. Such analysis can lead to optimized flow fields as well as
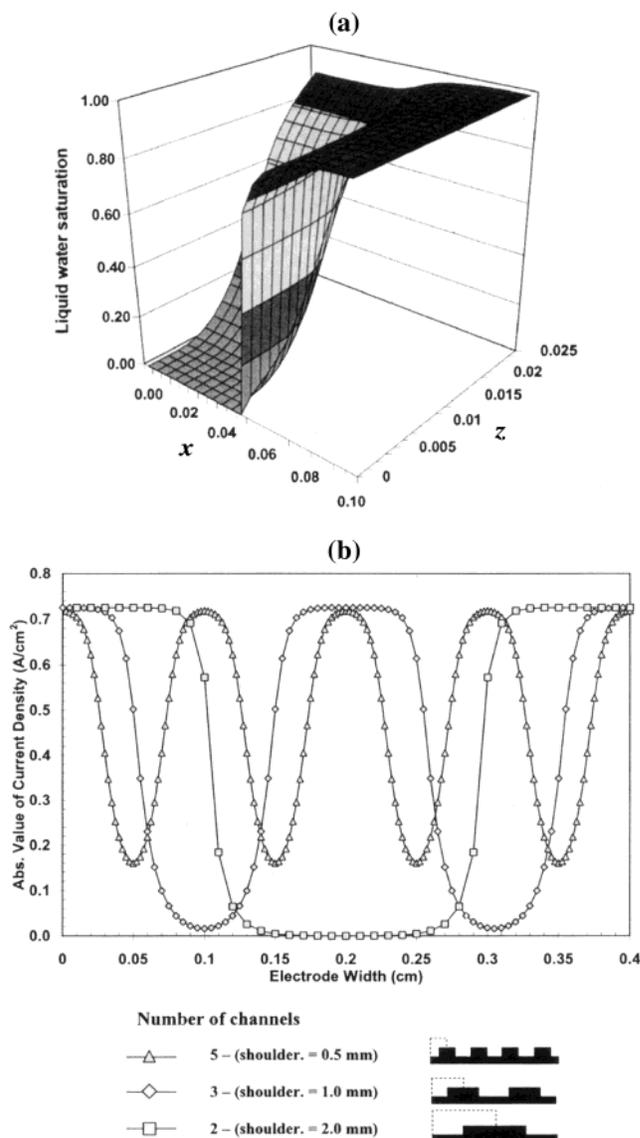
Figure 19. Liquid saturation and current density of the cathode as a function of position for the case of dry air fed at 60 °C. (a) Liquid saturation in the gas-diffusion layer where the channel goes from $x = 0$ to 0.05 cm and the rib is the rest; the total cathode overpotential is −0.5 V. (b) Current-density distributions for different channel/rib arrangements. (Reproduced with permission from ref 56. Copyright 2001 The Electrochemical Society, Inc.)

perhaps catalyst layers in terms of placing catalyst only where higher reaction rates are expected (i.e., minimize catalyst loading).

5.2. Three-Dimensional Models

The 3-D models try to capture all of the effects mentioned above, in both 2-D directions as well as in the 1-D sandwich.[51,54,60,76,77,80,82,87,119,124,125,279−281] The domain is as shown in Figure 1. 3-D models have the potential to accurately represent the true operation of a fuel cell. In principle, these models are the ones that should be used to obtain the best designs and optimization of various properties and operating conditions. However, while the current published models are complex on an overall global scale, they are usually not very detailed on the 1-D sandwich scale. For example, almost all of these models have

neither a robust membrane model nor a rigorous two-phase model. In addition, validation of these models is usually done by comparing only one polarization curve (normally because of the computational costs of the models), which may or may not be representative of the regimes in which the models are run.[84]

In terms of modeling, the equations are the same as those in section 4, with perhaps some simplifications. Additional boundary conditions are required due to the higher dimensionality of the equations, but these are relatively straightforward, such as no fluxes of gas species across the external boundary of the gas channels.

The general results of the 3-D models are more-or-less a superposition of the 2-D models discussed above. Furthermore, most of the 3-D models do not show significant changes in the 1-D sandwich in a local region. In other words, a pseudo-3-D approach would be valid in which the 1-D model is run at points in a 2-D mesh wherein both the channel and rib effects can easily be incorporated. Another pseudo-3-D approach is where the 2-D rib models are used and then moved along the channel, similar to the cases of the pseudo-2-D models described above.[87] This latter approach is similar to that by Baker and Darling.[281] In their model, they uncouple the different directions such that there is a 1-D model in the gas channel and multiple 2-D rib models. However, they neither treat the membrane nor have liquid water. In all, the use of CFD means that it is not significantly more complicated to run a complete 3-D model in all domains.

The 3-D models show that the flooding problems associated with the ribs and the oxygen depletion along the channel compound each other.[69,82,87] Thus, flooding is worse across from the ribs, and the reaction rate distribution is more nonuniform. However, as mentioned above, for nonhumidified feeds, the effects down the channel are more significant. This is seen in Figure 20, where the local current density can be associated with the oxygen concentration. Although the rib scale is a little hard to discern, there is a definite change in the current density along the length scale. The highest current density is obtained at the inlet because the cathode is less flooded and the oxygen concentration is highest. The current density drops and then increases near the exit due to the increase in the back flux of water from cathode to anode and a fully hydrated membrane. The figure clearly shows that there is an entrance region with large nonuniformities. The compounding of the 2-D effects shown by the 3-D models also results in the 2-D models underpredicting the water removal rate. This means that saturations are higher than expected in the diffusion media.[85]

In addition, the models demonstrated that the water balance is important and can alter potential and reactant location.[51,54,60] For example, the reaction distribution is closer to the channel than the rib near the inlet regions for humidified feeds. The reason is that, as the water moves from anode to cathode, there is more flooding, but the movement of water in this direction decreases along the channel because of lower current densities associated with lower oxygen
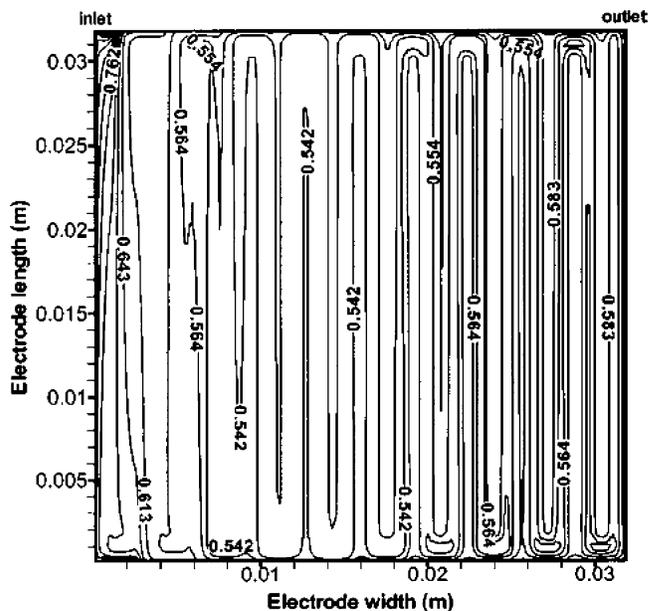
Figure 20. Local current density contours at a cell potential of 0.6 V for cocurrent flow of dry air and humidified hydrogen at 65 °C. (Reproduced with permission from ref 82. Copyright 2003 The Electrochemical Society, Inc.)

concentrations. In the same fashion, the 3-D models also show that ribs are beneficial if the anode is fed dry because of better membrane hydration, and again, this mainly occurs in an entrance region.[81] 3-D simulations with and without liquid water clearly show that, for humidified feeds, liquid water must be accounted for, especially if operating in the mass-transfer regime of the polarization curve.[84,85]

One of the benefits of a 3-D model is the ability to examine the effect of flow-field design. For example, Kumar et al.[279,280] showed that having hemispherical channels provides more convective flow through the gas-diffusion layers and better overall fuel-cell performance. Furthermore, they showed that there are benefits to having flow channels that have a saturated permeability comparable to that of the diffusion media. Once again, in these cases there is more convective-type flow through the diffusion media. Both of the above designs try to mimic interdigitated flow channels to a certain extent. Baker and Darling[281] showed that there is more convective flow through the diffusion media farther away from the U-turns in serpentine flow fields. They also demonstrated that at high current densities the flow field acts more as a single pass than at low current densities where the concentration is more uniform due to higher transport through the diffusion media between adjacent channels.

The inclusion of multidimensional effects is important to realistically mimic transport in the fuel cell. This is not to say that certain cases and factors cannot be collapsed to lower dimensionality, but one must be aware of higher dimensional effects, lest they become important.

6. Other Effects

To complete the discussion of the macroscopic fuel-cell models, two other effects should be examined. These effects can be important, have not really been

discussed so far, and alter the system of governing equations. The first effect is taking into account transport and generation of heat in the fuel cell. The reaction is an oxidation process that generates heat, mainly because of irreversibilities. Water condensation and evaporation are also important heat sources and sinks. The second effect is transient operation of a fuel cell. This is important in many instances such as automotive applications, where fuel cells are expected to undergo transients, especially during acceleration, start up, and shut down.

6.1. Nonisothermal Models

The discussion of nonisothermal effects has been delayed until this section because the models that account for such effects constitute a relatively small subset of the total number of models and have already been discussed above in other contexts.[15,16,25,26,45,60,71,80,82,84−86,90,107,125,126] Furthermore, the complex (i.e., multidimensional) models are the ones that usually take into account temperature effects. One result of the nonisothermal models is that the temperature distribution in the 1-D fuel-cell sandwich is basically uniform (around 1 °C or so), and thus, the isothermal assumption is usually valid for the sandwich. The cases where larger deviations from a uniform temperature distribution occur are in the inlets and outlets of the fuel cell and also depend on operating conditions, such as feed-gas humidity.

When discussing nonisothermal models, the focus is on those models that account for heat generation, consumption, and transfer. A distinction is made between this type of model and those that have properties and parameters that depend on temperature but assume a uniform temperature distribution. Many of the models discussed above fall into this latter category and allow for the effects of operating temperature changes but not a temperature gradient. For most conditions, the change in parameter values with temperature has a more significant impact than accounting for temperature gradients, although the two are coupled to a certain extent.

There are various changes that must be done to include nonisothermal effects. The most important is the addition of an energy conservation equation instead of setting the temperature to a constant; it is discussed below. The other changes are the inclusions of the appropriate thermal effects to the equations described above. To be rigorous, these effects need to be included, but they are usually negligible or are already accounted for. For example, a temperature distribution within an agglomerate can give different values of the effectiveness factor, but due to the size and properties of the agglomerate, it is sufficient to assume that it is at a uniform temperature. Another consideration is that, because the chemical potential is undefined in a nonuniform temperature field, a term must be added to account for this. Thus, a thermodynamically rigorous expression for the driving forces for transport must be used,

$$\mathbf{d}_{i,k} = c_{i,k}[\nabla \mu_{i,k} + \overline{S}_{i,k}\nabla T_k] \tag{67}$$

where $\overline{S}_{i,k}$ is the partial molar entropy of species i.

The addition of the temperature component comes from analysis leading to the Gibbs−Duhem equation.[282] In addition to the above driving force, expressions must be added that result in thermal diffusion.[139] However, because thermal diffusion is small relative to other effects such as conduction, and there are small gradients in temperature in fuel cells, this type of transport can be neglected. Similarly, the effect of diffusion on heat flux, the Dufour effect, is likewise neglected.[139] In addition, heats of mixing for ideal gases are zero, and for the other components they are assumed negligible.[283] Overall, because the above effects are neglected, if one follows the derivations given in section 4, then one obtains the same set of governing equations. Thus, the equations reviewed above remain valid for use in nonisothermal systems, as long as the above assumptions are accepted.

As mentioned, to include nonisothermal effects, an overall thermal energy balance needs to be added to the set of governing equations. The energy conservation equation can be written for phase k in the form[139,149]

$$\rho_k \hat{C}_{pk}\left(\frac{\partial T_k}{\partial t} + \mathbf{v}_k \cdot \nabla T_k\right) +$$
$$\left(\frac{\partial \ln \rho_k}{\partial \ln T_k}\right)_{p_k, x_{i,k}}\left(\frac{\partial p_k}{\partial t} + \mathbf{v}_k \cdot \nabla p_k\right) = Q_{k,p} - \nabla \cdot \mathbf{q}_k -$$
$$\tau : \nabla \mathbf{v}_k + \sum_i \overline{H}_{i,k} \nabla \cdot \mathbf{J}_{i,k} - \sum_i \overline{H}_{i,k} \mathcal{R}_{i,k} \tag{68}$$

In the above expression, the first term represents the accumulation and convective transport of enthalpy, where $\hat{C}_{pk}$ is the heat capacity of phase k. The second term is energy due to reversible work. For condensed phases this term is negligible, and an order-of-magnitude analysis for ideal gases with the expected pressure drop in a fuel cell demonstrates that this term is negligible compared to the others; therefore, it is ignored in all of the models.

The first two terms on the right side of eq 68 represent the net heat input by conduction and interphase transfer. The first is due to heat transfer between two phases

$$Q_{k,p} = h_{k,p} a_{k,p}(T_p - T_k) \tag{69}$$

where $h_{k,p}$ is the heat-transfer coefficient between phases k and p per interfacial area. Most often this term is used as a boundary condition, since it occurs only at the edges. However, in some modeling domains (e.g., along the channel) it may need to be incorporated as above. The second term is due to the heat flux in phase k

$$\mathbf{q}_k = -\sum_i \overline{H}_{i,k}\mathbf{J}_{i,k} - k_{T_k}^{\text{eff}}\nabla T_k \tag{70}$$

where $\overline{H}_{i,k}$ is the partial molar enthalpy of species i in phase k, $\mathbf{J}_{i,k}$ is the flux density of species i relative to the mass-average velocity of phase k

$$\mathbf{J}_{i,k} = \mathbf{N}_{i,k} - c_{i,k}\mathbf{v}_k \tag{71}$$

and $k_{T_k}^{\text{eff}}$ is the effective thermal conductivity of phase k. This means that it was corrected for the volume fraction of the phase by perhaps a Bruggeman equation (eq 42).

The third term on the right side of eq 68 represents viscous dissipation, the heat generated by viscous forces, where τ is the stress tensor. This term is also small, and all of the models except those of Mazumder and Cole[84,85] neglect it. The fourth term on the right side comes from enthalpy changes due to diffusion. Finally, the last term represents the change in enthalpy due to reaction

$$\sum_i \overline{H}_{i,k}\mathscr{R}_{i,k} = -\sum_h a_{1,k}i_{h,1-k}(\eta_{s_{h,1-k}} + \Pi_h) - \\ \sum_{p \neq k}\Delta H_l a_{k,p}r_{l,k-p} - \sum_g \Delta H_g R_{g,k} \quad (72)$$

where the expressions can be compared to those in the conservation-of-mass equation (eq 23). The above reaction terms include homogeneous reactions, interfacial reactions (e.g., evaporation), and interfacial electron-transfer reactions. The latter contains expressions for both the reversible and irreversible heat generation due to electrochemical reaction, as derived by Newman and Thomas-Alyea.[284] The irreversible heat generation is represented by the surface overpotential. The reason the electrode overpotential, which contains a surface overpotential, is not used is that the generation of heat is due to the reaction at the interface; thus, a reference electrode next to the interface is used. This point is discussed further below. The reversible heat generation is represented by the second term, Π_h, which is the Peltier coefficient for charge-transfer reaction h[285] and can be expressed as[284]

$$\Pi_h \approx \frac{T}{n_h F}\sum_i s_{i,k,h}\overline{S}_{i,k} = T\frac{\Delta S_h}{n_h F} \quad (73)$$

where ΔS_h is the entropy of reaction h. The above equation neglects transported entropy (hence, the approximate sign), and the summation includes all species that participate in the reaction (e.g., electrons, protons, oxygen, hydrogen, water). The models that take into account reversible heating either use values for ΔS_h for the two fuel-cell half reactions[26,45,71,80,90,125] or just do an overall energy balance where the total fuel-cell reaction entropy is used.[15,16,65,107]

Almost all of the models assume local thermal equilibrium between the various phases. The exceptions are the models of Berning et al.,[80,125] who use a heat-transfer coefficient to relate the gas temperature to the solid temperature. While this approach may be slightly more accurate, assuming a valid heat-transfer coefficient is known, it is not necessarily needed. Because of the intimate contact between the gas, liquid, and solid phases within the small pores of the various fuel-cell sandwich layers, assuming that all of the phases have the same temperature as each other at each point in the fuel cell is valid. Doing this eliminates the phase dependences in the above equations and allows for a single thermal energy equation to be written.

The assumption of local thermal equilibrium also means that an overall effective thermal conductivity is needed, because there is only a single energy equation. One way to calculate this thermal conductivity is to use Bruggeman factors,

$$k_T^{\text{eff}} = \sum_k \epsilon_k^{1.5}k_{T_k} \quad (74)$$

an expression that assumes that thermal conduction in the phases is in parallel. Some other models take the average as[25,80,84,85,125]

$$k_T^{\text{eff}} = -2k_s + \frac{1}{\dfrac{\epsilon_0}{2k_s + k_G} + \dfrac{1 - \epsilon_0}{3k_G}} \quad (75)$$

where k_G and k_s are the thermal conductivities of the gas and solid (both conductive and nonconductive components) phases, respectively. A final way to calculate an effective thermal conductivity is to realize that the thermal conductivity of the solid is the larger and use that value,[26,45,65] although the porosity and tortuosity should be considered for the different solid phases.

Most of the models use a simplified analogue of eq 68 where eqs 69, 70, and 72 have been substituted into it and local thermal equilibrium is assumed and the equation is summed over phases. The resultant equation is then further simplified for fuel cells

$$\sum_k \rho_k \hat{C}_{p_k}\left(\frac{\partial T}{\partial t} + \mathbf{v}_k\cdot\nabla T\right) = \sum_k h_{k,\text{ext}}a_{k,\text{ext}}(T_{\text{ext}} - T) + \\ \nabla\cdot(k_T^{\text{eff}}\nabla T) - \sum_k\sum_i \mathbf{J}_{i,k}\cdot\nabla\overline{H}_{i,k} + \\ \sum_{1-k}\sum_h a_{1,k}i_{h,1-k}(\eta_{s_{\text{ORR},1-k}} + \Pi_h) + \Delta H_{\text{evap}}r_{\text{evap}} \quad (76)$$

where the evaporation rate is given by eq 39. In the above equation, the summation over species i includes all reacting species including electrons and protons, the summation over $1 - k$ denotes summation over all reaction interfaces between phase k and the electronically conducting solid, and the subscript ext denotes heat transfer that is external to the control volume and is normally found only in the gas channels where there may be a heat-transfer plate, fluid, or reservoir. For boundary conditions, continuity in temperature and thermal flux serve as the internal boundary conditions. For the external boundary conditions, the inlet temperature is specified, and at the edges, either an external heat-transfer relation is used (if not already added into eq 76) or the wall is assumed to be adiabatic. The latter corresponds to a cell inside a stack, and the former to cells in contact with perhaps coolant plates.

In the gas channels, the models have convection of enthalpy, conduction through the graphite plates, and heat transfer to the ambient environment or cooling fluid if that case is being studied.[15,16,65,80,90,107,125,126] In the diffusion layers, there is conduction of heat but no convective motion. There is also no external heat transfer. However, there is Joule heating,[139,164,286] as discussed below. The cata-

lyst layers have the same thermal effects as the diffusion media, except that there is also heat generation, as discussed above. In the membrane, there is conduction, Joule heating, and some enthalpy that is carried by diffusion or convection. While most models account for this, some do not,[60,80,84,85,90,125] and some are only cathode models.[26,86,126] Also, some of the models assume that all of the water from the membrane vaporizes,[60,82,86,90] which consumes a lot of heat and is not necessarily correct; it depends on the membrane model being used and the conditions in the catalyst layer.

Joule heating is due to the passage of current. It can be derived from the third term on the right side of eq 76

$$-\sum_i \mathbf{J}_{i,1} \cdot \nabla \bar{H}_{i,1} = -\mathbf{i}_1 \cdot \nabla \Phi_1 = \frac{\mathbf{i}_1 \cdot \mathbf{i}_1}{\sigma^{eff}} \qquad (77)$$

The above is derived by using the definition of current density and relating the gradients of enthalpy and electrochemical potential for a system of uniform temperature. This type of heating can similarly be calculated for the ionically conducting phase where the ionic conductivity is used instead of the electronic conductivity. Joule heating is important in the membrane because a temperature change can cause an appreciable change in water content if the membrane is close to saturation.[41,63,94] Even though it can be important, not all of the models include it.[26,60,82,86,126]

Equation 76 is valid for local heat generation and analysis. However, there are some models that treat only heat transfer in the gas channels and assume that the fuel-cell sandwich remains isothermal,[15,16,107,129] an assumption that is arguably valid from other simulation results. In this approach, only thermal convection and external heat transfer in the gas channels are used, and an energy balance yields the total energy produced in the fuel-cell sandwich.[164,286,287] This energy balance has the form

$$Q = \sum_{k-p} \sum_h a_{k,p} i_{h,k-p} (U_{H_h} - V) \qquad (78)$$

where Q is the total heat generated per unit volume, V is the (observed) cell potential, the summations are over all the electron-transfer reactions and interfaces, and U_{H_h} is the enthalpy potential for reaction h,

$$U_{H_h} = \frac{\Delta H_h}{n_h F} = U_h - T \frac{\partial U_h}{\partial T} \qquad (79)$$

and is a function of temperature. Equation 78 is simple to use, since the necessary quantities are relatively easy to obtain. This is especially true if only a single fuel-cell reaction occurs, wherein the enthalpy of the overall reaction can be used directly with the observed current density per unit volume to yield Q. Equation 78 is good if just the amount, and not the precise location of heat generation, is required. An example is a pseudo-2-D model where
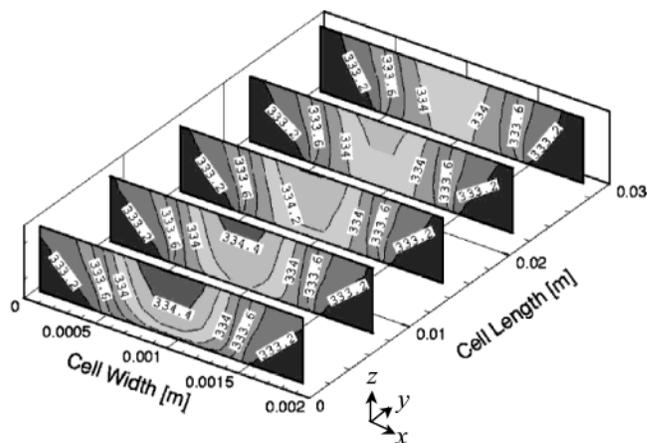
Figure 21. Temperature distribution in kelvin inside the cathode diffusion medium at a current density of 1.2 A/cm² and with saturated feeds. (Reproduced with permission from ref 80. Copyright 2003 The Electrochemical Society, Inc.)

the 1-D sandwich is taken to be isothermal and only the total heat generated in each sandwich layer is required.

Equation 78 can be used to show that the concentration overpotential due to gas diffusion does not generate heat. To do this, a virtual experiment is setup. First, the total amount of heat generation of a complete fuel cell is calculated. Next, one imagines that diffusion media are added to the fuel cell in such a way that the partial pressure of the reactant gases and all ohmic effects remain the same within the catalyst layers and fuel cell. Hence, only the partial pressures of the gases in the gas channels increase. According to eq 78, since the conditions are identical in the fuel cell, the heat generation is the same (i.e., no terms change). In other words, there is no heat generation due to this concentration overpotential. This can also be seen if the cell potential is divided into a summation of various overpotentials, where the effect of changing gas concentration in the diffusion media cancels. However, if the gases are not ideal, then some heat will be generated through the $\mathbf{J}_{i,1} \cdot \nabla \bar{H}_{i,1}$ term in eq 76.

The nonisothermal models allow for detailed temperature distributions to be generated, as shown in Figure 21. In the figure, the temperature is highest in the channel and decreases along the channel, because the rib has a higher thermal conductivity and the reaction rate is higher closer to the channel inlet. These effects have been seen with other models.[60,65,80] Although the temperature gradient is not large, it is greater in the cell sandwich than along the gas channel. The main reason is that condensation is occurring in the diffusion medium, which releases heat in addition to that released at the reaction sites. Whether the temperature is largest along the channel or in the sandwich depends on the length of the channels, the boundary conditions set at the channels (i.e., insulating or conductive), and the operating conditions. For example, with dry-gas feeds, the temperature gradients along the channel become larger, and the inlet region becomes susceptible to membrane dehydration, as seen with some

of the other models (for examples, see refs 15 and 60).

Overall, the models show that nonisothermal effects mainly influence the water balance and current distribution. The water balance affects the competition between membrane dehydration and mass-transfer limitations, both of which are functions of temperature. Because water vaporization has a high enthalpy change, the models that do not take into account liquid water and evaporation/condensation reactions[15,84,90,126] cannot explore many significant heat effects. On the other hand, models that always have a fully hydrated membrane are valid for only specific circumstances where there is always liquid water.[25,80,84,85,125] As discussed in the previous sections, this does not occur often, especially at the anode. Thus, a full membrane model is required, especially since membrane dehydration and temperature rise exacerbate each other.[65,128] In addition, pressure and temperature gradients can combine to produce significant effects on water management through evaporation and condensation of water (i.e., changing the partial pressure and vapor pressure of water).

To be complete in understanding and modeling water management, especially on a multidimensional or stack level, nonisothermal effects should be included. However, it is an adequate first approximation to assume that a sandwich and perhaps even a single cell are isothermal, as long as the dependence of the various parameters on temperature is included in the model. Finally, to be rigorous, some of the thermal effects assumed to be negligible could be added, such as heats of mixing of species into the membrane, temperature effects in the catalyst agglomerates, and thermal diffusion.

6.2. Transient Models

The other effect considered in this section deals with transients in a single fuel cell. The transient models examine step changes in potential and related phenomena (e.g., gas flow rates, water production, and current density). Hence, they are aimed at examining how a fuel-cell system handles different load requirements, which may occur during automotive operation or start up and shut down. They are not trying to model slow degradation processes that lead to failure or the transients associated with impedance experiments (i.e., potential or current oscillations). These types of models are discussed in section 7.

There are not many models that do transients, mainly because of the computational cost and complexity. The models that do have mainly been discussed above. In terms of modeling, the equations use the time derivatives in the conservation equations (eqs 23 and 68) and there is still no accumulation of current or charging of the double layer; that is, eq 27 still holds. The mass balance for liquid water requires that the saturation enter into the time derivative because it is the change in the water loading per unit time. However, this treatment is not necessarily rigorous because a water capacitance term should also be included,[234] although it can be neglected as a first approximation.

One of the first models to examine transients in polymer-electrolyte fuel cells was a stack-level model by Amphlett et al.[288] Their model is mainly empirical and examines temperature and gas flow rates. They showed that transient behavior lasts for a few minutes in a stack before a new steady state is reached. In a similar stack-level analysis, Yerramalla et al.[289] used a slightly more complicated single-cell model and examined the shape of the transients. They noticed voltage behavior that had oscillations in it and some leakage current. Their overall analysis was geared to the development of a controller for the stack.

In terms of the more complicated single-cell models, which have been discussed in various contexts above, van Bussel et al.[44] mainly examined the transient behavior of the water content of the membrane with their model. They clearly showed that coflow operation with dry gases as well as counterflow with dry gases and high stoichiometries all lead to cases where the membrane dries out and the fuel cell cannot operate for more than a few minutes. This analysis shows that the drying out of the membrane is a much faster process in an operating fuel cell than with a naked membrane, where dehydration occurs over a much longer time scale.[290] The modeling results also agreed with the transient uptake model of Nguyen and Vanderborgh,[291] which also showed that the initial development of the membrane water profile required a few minutes.

Um et al.[64] also examined a transient using their complex model. They saw that in a matter of tens of seconds the current density response reached steady state after a change in potential. However, their model did not include liquid water. The most complex model to examine transients is that of Natarajan and Nguyen.[56] It should be noted that although the model of Bevers et al.[26] has transient equations, they do not report any transient results. Natarajan and Nguyen included liquid saturation effects and water transport in their model. They clearly showed the flooding of the diffusion media and that it takes on the order of a couple of minutes for the profiles to develop.

The above models clearly demonstrated that the transient response of the electrical phenomena in a fuel cell is fast. The limiting time constant in the fuel cell is the liquid-water transport and its associated effects, which agree with experimental findings.[292,293] This time constant causes a slow approach to steady state that can be on the order of tens of minutes in certain circumstances.[292] However, the majority of the change in the parameters of interest (power, current density, etc.) occurs within a much shorter time, and although the approach due to liquid water is long, the overall change in the parameter values is minor. For example, with a change in potential, the current density will reach a significant fraction of its steady-state value in a short time and then slowly decay toward it.

Some other general comments can also be made. For a stack, the interconnectivity of the cells means that the overall response will exhibit slower time constants than those for a single cell. However, the stack response (at least in terms of electrical vari-

ables) is still probably faster than the responses of the other components in the fuel-cell system such as compressors and so forth (for example, see ref 294). In the final analysis, as a first try, transient behavior of a fuel cell can be adequately modeled using a pseudo-steady-state model. This type of approach would involve stepping the single-cell model through various steady states, where the operating conditions such as potential, current, or flow rates change. Of course, the stepping rate would have to be determined. The approach is the same as assuming instantaneous achievement of steady state, or in other words infinitesimal time constants. If more specific phenomena need to be described such as liquid-water transport, then a full transient model should be used. Finally, due to load-leveling devices and possible hybridization of a fuel-cell system, transient models should be explored only after the relevant effects described in the preceding sections (e.g., flooding) are examined, or if specific phenomena such as start up from freeze are being considered.

7. Other Models

Other types and aspects of polymer-electrolyte fuel cells have also been modeled. In this section, those models are quickly reviewed. This section is written more to inform than to analyze the various models. The outline of this section in terms of models is stack models, impedance models, direct-methanol fuel-cell models, and miscellaneous models.

As mentioned above, stack models are useful for analyzing full system performance including perhaps auxiliary components in the system such as compressors. In terms of equations, almost all of the models use simple global balances and equations because single cells are not the focus of the models; thus, they use equations similar to eqs 21 and 78. In terms of other equations, normally they use typical flow and heat balances as well as the appropriate current and voltage relations, which take into account how the cells are connected together. The stack models can be separated into two categories, those that consider the stack only[45,288,289,295-299] and those that consider a whole power system.[100,294,300,301]

The models that examine only stacks focus mainly on the temperature distribution within the stack. As mentioned, there is a much higher temperature gradient in the stack than in a single cell, and it provides design information in terms of coolant flow rate, among other things.[45,296,298] Also, as mentioned above, transient effects have also been examined.[288,289] Lee et al.[298,299] examined many different profiles in the stack including temperature, relative humidity, pressure, and current density, and their models can be used to predict flooding and various gradients in the stack. Similarly, the model of Thirumalai and White[297] examined reactant distribution and design of the flow field and manifold.

As mentioned, there are also models of complete fuel-cell power systems in which the stack is but one component. These models have the benefit of examining true designs and the interconnections between components, but they usually require an even weaker model of an individual fuel cell. In fact, the entire fuel-cell stack may be modeled with only single equations in the form of eqs 21 and 78.[100,300] The models show such tradeoffs as compressor power required and performance gain due to pressurized and humidified feeds. In terms of the models, Ahmed et al.[100,300] considered the total water requirements needed both for the fuel cell and for the reformer reactors. Cownden et al.[300] looked mainly at the total system power and saw the effects of compressors, pressure drops, coolant flows, and the efficiencies of the various components in the system. Ahluwalia et al.[301] studied the gain in overall stack performance and design when high-temperature polymer-electrolyte systems are considered. Finally, the model of De Francesco and Arato[294] looks at transients and start-up conditions and procedures. Overall, while the stack models use simplified and usually empirical equations for a single cell, they provide benefits in actually designing operating systems. In these cases, the data for the empirical expressions are known, and complex modeling may not be required.

The next set of models examined in this section is impedance models. Impedance is often used to determine parameters and understand how the fuel cell is operating. By applying only a small perturbation during operation, the system can be studied in situ. There are many types of impedance models. They range from very simple analyses to taking a complete fuel-cell model and shifting it to the frequency domain. The very simple models use a simple equivalent circuit just to understand some general aspects (for examples, see refs 302−304).

The next more complicated models focus on analyzing the impedance spectra using complex equivalent circuits.[103,137,221,305−312] Most of these models use a series of resistors to represent transport in the membrane and diffusion media. The porous electrodes are modeled similarly to Figure 10, with the addition of a double-layer capacitance term in parallel with each charge-transfer resistance. Most of the models show such effects as increased high-frequency resistance as the membrane dehydrates and an increased low-frequency loop as flooding occurs. The model of Wang et al.[306] also considers how carbon monoxide affects performance in the anode. Out of these models, the one of Eikerling and Kornyshev[137] is the most sophisticated. It shows specifically how ohmic and oxygen limitations affect the impedance of the cathode. With such a model, meaningful analysis of experimental impedance plots can be made and governing phenomena noted, as well as the determination of general transport parameters such as the resistance of the membrane.

While a good equivalent-circuit representation of the transport processes in a fuel cell can lead to an increased understanding, it is not as good as taking a 1-D sandwich model and taking it into the frequency domain. These models typically analyze the cathode side of the fuel cell.[102,313,314] The most comprehensive is probably that of Springer et al.[102] The use of impedance models allows for the calculation of parameters, like gas-phase tortuosity, which cannot be determined easily by other means, and can also allow for the separation of diffusion and migra-

tion effects. Overall, impedance is a very powerful experimental tool, but its results are only as good as the model used to analyze it.

The next models that should be mentioned are those for direct-methanol fuel cells.[68,117,130−132,295,315−325] A direct-methanol fuel cell is very similar to the hydrogen fuel cells in this review, with the exception of the fuel. In a direct-methanol fuel cell, methanol is fed instead of hydrogen and reacts according to the reaction

$$CH_3OH + H_2O \rightarrow CO_2 + 6H^+ + 6e^- \quad (80)$$

and the cathode ORR (eq 2) is the same. The design of the fuel cell is the same as the polymer-electrolyte models described above. The methanol reaction is much slower than hydrogen oxidation and is a significant source of performance loss for the direct-methanol fuel cells. However, because methanol is a liquid, the membrane is always fully hydrated. Even though the membrane has better conductivity, a fully hydrated membrane also means that there is a significant amount of methanol crossover. This crossover is one reason that thicker membranes are used in methanol fuel cells than in hydrogen ones. Treatment of the transport phenomena becomes much more complex due to the presence of methanol[130,131] and also because there is liquid on both sides of the fuel cell.

In terms of modeling, all of the different types of models discussed above have been used. The major problems are methanol crossover, flooding, the kinetics of the cathode, and predominately mass-transfer and reaction of methanol at the anode. It is beyond the scope of this review to discuss all of the models for direct-methanol fuel cells. The major ones are listed in the references and have been mentioned here only because of their similarity to those discussed in this article. The governing phenomena and equations are basically the same with only slight variations to take into account methanol in the membrane, different anode kinetics, and diffusion of methanol in water instead of hydrogen in water vapor. It should be noted that direct-methanol fuel cells are being considered for portable applications due to their more energy-dense fuel and simple liquid-injection systems, among other things.

Finally, there are some miscellaneous polymer-electrolyte fuel cell models that should be mentioned. The models of Okada and co-workers[42,43,326] have examined how impurities in the water affect fuel-cell performance. They have focused mainly on ionic species such as chlorine and sodium and show that even a small concentration, especially next to the membrane at the cathode, impacts the overall fuel-cell performance significantly. There are also some models that examine having free convection for gas transfer into the fuel cell.[327−329] These models are also for very miniaturized fuel cells, so that free convection can provide enough oxygen. The models are basically the same as the ones above, but because the cell area is much smaller, the results and effects can be different. For example, free convection is used for both heat transfer and mass transfer, and the small

length scale means that such effects as Knudsen diffusion and water droplet formation and flooding can be more important. These models are normally 3-D and focus more on the flow-field design and the gas channels than on the complex relationships within the fuel-cell sandwich.

The final group of models is those that incorporate possible failure mechanisms.[330−333] These failure mechanisms are time or condition dependent and are not the same as the effects examined in earlier sections, such as carbon monoxide poisoning, that was also valid for steady-state operation. The model by Darling and Meyers[330] examined platinum catalyst loss as the potential is cycled. This is something that has also been observed in phosphoric-acid fuel cells[334,335] and can occur during start up and shut down. Similar to the case of the Darling and Meyers model, Wendt et al.[331] examined catalyst aging due to changing catalyst morphology and, to a lesser extent, accumulation of impurities. The models of Jiang and Chu[332] and Fowler et al.[333] examined slow voltage degradation over time for a cell stack and a single cell, respectively. They do this by including time-dependent rate constants for the kinetic reactions as well as a membrane deterioration term that limits the maximum water content of the membrane. Both use semiempirical equations to model the fuel-cell behavior, but they are some of the first to model fuel-cell failure. The above models are notable because durability issues are becoming increasingly significant and have not received much attention in the literature either theoretically or experimentally (for examples, see refs 336−338).

8. Summary

In this review, we have examined the different models for polymer−electrolyte fuel cells operating with hydrogen. The major focus has been on transport of the various species within the fuel cell. The different regions of the fuel cell were examined, and their modeling methodologies and equations were elucidated. In particular, the 1-D fuel-cell sandwich was discussed thoroughly because it is the most important part of the fuel-cell assembly. Models that included other effects such as temperature gradients and transport in other directions besides through the fuel-cell sandwich were also discussed.

Models were not directly compared to each other; instead they were broken down into their constitutive parts. The reason for this is that validation of the models is usually accomplished by comparison of simulation to experimental polarization data (e.g., Figure 3). However, other data can also be used such as the net flux of water through the membrane. In fitting these data, the models vary not only in their complexity and treatments but also in their number and kind of fitting parameters. This is one reason it is hard to justify one approach over another by just looking at the modeling results. In general, it seems reasonable that the more complex models, which are based on physical arguments and do not contain many fitting parameters, are perhaps closest to reality. Of course, this assumes that they fit the experimental data and observations. This last point

has been overlooked in the validation of many models. For example, a model may fit the data very well for certain operating conditions, but if it does not at least predict the correct trend when one of those conditions is changed, then the model is shown to be valid only within a certain operating range.

This review has highlighted the important effects that should be modeled. These include two-phase flow of liquid water and gas in the fuel-cell sandwich, a robust membrane model that accounts for the different membrane transport modes, nonisothermal effects, especially in the directions perpendicular to the sandwich, and multidimensional effects such as changing gas composition along the channel, among others. For any model, a balance must be struck between the complexity required to describe the physical reality and the additional costs of such complexity. In other words, while more complex models more accurately describe the physics of the transport processes, they are more computationally costly and may have so many unknown parameters that their results are not as meaningful. Hopefully, this review has shown and broken down for the reader the vast complexities of transport within polymer-electrolyte fuel cells and the various ways they have been and can be modeled.

9. Acknowledgments

10. Nomenclature

a_i^α	activity of species i in phase α
$a_{k,p}$	interfacial surface area between phases k and p per unit volume, 1/cm
$a_{1,2}^\circ$	interfacial area between the electronically conducting and membrane phases with no flooding, 1/cm
A_{agg}	specific external surface area of the agglomerate, 1/cm
A_{Pt}	reactive surface area of platinum, cm²/g
b	Tafel slope, defined by eq 14 for the ORR, V
$c_{i,k}$	interstitial concentration of species i in phase k, mol/cm³
c_T	total solution concentration or molar density, mol/cm³
$\hat{C}_{pk}$	heat capacity of phase k, J/g·K
$\mathbf{d}_i$	driving force per unit volume acting on species i in phase k, J/cm⁴
D_i	Fickian diffusion coefficient of species i in a mixture, cm²/s
D_S	capillary diffusivity, cm²/s
$D_{i,j}$	diffusion coefficient of i in j, cm²/s
D_{K_i}	Knudsen diffusion coefficient of species i, cm²/s
E	effectiveness factor
F	Faraday's constant, 96 487 C/equiv
g	acceleration due to gravity, cm/s²
$h_{k,p}$	heat-transfer coefficient between phases k and p, J/cm²·s·K
$\overline{H}_{i,k}$	partial molar enthalpy of species i in phase k, J/mol
$H_{i,j}$	Henry's constant for species i in component j, mol/cm³·kPa

ΔH_l	heat or enthalpy of reaction l, J/mol
i	superficial current density through the membrane, A/cm²
$\mathbf{i}_k$	current density in phase k, A/cm²
i_{0_h}	exchange current density for reaction h, A/cm²
$i_{h,k-p}$	transfer current density of reaction h per interfacial area between phases k and p, A/cm²
i_{lim}	limiting current density, A/cm²
$\mathbf{J}_{i,k}$	flux density of species i in phase k relative to the mass-average velocity of phase k, mol/cm²·s
k	effective hydraulic permeability, cm²
k'	ORR rate constant as defined by eq 61, 1/s
k^*	ORR rate constant in Figure 11, cm/s
k_{T_k}	thermal conductivity of phase k, J/cm²·K
k_r	relative hydraulic permeability
k_{sat}	saturated hydraulic permeability, cm²
k_Φ	electrokinetic permeability, cm²
L	catalyst layer thickness, cm
m	parameter in the polarization equation (eq 20)
m_{Pt}	loading of platinum, g/cm²
M_i	molecular weight of species i, g/mol
$M_i^{z_i}$	symbol for the chemical formula of species i in phase k having charge z_i
n	parameter in the polarization equation (eq 20)
n_h	number of electrons transferred in electrode reaction h
$\mathbf{N}_{i,k}$	superficial flux density of species i in phase k, mol/cm²·s
p_i	partial pressure of species i, kPa
p_C	capillary pressure, kPa
p_k	total pressure of phase k, kPa
p_w^{vap}	vapor pressure of water, kPa
$\mathbf{q}_k$	superficial heat flux through phase k, J/cm²·s
Q	total amount of heat generated, J/cm²·s
$Q_{k,p}$	heat flux transferred between phases k and p, J/cm³·s
r	pore radius, cm
r_{evap}	rate of evaporation, mol/cm³·s
$r_{l,k-p}$	rate of reaction l per unit of interfacial area between phases k and p, mol/cm²·s
R	ideal-gas constant, 8.3143 J/mol·K
R_{agg}	agglomerate radius, cm
$R_{g,k}$	rate of homogeneous reaction g in phase k, mol/cm³·s
$R_{i,j}$	resistance of resistor i,j in Figure 10 where ct stands for charge-transfer, Ω·cm²
R'	total ohmic resistance, Ω·cm²
$\mathscr{R}_{i,k}$	total rate of reaction of species i in phase k, mol/cm³·s
$s_{i,k,l}$	stoichiometric coefficient of species i in phase k participating in reaction l
S	liquid saturation
$\overline{S}_{i,k}$	molar entropy of species i in phase k, J/mol·K
ΔS_h	entropy of reaction h, J/mol·K
t	time, s
T	absolute temperature, K
T_k	absolute temperature of phase k, K
u_i	mobility of species i, cm²·mol/J·s
U_h	reversible cell potential of reaction h, V
U'	potential intercept for a polarization equation, V
U_h^θ	standard potential of reaction h, for oxygen reduction, 1.229 V at 25 °C
U_{H_h}	enthalpy potential, V
$\mathbf{v}_k$	superficial velocity of phase k, cm/s
V	cell potential, V
$\overline{V}_i$	(partial) molar volume of species i, cm³/mol
$W_{O_2}^{diff}$	molar flow rate of oxygen to the agglomerate, mol/cm³·s
x	distance across the flow field, cm
$x_{i,k}$	mole fraction of species i in phase k

y	distance along the flow-field channel, cm
z	distance across the cell sandwich, cm
z_i	valence or charge number of species i

Greek Letters

α_a	anodic transfer coefficient
α_c	cathodic transfer coefficient
α_w	water transport coefficient, $mol^2/J \cdot cm \cdot s$
β	net water flux per proton flux through the membrane
γ	surface tension, N/cm
δ_n	diffusion length or thickness of region n, cm
ζ	characteristic length, cm
ϵ_k	volume fraction of phase k
ϵ_0	bulk porosity
ν_k	kinematic viscosity of phase k, cm^2/s
ξ	electroosmotic coefficient
Π_h	Peltier coefficient for charge-transfer reaction h, V
ρ_k	density of phase k, g/cm^3
σ_0	standard conductivity in the electronically conducting phase, S/cm
$\eta_{h,k-p}$	electrode overpotential of reaction h between phases k and p (see eq 10), V
$\eta_{s_{h,k-p}}$	surface overpotential of reaction h between phases k and p (see eq 11), V
η^*	dimensionless overpotential in Figure 11
θ	contact angle, deg
κ	conductivity of the ionically conducting phase, S/cm
λ	moles of water per mole of sulfonic acid sites
λ_L	relative mobility of the liquid phase
μ	viscosity, Pa·s
μ_i	(electro)chemical potential of species i, J/mol
μ_i^α	electrochemical potential of species i in phase α, J/mol
τ	stress tensor, kPa
τ_k	tortuosity of phase k
ϕ	Thiele modulus, defined by eq 60 for the ORR
Φ_k	potential in phase k, V
ψ	dimensionless parameter in Figure 11

Subscripts/Superscripts

1	electronically conducting phase
2	ionically conducting phase
agg	agglomerate
CL	catalyst layer
eff	effective value, corrected for tortuosity and porosity
ext	external to the control volume
f	fixed ionic site in the membrane
film	film covering the agglomerate
g	homogeneous reaction number
G	gas phase
h	electron-transfer reaction number
HOR	hydrogen-oxidation reaction
i	generic species
j	generic species
k	generic phase
l	heterogeneous reaction number
L	liquid phase
m	mixture
ORR	oxygen-reduction reaction
p	generic phase
ref	parameter evaluated at the reference conditions
s	solid phase
w	water

11. References

(1) Giner, J.; Hunter, C. *J. Electrochem. Soc.* **1969**, *116*, 1124.
(2) Cutlip, M. B. *Electrochim. Acta* **1975**, *20*, 767.
(3) Cutlip, M. B.; Yang, S. C.; Stonehart, P. *J. Electrochem. Soc.* **1986**, *133*, C299.
(4) Cutlip, M. B.; Yang, S. C.; Stonehart, P. *Electrochim. Acta* **1991**, *36*, 547.
(5) Iczkowski, R. P.; Cutlip, M. B. *J. Electrochem. Soc.* **1980**, *127*, 1433.
(6) Newman, J.; Tiedemann, W. *AIChE J.* **1975**, *21*, 25.
(7) Newman, J. S.; Tobias, C. W. *J. Electrochem. Soc.* **1962**, *109*, 1183.
(8) Paganin, V. A.; Ticianelli, E. A.; Gonzalez, E. R. *J. Appl. Electrochem.* **1996**, *26*, 297.
(9) Parthasarathy, A.; Srinivasan, S.; Appleby, A. J.; Martin, C. R. *J. Electrochem. Soc.* **1992**, *139*, 2530.
(10) Parthasarathy, A.; Srinivasan, S.; Appleby, A. J.; Martin, C. R. *J. Electrochem. Soc.* **1992**, *139*, 2856.
(11) Ticianelli, E. A.; Derouin, C. R.; Redondo, A.; Srinivasan, S. *J. Electrochem. Soc.* **1988**, *135*, 2209.
(12) Kim, J.; Lee, S. M.; Srinivasan, S.; Chamberlin, C. E. *J. Electrochem. Soc.* **1995**, *142*, 2670.
(13) Bernardi, D. M.; Verbrugge, M. W. *J. Electrochem. Soc.* **1992**, *139*, 2477.
(14) Springer, T. E.; Zawodzinski, T. A.; Gottesfeld, S. *J. Electrochem. Soc.* **1991**, *138*, 2334.
(15) Fuller, T. F.; Newman, J. *J. Electrochem. Soc.* **1993**, *140*, 1218.
(16) Nguyen, T. V.; White, R. E. *J. Electrochem. Soc.* **1993**, *140*, 2178.
(17) Wang, J.-T.; Savinell, R. F. *Electrochim. Acta* **1992**, *37*, 2737.
(18) Chan, D. S.; Wan, C. C. *J. Power Sources* **1994**, *50*, 261.
(19) Rho, Y. W.; Srinivasan, S.; Kho, Y. T. *J. Electrochem. Soc.* **1994**, *141*, 2089.
(20) Amphlett, J. C.; Baumert, R. M.; Mann, R. F.; Peppley, B. A.; Roberge, P. R.; Harris, T. J. *J. Electrochem. Soc.* **1995**, *142*, 1.
(21) Amphlett, J. C.; Baumert, R. M.; Mann, R. F.; Peppley, B. A.; Roberge, P. R.; Harris, T. J. *J. Electrochem. Soc.* **1995**, *142*, 9.
(22) Ticianelli, E. A. *J. Electronanal. Chem.* **1995**, *387*, 1.
(23) Mosdale, R.; Srinivasan, S. *Electrochim. Acta* **1995**, *40*, 413.
(24) West, A. C.; Fuller, T. F. *J. Appl. Electrochem.* **1996**, *26*, 557.
(25) Gurau, V.; Liu, H.; Kakac, S. *AIChE J.* **1998**, *44*, 2414.
(26) Bevers, D.; Wohr, M.; Yasuda, K.; Oguro, K. *J. Appl. Electrochem.* **1997**, *27*, 1254.
(27) Broka, K.; Ekdunge, P. *J. Appl. Electrochem.* **1997**, *27*, 281.
(28) Eikerling, M.; Kornyshev, A. A. *J. Electronanal. Chem.* **1998**, *453*, 89.
(29) de Sena, D. R.; Ticianelli, E. A.; Gonzalez, E. R. *Electrochim. Acta* **1998**, *43*, 3755.
(30) Antoine, O.; Bultel, Y.; Durand, R.; Ozil, P. *Electrochim. Acta* **1998**, *43*, 3681.
(31) Bultel, Y.; Ozil, P.; Durand, R. *J. Appl. Electrochem.* **1998**, *28*, 269.
(32) Bultel, Y.; Ozil, P.; Durand, R. *Electrochim. Acta* **1998**, *43*, 1077.
(33) Bultel, Y.; Ozil, P.; Durand, R. *J. Appl. Electrochem.* **1999**, *29*, 1025.
(34) Gloaguen, F.; Durand, R. *J. Appl. Electrochem.* **1997**, *27*, 1029.
(35) Gloaguen, F.; Convert, P.; Gamburzev, S.; Velev, O. A.; Srinivasan, S. *Electrochim. Acta* **1998**, *43*, 3767.
(36) Perry, M. L.; Newman, J.; Cairns, E. J. *J. Electrochem. Soc.* **1998**, *145*, 5.
(37) Kulikovsky, A. A.; Divisek, J.; Kornyshev, A. A. *J. Electrochem. Soc.* **1999**, *146*, 3981.
(38) Paddison, S. J.; Zawodzinski, T. A. *Solid State Ionics* **1998**, *115*, 333.
(39) Okada, T.; Xie, G.; Meeg, M. *Electrochim. Acta* **1998**, *43*, 2141.
(40) Eikerling, M.; Kharkats, Y. I.; Kornyshev, A. A.; Volfkovich, Y. M. *J. Electrochem. Soc.* **1998**, *145*, 2684.
(41) Futerko, P.; Hsing, I. M. *J. Electrochem. Soc.* **1999**, *146*, 2049.
(42) Okada, T. *J. Electroanal. Chem.* **1999**, *465*, 1.
(43) Okada, T. *J. Electroanal. Chem.* **1999**, *465*, 18.
(44) van Bussel, H.; Koene, F. G. H.; Mallant, R. *J. Power Sources* **1998**, *71*, 218.
(45) Wohr, M.; Bolwin, K.; Schnurnberger, W.; Fischer, M.; Neubrand, W.; Eigenberger, G. *Int. J. Hydrogen Energy* **1998**, *23*, 213.
(46) Kazim, A.; Liu, H. T.; Forges, P. *J. Appl. Electrochem.* **1999**, *29*, 1409.
(47) Singh, D.; Lu, D. M.; Djilali, N. *Int. J. Eng. Sci.* **1999**, *37*, 431.
(48) Yi, J. S.; Nguyen, T. V. *J. Electrochem. Soc.* **1999**, *146*, 38.
(49) Boyer, C. C.; Anthony, R. G.; Appleby, A. J. *J. Appl. Electrochem.* **2000**, *30*, 777.
(50) Baschuk, J. J.; Li, X. *J. Power Sources* **2000**, *86*, 181.
(51) Dutta, S.; Shimpalee, S.; Van Zee, J. W. *J. Appl. Electrochem.* **2000**, *30*, 135.
(52) He, W.; Yi, J. S.; Nguyen, T. V. *AIChE J.* **2000**, *46*, 2053.
(53) Chan, S. H.; Tun, W. A. *Chem. Eng. Technol.* **2001**, *24*, 51.
(54) Dutta, S.; Shimpalee, S.; Van Zee, J. W. *Int. J. Heat Mass Transfer* **2001**, *44*, 2029.
(55) Janssen, G. J. M. *J. Electrochem. Soc.* **2001**, *148*, A1313.
(56) Natarajan, D.; Nguyen, T. V. *J. Electrochem. Soc.* **2001**, *148*, A1324.
(57) Wang, Z. H.; Wang, C. Y.; Chen, K. S. *J. Power Sources* **2001**, *94*, 40.
(58) Wang, C. Y.; Cheng, P. *Int. J. Heat Mass Transfer* **1996**, *39*, 3607.
(59) Wang, C. Y.; Cheng, P. *Adv. Heat Transfer* **1997**, *30*, 93.

(60) Shimpalee, S.; Dutta, S. *Numer. Heat Transfer, Part A* **2000**, *38*, 111.
(61) Hsing, I. M.; Futerko, P. *Chem. Eng. Sci.* **2000**, *55*, 4209.
(62) Futerko, P.; Hsing, I. M. *Electrochim. Acta* **2000**, *45*, 1741.
(63) Thampan, T.; Malhotra, S.; Tang, H.; Datta, R. *J. Electrochem. Soc.* **2000**, *147*, 3242.
(64) Um, S.; Wang, C.-Y.; Chen, K. S. *J. Electrochem. Soc.* **2000**, *147*, 4485.
(65) Costamagna, P. *Chem. Eng. Sci.* **2001**, *56*, 323.
(66) Dohle, H.; Kornyshev, A. A.; Kulikovsky, A. A.; Mergel, J.; Stolten, D. *Electrochem. Commun.* **2001**, *3*, 73.
(67) Kornyshev, A. A.; Kulikovsky, A. A. *Electrochim. Acta* **2001**, *46*, 4389.
(68) Kulikovsky, A. A. *Electrochem. Commun.* **2001**, *3*, 572.
(69) Kulikovsky, A. A. *Fuel Cells* **2001**, *1*, 162.
(70) Eikerling, M.; Kornyshev, A. A.; Kuznetsov, A. M.; Ulstrup, J.; Walbran, S. *J. Phys. Chem. B* **2001**, *105*, 3646.
(71) Rowe, A.; Li, X. G. *J. Power Sources* **2001**, *102*, 82.
(72) Thampan, T.; Malhotra, S.; Zhang, J. X.; Datta, R. *Catal. Today* **2001**, *67*, 15.
(73) Shimpalee, S.; Lee, W. K.; Van Zee, J. W. The Electrochemical Society Extended Abstracts, September 2–7, 2001; Abstract 458.
(74) Weber, A. Z.; Darling, R. M.; Newman, J. *J. Electrochem. Soc.*, in press.
(75) Chu, H.-S.; Yeh, C.; Chen, F. *J. Power Sources* **2002**, *123*, 1.
(76) Um, S.; Wang, C. Y. *J. Power Sources* **2004**, *125*, 40.
(77) Zhukovsky, K. V. *AIChE J.* **2003**, *49*, 3029.
(78) Pisani, L.; Murgia, G.; Valentini, M.; D'Aguanno, B. *J. Electrochem. Soc.* **2002**, *149*, A898.
(79) You, L. X.; Liu, H. T. *Int. J. Heat Mass Transfer* **2002**, *45*, 2277.
(80) Berning, T.; Djilali, N. *J. Electrochem. Soc.* **2003**, *150*, A1598.
(81) Kulikovsky, A. A. *J. Electrochem. Soc.* **2003**, *150*, A1432.
(82) Lee, W. K.; Shimpalee, S.; Van Zee, J. W. *J. Electrochem. Soc.* **2003**, *150*, A341.
(83) Kulikovsky, A. A. *Electrochem. Commun.* **2002**, *4*, 527.
(84) Mazumder, S.; Cole, J. V. *J. Electrochem. Soc.* **2003**, *150*, A1503.
(85) Mazumder, S.; Cole, J. V. *J. Electrochem. Soc.* **2003**, *150*, A1510.
(86) Nam, J. H.; Kaviany, M. *Int. J. Heat Mass Transfer* **2003**, *46*, 4595.
(87) Natarajan, D.; Nguyen, T. V. *J. Power Sources* **2003**, *115*, 66.
(88) Weber, A. Z.; Newman, J. In *Advanced Materials for Fuel Cells and Batteries*; Ehrlich, G., Arora, P., Ofer, D., Savinell, R. F., Zawodinski, T., D'Souza, F., Eds.; The Electrochemical Society Proceeding Series: Pennington, NJ, 2003.
(89) Weber, A. Z.; Newman, J. *J. Electrochem. Soc.* **2003**, *150*, A1008.
(90) Siegel, N. P.; Ellis, M. W.; Nelson, D. J.; von Spakovsky, M. R. *J. Power Sources* **2003**, *115*, 81.
(91) Pisani, L.; Valentini, M.; Murgia, G. *J. Electrochem. Soc.* **2003**, *150*, A1558.
(92) Choi, P.; Datta, R. *J. Electrochem. Soc.* **2003**, *150*, E601.
(93) Weber, A. Z.; Newman, J. In *Proton Conducting Membrane Fuel Cells III*; Van Zee, J. W., Fuller, T. F., Gottesfeld, S., Murthy, M., Eds.; The Electrochemical Society Proceeding Series: Pennington, NJ, 2002.
(94) Weber, A. Z.; Newman, J. *J. Electrochem. Soc.* **2004**, *151*, A311.
(95) Murgia, G.; Pisani, L.; Valentini, M.; D'Aguanno, B. *J. Electrochem. Soc.* **2002**, *149*, A31.
(96) Kulikovsky, A. A. *Electrochem. Commun.* **2002**, *4*, 318.
(97) Kulikovsky, A. A. *Electrochem. Commun.* **2002**, *4*, 845.
(98) Jaouen, F.; Lindbergh, G.; Sundholm, G. *J. Electrochem. Soc.* **2002**, *149*, A437.
(99) Hertwig, K.; Martens, L.; Karwoth, R. *Fuel Cells* **2002**, *2*, 61.
(100) Ahmed, S.; Kopasz, J.; Kumar, R.; Krumpelt, M. *J. Power Sources* **2002**, *112*, 519.
(101) Springer, T. E.; Wilson, M. S.; Gottesfeld, S. *J. Electrochem. Soc.* **1993**, *140*, 3513.
(102) Springer, T. E.; Zawodzinski, T. A.; Wilson, M. S.; Gottesfeld, S. *J. Electrochem. Soc.* **1996**, *143*, 587.
(103) Springer, T. E.; Raistrick, I. D. *J. Electrochem. Soc.* **1989**, *136*, 1594.
(104) Springer, T. E.; Rockward, T.; Zawodzinski, T. A.; Gottesfeld, S. *J. Electrochem. Soc.* **2001**, *148*, A11.
(105) Ridge, S. J.; White, R. E.; Tsou, Y.; Beaver, R. N.; Eisman, G. A. *J. Electrochem. Soc.* **1989**, *136*, 1902.
(106) Weisbrod, K. R.; Grot, S. A.; Vanderborgh, N. E. In *First International Symposium on Proton Conducting Membrane Fuel Cells*; Landgrebe, A. R., Gottesfeld, S., Halpert, G., Eds.; The Electrochemical Society Proceeding Series; Pennington, NJ, 1995; Vol. PV 95–23.
(107) Yi, J. S.; Nguyen, T. V. *J. Electrochem. Soc.* **1998**, *145*, 1149.
(108) Wood, D. L.; Yi, Y. S.; Nguyen, T. V. *Electrochim. Acta* **1998**, *43*, 3795.
(109) Ge, S.-H.; Yi, B.-L. *J. Power Sources* **2003**, *124*, 1.
(110) Bernardi, D. M.; Verbrugge, M. W. *AIChE J.* **1991**, *37*, 1151.
(111) Verbrugge, M. W.; Hill, R. F. *J. Electrochem. Soc.* **1990**, *137*, 886.
(112) Bernardi, D. M. *J. Electrochem. Soc.* **1990**, *137*, 3344.
(113) Chan, S. H.; Goh, S. K.; Jiang, S. P. *Electrochim. Acta* **2003**, *48*, 1905.

(114) Marr, C.; Li, X. G. *J. Power Sources* **1999**, *77*, 17.
(115) Baschuk, J. J.; Li, X. G. *Int. J. Energy Res.* **2003**, *27*, 1095.
(116) Baschuk, J. J.; Rowe, A. M.; Li, X. G. *J. Energy Resour. Technol.* **2003**, *125*, 94.
(117) Murgia, G.; Pisani, L.; Shukla, A. K.; Scott, K. *J. Electrochem. Soc.* **2003**, *150*, A1231.
(118) Pisani, L.; Murgia, G.; Valentini, M.; D'Aguanno, B. *J. Power Sources* **2002**, *108*, 192.
(119) Zhou, T.; Liu, H. *Int. J. Trans. Phenom.* **2001**, *3*, 177.
(120) Gurau, V.; Barbir, F.; Liu, H. *J. Electrochem. Soc.* **2000**, *147*, 2468.
(121) You, L. X.; Liu, H. T. *Int. J. Hydrogen Energy* **2001**, *26*, 991.
(122) Pasaogullari, U.; Wang, C. Y. 204th Meeting of the Electrochemical Society, Orlando, FL, 2003; Abstract 1103.
(123) Pasaogullari, U.; Wang, C. Y. *J. Electrochem. Soc.* **2004**, *151*, A399.
(124) Meng, H.; Wang, C. Y. *J. Electrochem. Soc.* **2004**, *151*, A358.
(125) Berning, T.; Lu, D. M.; Djilali, N. *J. Power Sources* **2002**, *106*, 284.
(126) Bradean, R.; Promislow, K.; Wetton, B. *Numer. Heat Transfer, Part A* **2002**, *42*, 121.
(127) Newman, J. *Electrochim. Acta* **1979**, *24*, 223.
(128) Fuller, T. F. Ph.D. Dissertation, University of California–Berkeley, 1992.
(129) Dannenberg, K.; Ekdunge, P.; Lindbergh, G. *J. Appl. Electrochem.* **2000**, *30*, 1377.
(130) Meyers, J. P.; Newman, J. *J. Electrochem. Soc.* **2002**, *149*, A710.
(131) Meyers, J. P.; Newman, J. *J. Electrochem. Soc.* **2002**, *149*, A718.
(132) Meyers, J. P.; Newman, J. *J. Electrochem. Soc.* **2002**, *149*, A729.
(133) Weber, A.; Darling, R.; Meyers, J.; Newman, J. In *Handbook of Fuel Cells: Fundamentals, Technology, and Applications*; Vielstich, W., Lamm, A., Gasteiger, H. A., Eds.; John Wiley & Sons: New York, 2003; Vol. 1.
(134) Weber, A. Z.; Newman, J. *J. Electrochem. Soc.* **2004**, *151*, A326.
(135) Kulikovsky, A. A. *Electrochem. Commun.* **2003**, *5*, 530.
(136) Eikerling, M.; Paddison, S. J.; Zawodzinski, T. A. *J. New Mater. Electrochem. Syst.* **2002**, *5*, 15.
(137) Eikerling, M.; Kornyshev, A. A. *J. Electroanal. Chem.* **1999**, *475*, 107.
(138) Eikerling, M.; Kornyshev, A. A.; Stimming, U. *J. Phys. Chem. B* **1997**, *101*, 10807.
(139) Newman, J. S. *Electrochemical Systems*, 2nd ed.; Prentice Hall: Englewood Cliffs, NJ, 1991.
(140) Bard, A. J.; Faulkner, L. R. *Electrochemical Methods: Fundamentals and Applications*, 2nd ed.; John Wiley & Sons: New York, 2001.
(141) Bockris, J. O'M.; Reddy, A. K. N. *Modern Electrochemistry*; Plenum Press: New York, 1973.
(142) Perry, R. H.; Green, D. W. *Perry's Chemical Engineers' Handbook*, 7th ed.; McGraw-Hill: New York, 1997.
(143) Latimer, W. *Oxidation Potentials*, 2nd ed.; Prentice-Hall: Englewood Cliffs, NJ, 1952.
(144) Lewis, G.; Randall, M. *International Critical Tables*; McGraw-Hill: New York, 1930.
(145) Vetter, K. J. *Electrochemical Kinetics*; Academic Press: New York, 1967.
(146) Wang, J. X.; Brankovic, S. R.; Zhu, Y.; Hanson, J. C.; Adzic, R. R. *J. Electrochem. Soc.* **2003**, *150*, A1108.
(147) Maruyama, J.; Inaba, M.; Katakura, K.; Ogumi, Z.; Takehara, Z. *J. Electroanal. Chem.* **1998**, *447*, 201.
(148) Mello, R. M. Q.; Ticianelli, E. A. *Electrochim. Acta* **1997**, *42*, 1031.
(149) Bird, R. B.; Stewart, W. E.; Lightfoot, E. N. *Transport Phenomena*, 2nd ed.; John Wiley & Sons: New York, 2002.
(150) Appleby, A. J. *J. Electrochem. Soc.* **1970**, *117*, 328.
(151) Kinoshita, K. *Electrochemical Oxygen Technology*; John Wiley & Sons: New York, 1992.
(152) Beattie, P. D.; Basura, V. I.; Holdcroft, S. *J. Electroanal. Chem.* **1999**, *468*, 180.
(153) Rho, Y. W.; Velev, O. A.; Srinivasan, S. *J. Electrochem. Soc.* **1994**, *141*, 2084.
(154) Parthasarathy, A.; Dave, B.; Srinivasan, S.; Appleby, A. J.; Martin, C. R. *J. Electrochem. Soc.* **1992**, *139*, 1634.
(155) Parthasarathy, A.; Srinivasan, S.; Appleby, A. J.; Martin, C. R. *J. Electroanal. Chem.* **1992**, *339*, 101.
(156) Perez, J.; Gonzalez, E. R.; Ticianelli, E. A. *J. Electrochem. Soc.* **1998**, *145*, 2307.
(157) Uribe, F. A.; Springer, T. E.; Gottesfeld, S. *J. Electrochem. Soc.* **1992**, *139*, 765.
(158) Gasteiger, H. A.; Gu, W.; Makharia, R.; Mathias, M. F.; Sompalli, B. In *Handbook of Fuel Cells: Fundamentals, Technology, and Applications*; Vielstich, W., Lamm, A., Gasteiger, H. A., Eds.; John Wiley & Sons: New York, 2003; Vol. 3.
(159) Sena, D. R.; Ticianelli, E. A.; Paganin, V. A.; Gonzalez, E. R. *J. Electroanal. Chem.* **1999**, *477*, 164.
(160) Lee, S. J.; Mukerjee, S.; McBreen, J.; Rho, Y. W.; Kho, Y. T.; Lee, T. H. *Electrochim. Acta* **1998**, *43*, 3693.
(161) Liebhafsky, H. A.; Cairns, E. J.; Grubb, W. T.; Niedrach, L. W. In *Fuel Cell Systems*; Young, G. J., Linden, H. R., Eds.; American Chemical Society: Washington, DC, 1965; Vol. 47.

(162) Passalacqua, E.; Lufrano, F.; Squadrito, G.; Patti, A.; Giorgi, L. *Electrochim. Acta* **2001**, *46*, 799.
(163) Squadrito, G.; Maggio, G.; Passalacqua, E.; Lufrano, F.; Patti, A. *J. Appl. Electrochem.* **1999**, *29*, 1449.
(164) Newman, J. *Ind. Eng. Chem. Res.* **1995**, *34*, 3208.
(165) Kreuer, K. D. *Chem. Rev.* **2004**, *104*, 4637.
(166) Paddison, S. J.; Paul, R.; Zawodzinski, T. A. *J. Electrochem. Soc.* **2000**, *147*, 617.
(167) Khalatur, P. G.; Talitskikh, S. K.; Khokhlov, A. R. *Macromol. Theory Simul.* **2002**, *11*, 566.
(168) Krueger, J. J.; Simon, P. P.; Ploehn, H. J. *Macromolecules* **2002**, *35*, 5630.
(169) Li, T.; Wlaschin, A.; Balbuena, P. B. *Ind. Eng. Chem. Res.* **2001**, *40*, 4789.
(170) Paddison, S. J.; Paul, R.; Zawodzinski, T. A. *J. Chem. Phys.* **2001**, *115*, 7753.
(171) Paul, R.; Paddison, S. J. *J. Chem. Phys.* **2001**, *115*, 7762.
(172) Paddison, S. J. *J. New Mater. Electrochem. Syst.* **2001**, *4*, 197.
(173) Vishnyakov, A.; Neimark, A. V. *J. Phys. Chem. B* **2001**, *105*, 7830.
(174) Mologin, D. A.; Khalatur, P. G.; Kholhlov, A. R. *Macromol. Theory Simul.* **2002**, *11*, 587.
(175) Spohr, E.; Commer, P.; Kornyshev, A. A. *J. Phys. Chem. B* **2002**, *106*, 10560.
(176) Vishnyakov, A.; Neimark, A. V. *J. Phys. Chem. B* **2000**, *104*, 4471.
(177) Vishnyakov, A.; Neimark, A. V. *J. Phys. Chem. B* **2001**, *105*, 9586.
(178) Din, X. D.; Michaelides, E. E. *AIChE J.* **1998**, *44*, 35.
(179) Commer, P.; Cherstvy, A. G.; Spohr, E.; Kornyshev, A. A. *Fuel Cells* **2002**, *2*, 127.
(180) Jinnouchi, R.; Okazaki, K. *Microscale Thermophys. Eng.* **2003**, *7*, 15.
(181) Yeo, S. C.; Eisenberg, J. *J. Appl. Polym. Sci.* **1977**, *21*, 875.
(182) Hsu, W. Y.; Gierke, T. D. *J. Membr. Sci.* **1983**, *13*, 307.
(183) Eisenberg, A. *Macromolecules* **1970**, *3*, 147.
(184) Yeager, H. L.; Steck, A. *J. Electrochem. Soc.* **1981**, *128*, 1880.
(185) Eisenberg, A. *Bull. Am. Phys. Soc.* **1969**, *14*, 382.
(186) Dreyfus, B. *J. Polym. Sci., Part B: Polym. Phys.* **1983**, *21*, 2337.
(187) Koter, S. *J. Membr. Sci.* **2000**, *166*, 127.
(188) Datye, V. K.; Taylor, P. L.; Hopfinger, A. J. *Macromolecules* **1984**, *17*, 1704.
(189) Mauritz, K. A.; Rogers, C. E. *Macromolecules* **1985**, *18*, 483.
(190) Pintauro, P. N.; Verbrugge, M. W. *J. Membr. Sci.* **1989**, *44*, 197.
(191) Uitto, O. D.; White, H. S.; Aoki, K. *Anal. Chem.* **2002**, *74*, 4577.
(192) Guzmangarcia, A. G.; Pintauro, P. N.; Verbrugge, M. W.; Hill, R. F. *AIChE J.* **1990**, *36*, 1061.
(193) Tandon, R.; Pintauro, P. N. *J. Membr. Sci.* **1997**, *136*, 207.
(194) Wendt, R. P.; Klein, E.; Lynch, S. *J. Membr. Sci.* **1976**, *1*, 165.
(195) Cwirko, E. H.; Carbonell, R. G. *J. Membr. Sci.* **1992**, *67*, 227.
(196) Bontha, J. R.; Pintauro, P. N. *Chem. Eng. Sci.* **1994**, *49*, 3835.
(197) Koter, S. *J. Membr. Sci.* **2002**, *206*, 201.
(198) Narebska, A.; Koter, S.; Kujawski, W. *Desalination* **1984**, *51*, 3.
(199) Yang, Y. H.; Pintauro, P. N. *AIChE J.* **2000**, *46*, 1177.
(200) Pintauro, P. N.; Bennion, D. N. *Ind. Eng. Chem. Fundam.* **1984**, *23*, 234.
(201) Capeci, S. W.; Pintauro, P. N.; Bennion, D. N. *J. Electrochem. Soc.* **1989**, *136*, 2876.
(202) Schroeder, P. *Z. Phys. Chem.* **1903**, *45*, 57.
(203) Mann, R. F.; Amphlett, J. C.; Hooper, M. A. I.; Jensen, H. M.; Peppley, B. A.; Roberge, P. R. *J. Power Sources* **2000**, *86*, 173.
(204) Leddy, J.; Iverson, A. E.; Vanderborgh, N. E. In *Electrochemical and Thermal Modeling of Battery, Fuel Cell, and Photoenergy Conversion Systems*; Selman, J. R., Maru, H. C., Eds.; The Electrochemical Society Proceeding Series; Pennington, NJ, 1986; Vol. PV 86−12.
(205) Einstein, A. *Ann. Phys.* **1905**, *17*, 549.
(206) Nernst, W. *Z. Phys. Chem.* **1888**, *2*, 613.
(207) Okada, T.; Xie, G.; Tanabe, Y. *J. Electronanal. Chem.* **1996**, *413*, 49.
(208) Bennion, D. N. *Mass Transport of Binary Electrolyte Solutions in Membranes*; Water Resources Center Desalination Report No. 4; Department of Engineering, University of California−Los Angeles: 1966.
(209) Pintauro, P. N.; Bennion, D. N. *Ind. Eng. Chem. Fundam.* **1984**, *23*, 230.
(210) Auclair, B.; Nikonenko, V.; Larchet, C.; Metayer, M.; Dammak, L. *J. Membr. Sci.* **2002**, *195*, 89.
(211) Koter, S.; Hamann, C. H. *J. Non-Equilib. Thermodyn.* **1990**, *15*, 315.
(212) Meyers, J. P. Ph.D. Dissertation, University of California−Berkeley, 1998.
(213) Verbrugge, M. W.; Hill, R. F. *J. Electrochem. Soc.* **1990**, *137*, 3770.
(214) Verbrugge, M. W.; Hill, R. F. *J. Electrochem. Soc.* **1990**, *137*, 1131.
(215) Schlogl, R. *Z. Phys. Chem.* **1955**, *3*, 73.
(216) Mason, E. A.; Malinauskas, A. P. *Gas Transport in Porous Media: The Dusty-Gas Model*; Elsevier: Amsterdam, 1983.

(217) Buchi, F. N.; Scherer, G. G. *J. Electrochem. Soc.* **2001**, *148*, A183.
(218) Kreuer, K. D. *Solid State Ionics* **1997**, *97*, 1.
(219) De La Rue, R. E.; Tobias, C. W. *J. Electrochem. Soc.* **1959**, *106*, 827.
(220) Bruggeman, D. A. G. *Ann. Phys.* **1935**, *24*, 636.
(221) Li, G.; Pickup, P. P. *J. Electrochem. Soc.* **2003**, *150*, C745.
(222) Bernardi, D. M. Ph.D. Dissertation, University of California, 1986.
(223) Dullien, F. A. L. *Porous Media: Fluid Transport and Pore Structure*, 2nd ed.; Academic Press: New York, 1992.
(224) Knudsen, M. *The Kinetic Theory of Gases*; Methuen: London, 1934.
(225) Rothfeld, L. B. *AIChE J.* **1963**, *9*, 19.
(226) Weber, A. Z.; Newman, J. *Int. Commun. Heat Mass Transfer*, in press.
(227) Passalacqua, E.; Squadrito, G.; Lufrano, F.; Patti, A.; Giorgi, L. *J. Appl. Electrochem.* **2001**, *31*, 449.
(228) Tucker, M. C.; Odgaard, M.; Yde-Anderson, S.; Thomas, J. O. 203rd Meeting of the Electrochemical Society, Paris, 2003; Abstract 1235.
(229) Jordan, L. R.; Shukla, A. K.; Behrsing, T.; Avery, N. R.; Muddle, B. C.; Forsyth, M. *J. Power Sources* **2000**, *86*, 250.
(230) Jordan, L. R.; Shukla, A. K.; Behrsing, T.; Avery, N. R.; Muddle, B. C.; Forsyth, M. *J. Appl. Electrochem.* **2000**, *30*, 641.
(231) Kong, C. S.; Kim, D.-Y.; Lee, H.-K.; Shul, Y.-G.; Lee, T.-H. *J. Power Sources* **2002**, *108*, 185.
(232) Wilson, M. S. U.S. Patent 5,641,586, 1995.
(233) Miller, C. T.; Christakos, G.; Imhoff, P. T.; McBride, J. F.; Pedit, J. A.; Trangenstein, J. A. *Adv. Water Resources* **1998**, *21*, 77.
(234) Bear, J. *Dynamics of Fluids in Porous Media*; Dover Publications: New York, 1988.
(235) Smith, W. O. *Physics* **1933**, *4*, 425.
(236) Leverett, M. C. *Trans. Am. Inst. Min., Metall. Pet. Eng.* **1941**, *142*, 152.
(237) Fischer, A.; Jindra, J.; Wendt, H. *J. Appl. Electrochem.* **1998**, *28*, 277.
(238) Ticianelli, E. A.; Beery, J. G.; Srinivasan, S. *J. Appl. Electrochem.* **1991**, *21*, 597.
(239) Cheng, X.; Yi, B.; Han, M.; Zhang, J.; Qiao, Y.; Yu, J. *J. Power Sources* **1999**, *79*, 75.
(240) Uchida, M.; Aoyama, Y.; Eda, N.; Ohta, A. *J. Electrochem. Soc.* **1995**, *142*, 4143.
(241) *Handbook of Fuel Cells: Fundamentals, Technology, and Applications, Vol. 2−Electrocatalysis*; Vielstich, W., Lamm, A., Gasteiger, H. A., Eds.; John Wiley & Sons: New York, 2003.
(242) Mukerjee, S. *J. Appl. Electrochem.* **1990**, *20*, 537.
(243) Markovic, N. M.; Schmidt, T. J.; Stamenkovic, V.; Ross, P. N. *Fuel Cells* **2001**, *1*, 105.
(244) Vogel, W.; Lundquist, J.; Ross, P.; Stonehart, P. *Electrochim. Acta* **1975**, *20*, 79.
(245) Zhang, J. X.; Thampan, T.; Datta, R. *J. Electrochem. Soc.* **2002**, *149*, A765.
(246) Bellows, R. J.; MarucchiSoos, E. P.; Buckley, D. T. *Ind. Eng. Chem. Res.* **1996**, *35*, 1235.
(247) Stonehar, P. *Electrochim. Acta* **1967**, *12*, 1185.
(248) Bhatia, K. K.; Wang, C.-Y. *Electrochim. Acta* **2004**, *49*, 2333.
(249) Grens, E. A.; Turner, R. M.; Katan, T. *Adv. Energy Convers.* **1964**, *4*, 109.
(250) Chirkov, Y. G. *Elektrokhimiya* **1975**, *11*, 36.
(251) Chirkov, Y. G. *Elektrokhimiya* **1972**, *7*, 1826.
(252) Viitanen, M.; Lampinen, M. J. *J. Power Sources* **1990**, *32*, 207.
(253) Grens, E. A. *Ind. Eng. Chem. Fundam.* **1966**, *5*, 542.
(254) Yang, S. C.; Cutlip, M. B.; Stonehart, P. *Electrochim. Acta* **1990**, *35*, 869.
(255) Yang, S. C.; Cutlip, M. B.; Stonehart, P. *Electrochim. Acta* **1989**, *34*, 703.
(256) Vogel, W.; Bradford, A.; Lundquist, J. *Electrochim. Acta* **1972**, *17*, 1735.
(257) Bjornbom, P. *Electrochim. Acta* **1987**, *32*, 115.
(258) Srinivasan, S.; Hurwitz, H. D. *Electrochim. Acta* **1967**, *12*, 495.
(259) Srinivasan, S.; Hurwitz, H. D.; Bockris, J. O'M. *J. Chem. Phys.* **1967**, *46*, 3108.
(260) Bultel, Y.; Ozil, P.; Durand, R. *J. Appl. Electrochem.* **2000**, *30*, 1369.
(261) Euler, J.; Nonnenmacher, W. *Electrochim. Acta* **1960**, *2*, 268.
(262) Bockris, J. O'M.; Srinivasan, S. *Fuel Cells: Their Electrochemistry*; McGraw-Hill: New York, 1969.
(263) DeVidts, P.; White, R. E. *J. Electrochem. Soc.* **1997**, *144*, 1343.
(264) Gloaguen, F.; Andolfatto, F.; Durand, R.; Ozil, P. *J. Appl. Electrochem.* **1994**, *24*, 863.
(265) Fogler, H. S. *Elements of Chemical Reaction Engineering*, 2nd ed.; Prentice Hall: Upper Saddle River, NJ, 1992.
(266) Thiele, E. W. *Ind. Eng. Chem.* **1939**, *31*, 916.
(267) Fuller, T. F.; Luczak, F. J.; Wheeler, D. J. *J. Electrochem. Soc.* **1995**, *142*, 1752.
(268) Stonehart, P.; Ross, P. N. *Electrochim. Acta* **1976**, *21*, 441.
(269) Maja, M.; Tosco, P.; Vanni, M. *J. Electrochem. Soc.* **2003**, *148*, A1368.
(270) Qi, Z. G.; Kaufman, A. *J. Power Sources* **2002**, *109*, 38.

(271) Wilson, M. S.; Valerio, J. A.; Gottesfeld, S. *Electrochim. Acta* **1995**, *40*, 355.
(272) Janssen, G. J. M.; Overvelde, M. L. J. *J. Power Sources* **2001**, *101*, 117.
(273) Patankar, S. *Numerical Heat Transfer and Fluid Flow*; Hemisphere Publishing Corporation: Bristol, PA, 1980.
(274) Suares, G. E.; Kosanovich, K. A. *Ind. Eng. Chem. Res.* **1997**, *36*, 4264.
(275) Duan, T.; Weidner, J. W.; White, R. E. *J. Power Sources* **2002**, *107*, 24.
(276) Wang, C. Y. *Chem. Rev.* **2004**, *104*, 4727.
(277) McCabe, W. L.; Smith, J. C.; Harriott, P. *Unit Operations of Chemical Engineering*, 5th ed.; McGraw-Hill, Inc.: New York, 1993.
(278) Meyers, J. P.; Villwock, R. D.; Darling, R. M.; Newman, J. In *Advances in Mathematical Modeling and Simulation of Electrochemical Processes and Oxygen Depolarized Cathodes and Activated Cathodes for Chlor-Alkali Processes*; Van Zee, J. W., Fuller, T. F., Foller, P. C., Hine, F., Eds.; The Electrcohemical Society Proceedings Series; Pennington, NJ, 1998; Vol. PV 98–10.
(279) Kumar, A.; Reddy, R. G. *J. Power Sources* **2003**, *114*, 54.
(280) Kumar, A.; Reddy, R. G. *J. Power Sources* **2003**, *113*, 11.
(281) Baker, D. R.; Darling, R. M. *Int. J. Trans. Phenom.* **2001**, *3*, 177.
(282) Hirschfelder, J. O.; Curtiss, C. F.; Bird, R. B. *Molecular Theory of Gases and Liquids*; John Wiley & Sons: New York, 1954.
(283) Thomas, K. E.; Newman, J. *J. Electrochem. Soc.* **2003**, *150*, A176.
(284) Newman, J.; Thomas-Alyea, K. E. *Electrochemical Systems*, 3rd ed.; John Wiley & Sons: New York, 2004.
(285) Agar, J. N. In *Advances in Electrochemistry and Electrochemical Engineering*; Delahay, P., Ed.; John Wiley & Sons: New York, 1963; Vol. 3.
(286) Rao, L.; Newman, J. *J. Electrochem. Soc.* **1997**, *144*, 2697.
(287) Bernardi, D. M.; Pawlikowski, E.; Newman, J. *J. Electrochem. Soc.* **1985**, *132*, 5.
(288) Amphlett, J. C.; Mann, R. F.; Peppley, B. A.; Roberge, P. R.; Rodrigues, A. *J. Power Sources* **1996**, *61*, 183.
(289) Yerramalla, S.; Davari, A.; Feliachi, A.; Biswas, T. *J. Power Sources* **2003**, *124*, 104.
(290) Zawodzinski, T. A.; Derouin, C. R.; Radzinski, S.; Sherman, R.; Smith, V. T.; Springer, T. E.; Gottesfeld, S. *J. Electrochem. Soc.* **1993**, *140*, 1041.
(291) Nguyen, T. V.; Vanderborgh, N. E. *J. Membr. Sci.* **1998**, *143*, 235.
(292) He, W. S.; Lin, G. Y.; Van Nguyen, T. *AIChE J.* **2003**, *49*, 3221.
(293) Mosdale, R.; Gebel, G.; Pineri, M. *J. Membr. Sci.* **1996**, *118*, 269.
(294) De Francesco, M.; Arato, E. *J. Power Sources* **2002**, *108*, 41.
(295) Scott, K.; Argyropoulos, P.; Taama, W. M. *Chem. Eng. Res. Des.* **2000**, *78*, 881.
(296) Maggio, G.; Recupero, V.; Mantegazza, C. *J. Power Sources* **1996**, *62*, 167.
(297) Thirumalai, D.; White, R. E. *J. Electrochem. Soc.* **1997**, *144*, 1717.
(298) Lee, J. H.; Lalk, T. R.; Appleby, A. J. *J. Power Sources* **1998**, *70*, 258.
(299) Lee, J. H.; Lalk, T. R. *J. Power Sources* **1998**, *73*, 229.
(300) Cownden, R.; Nahon, M.; Rosen, M. *Int. J. Hydrogen Energy* **2001**, *26*, 615.
(301) Ahluwalia, R. K.; Doss, E. D.; Kumar, R. *J. Power Sources* **2003**, *117*, 45.
(302) Paganin, V. A.; Oliveira, C. L. F.; Ticianelli, E. A.; Springer, T. E.; Gonzalez, E. R. *Electrochim. Acta* **1998**, *43*, 3761.
(303) Brett, D. J. L.; Atkins, S.; Brandon, N. P.; Vesovic, V.; Vasileiadis, N.; Kucernak, A. *Electrochem. Solid-State Lett.* **2003**, *6*, A63.

(304) Andreaus, B.; McEvoy, A. J.; Scherer, G. G. *Electrochim. Acta* **2002**, *47*, 2223.
(305) Wagner, N. *J. Appl. Electrochem.* **2002**, *32*, 859.
(306) Wang, X.; Hsing, I. M.; Leng, Y. J.; Yue, P. L. *Electrochim. Acta* **2001**, *46*, 4397.
(307) Ciureanu, M.; Roberge, R. *J. Phys. Chem. B* **2001**, *105*, 3531.
(308) Sorensen, T. S.; Kjelstrup, S. *J. Colloid Interface Sci.* **2002**, *248*, 355.
(309) Bultel, Y.; Genies, L.; Antoine, O.; Ozil, P.; Durand, R. *J. Electroanal. Chem.* **2002**, *527*, 143.
(310) Yuh, C. Y.; Selman, J. R. *AIChE J.* **1988**, *34*, 1949.
(311) Raistrick, I. D. *Electrochim. Acta* **1990**, *35*, 1579.
(312) Fritts, S. D.; Savinell, R. F. *J. Power Sources* **1989**, *28*, 301.
(313) Guo, Q.; Cayetano, M.; Tsou, Y.-M.; De Castro, E. S.; White, R. E. *J. Electrochem. Soc.* **2003**, *150*, A1440.
(314) Jaouen, F.; Lindbergh, G. *J. Electrochem. Soc.* **2003**, *150*, A1699.
(315) Scott, K.; Argyropoulos, P.; Sundmacher, K. *J. Electronanal. Chem.* **1999**, *477*, 97.
(316) Scott, K.; Taama, W. M.; Argyropoulos, P.; Sundmacher, K. *J. Power Sources* **1999**, *83*, 204.
(317) Scott, K.; Taama, W. M.; Kramer, S.; Argyropoulos, P.; Sundmacher, K. *Electrochim. Acta* **1999**, *45*, 945.
(318) Baxter, S. F.; Battaglia, V. S.; White, R. E. *J. Electrochem. Soc.* **1999**, *146*, 437.
(319) Fan, J. R.; Hu, G. L.; Yao, J.; Cen, K. F. *Energy Fuels* **2002**, *16*, 1591.
(320) Argyropoulos, P.; Scott, K.; Shukla, A. K.; Jackson, C. *Fuel Cells* **2002**, *2*, 78.
(321) Argyropoulos, P.; Scott, K.; Taama, W. M. *Chem. Eng. J.* **1999**, *73*, 217.
(322) Argyropoulos, P.; Scott, K.; Taama, W. M. *J. Power Sources* **1999**, *79*, 169.
(323) Argyropoulos, P.; Scott, K.; Taama, W. M. *J. Appl. Electrochem.* **2000**, *30*, 899.
(324) Birgersson, E.; Nordlund, J.; Ekstrom, H.; Vynnycky, M.; Lindbergh, G. *J. Electrochem. Soc.* **2003**, *150*, A1368.
(325) Andrian, S. V.; Meusinger, J. *J. Power Sources* **2000**, *91*, 193.
(326) Okada, T. *J. New Mater. Electrochem. Syst.* **2001**, *4*, 209.
(327) Li, P. W.; Schaefer, L.; Wang, Q. M.; Zhang, T.; Chyu, M. K. *J. Power Sources* **2003**, *115*, 90.
(328) Li, P. W.; Zhang, T.; Wang, Q. M.; Schaefer, L.; Chyu, M. K. *J. Power Sources* **2003**, *114*, 63.
(329) Chu, D.; Jiang, R. Z. *J. Power Sources* **1999**, *83*, 128.
(330) Darling, R. M.; Meyers, J. P. *J. Electrochem. Soc.* **2003**, *150*, A1523.
(331) Wendt, H.; Brenscheidt, T.; Fischer, A. *Philos. Trans. R. Soc. London, Ser. A* **1996**, *354*, 1627.
(332) Jiang, R. Z.; Chu, D. *J. Power Sources* **2001**, *92*, 193.
(333) Fowler, M. W.; Mann, R. F.; Amphlett, J. C.; Peppley, B. A.; Roberge, P. R. *J. Power Sources* **2002**, *106*, 274.
(334) Aragane, J.; Murahashi, T.; Odaka, T. *J. Electrochem. Soc.* **1988**, *135*, 844.
(335) Honji, A.; Mori, T.; Tamura, K.; Hishinuma, Y. *J. Electrochem. Soc.* **1988**, *135*, 355.
(336) Liu, W.; Ruth, K.; Rusch, G. *J. New Mater. Electrochem. Syst.* **2001**, *4*, 227.
(337) Pozio, A.; Silva, R. F.; De Francesco, M.; Giorgi, L. *Electrochim. Acta* **2003**, *48*, 1543.
(338) Kiwi, J.; Denisov, N.; Gak, Y.; Ovanesyan, N.; Buffat, P. A.; Suvorova, E.; Gostev, F.; Titov, A.; Sarkison, O.; Albers, P.; Nadtochenko, V. *Langmuir* **2002**, *18*, 9054.